FLEXURAL STRENGTHENING OF TWO-WAY SLABS USING CFRP EXTERNAL LAMINATES

By

Shams Abbas Naqvi

Presented to the Faculty of Graduate School of

The University of Texas at Arlington in Partial fulfillment

of the Requirements

for the Degree Program of

Master of Science in Structures and Applied Mechanics

The University of Texas at Arlington

May 2021

Acknowledgements

Firstly, I would like to thank the almighty Allah (SWT) for allowing me to bring this effort to completion. I would like to thank and deeply appreciate the sincere gratitude of my graduate advisor Dr. Nur Yazdani for his diligent support throughout my graduate studies. I would also like to thank him for providing me with this wonderful opportunity to work under his guidance.

Secondly, I would like to thank Dr. Eyosias Beneberu for his continuous guidance and positive feedback. I am also grateful to my committee members, Drs. Jalali & Najafi for their support and recommendations.

I am deeply thankful to Amy Florius for her continuous support. I would also like to thank Ahmed Alateeq, Habeeb Karzan, Gary Ebner, Mitesh Shah, Harjas Singh Chauhan, Ananta Ranjit, and Sachin Yadav for all their support during the experimental testing.

I am deeply grateful to my family, who were always there by my side and supported me in every step of my education.

Abstract

FLEXURAL STRENGTHENING OF TWO-WAY SLABS USING CFRP EXTERNAL LAMINATES

Shams Abbas Naqvi, MS

The University of Texas at Arlington, 2021

Supervising Professor: Nur Yazdani, PhD

Deterioration of reinforced concrete structures with time is a common phenomenon, which often leads to reduction in the load carrying capacity. To meet the coding requirements, strengthening of these structures is of utmost importance. Composite materials, such as Carbon Fiber Reinforced Polymers (CFRP), have shown effective results in external strengthening of these structures. However, premature delamination of CFRPs can decrease their efficiency. Recently, pre-saturated CFRP (PS-CFRP), a new type of CFRP pre-impregnated with epoxy resin, was introduced. Previous research has shown that PS-CFRP has shown improved results as compared to regular CFRP (R-CFRP) for strengthening beams and columns. However, no research has been conducted on flexural strengthening of two-way slabs using PS-CFRP.

The purpose of this study is to evaluate external strengthening of two-way slabs using R-CFRP and PS-CFRP and to compare the results of the two methods. To facilitate this process, two full-scale reinforced concrete two-way slabs were cast and externally retrofitted. These slabs were then tested until failure under concentrated loading. A numerical model was also developed on ABAQUS to study the behavior of CFRP bonded to concrete slabs based on a previous study. The results showed that strengthening the RC two-way slabs using PS-CFRP is more effective than

using R-CFRP. The ultimate load capacity of the slab strengthened with PS-CFRP was 14.29% higher than the slab strengthened by R-CFRP. The slab strengthened using PS-CFRP also demonstrated more ductile behavior compared to R-CFRP. The numerical model developed in this current study validated the experimental results.

Table of Contents

List of Figures

List of Tables

Chapter 1
Introduction

1.1 Background

Older structures degrade over time and often do not meet the current structural standards for load bearing capacity (Fathelbab et al., 2014). Consequently, the structures are more likely to suffer from structural degradation due to the corrosion of reinforcing steel bars, adverse weather conditions, cracking, etc. As a result, structural strengthening has become an essential requirement for the longevity of structures, causing various strengthening techniques to emerge in the market (Sudha et al., 2017).

Compared to other techniques, Fiber Reinforced Polymer (FRP) strengthening is typically the most effective, providing high-quality structural results, less installation time, and a moderate cost compared to other approaches (Pandey, 2018). Moreover, the use of FRP strengthening techniques has significantly increased for retrofitting old structures for many structural engineering projects. Previous research has shown FRP in older structures leads to an increase in the strength of columns, beams, and one-way slabs (Fathelbab et al., 2014). Additionally, the flexural capacity of the concrete beam and one-way slabs increased after bonding the FRP laminates on the tension side (Fathelbab et al., 2014).

To effectively strengthen structures, the most common type of FRP materials used are Carbon Fiber Reinforced Polymers (CFRPs) and Glass Fiber Reinforced Polymers (GFRPs). The use of CFRPs has grown rapidly in the construction industry, specifically in structural retrofitting, due to the strengthening property of CFRP. CFRPs are moreover high strength, lightweight, non-corrosive, and easy-to-install materials. Furthermore, CFRPs have several practical applications; for example, they can be used to strengthen floor slabs.

The floor system is a major part of the building structure, and the cost of the structure is greatly affected by the quality of the floor system. An example of a deteriorated reinforced concrete (RC) structure is show in Fig. 1.1. The figure illustrates a garage floor slab over an area of the basement with severe spalling and cracking. Additionally, salt from vehicles during the winter has penetrated the slab and caused corrosion of the embedded reinforcing steel (Structural Dynamics, Inc., 2021). For the floor to remain in service, it would need to be retrofitted or replaced. Replacing the entire floor system would be very costly. Therefore, engineers worldwide are developing different techniques, such as FRP strengthening to restore the floor system.

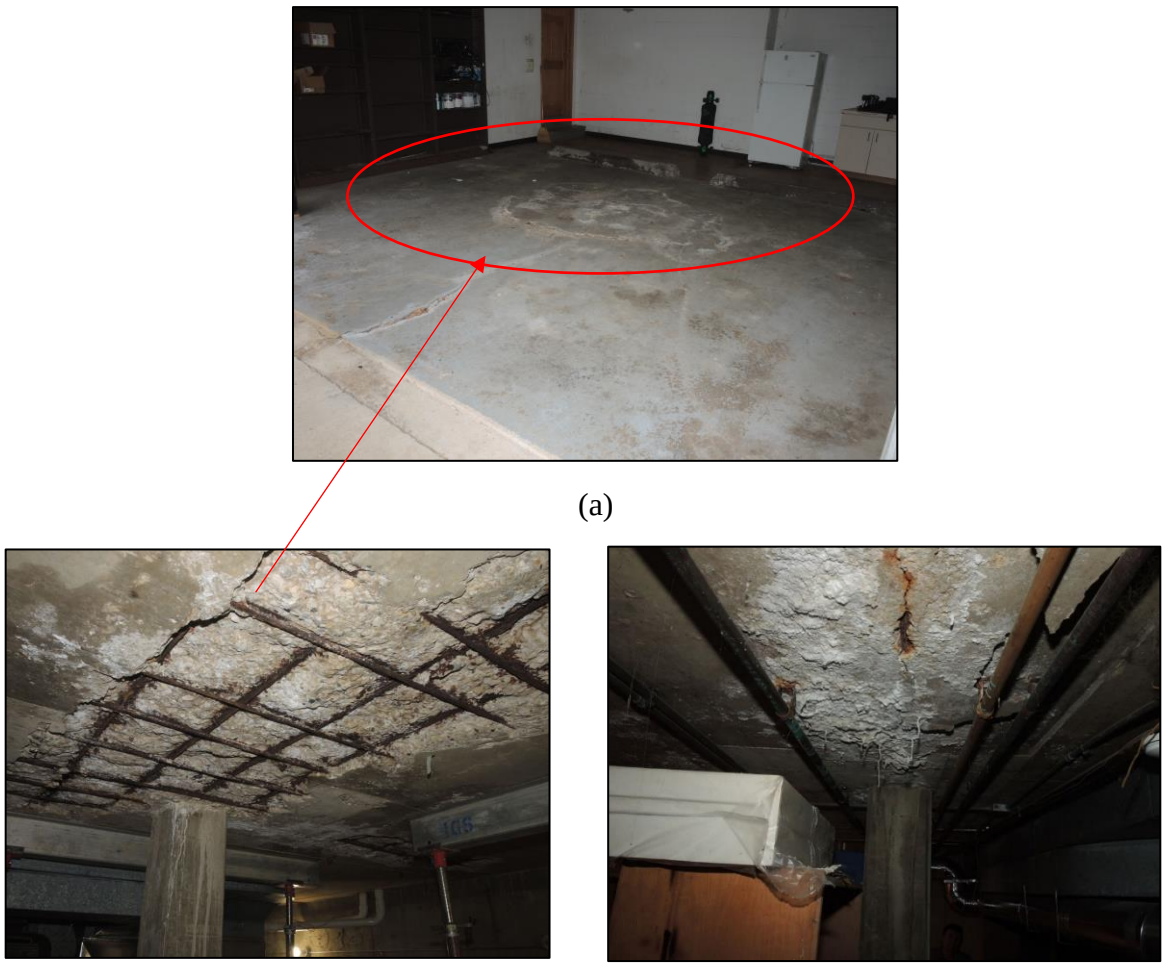

(a)

(b)

(c)

Fig 1.1: Deteriorated reinforced concrete slabs (a) Severe spalling and cracking of slab (b) Exposed corroded steel rebar (bottom view) (c) Corroding of steel and deflected slab

Little research has been conducted on the strengthening of RC slabs, specifically two-way slabs, using FRP materials. Certain studies explored the strengthening of one-way slabs using FRP materials or steel in which slabs were treated in a similar manner to beams (Ebead & Marzouk, 2002; Karbhari et al., 1994; Kikukawa et al., 1998).

Two-way slabs of low and medium reinforcement ratios are subject to flexural failure rather than punching shear failure. Hence, using CFRPs to enhance two-way slabs in flexure is more practical since they are easier to handle and install. The flexural capacity of two-way slabs can increase to an average of 35.5% over that of the non-strengthened specimen using CFRP (Ebead & Marzouk, 2004). Fig 1.2 illustrates strengthening of slabs using CFRP.

Fig 1.2: Slab strengthening using externally bonded CFRP (Horse Construction, 2021).

Externally bonded CFRP is one of the most superior repairing techniques (Sudha et al., 2017). However, it has a major drawback of debonding, which may occur at less than 50% of CFRP tensile strength capacity where up to half of its tensile capacity is ineffective (Orton et al., 2008). Previous studies have showed that the use of mechanical anchors, fan anchors, and u-wraps,

assisted with mitigating debonding and utilizing the maximum capacity of the CFRP (Anil & Belgin, 2010; Elsafty et al., 2013). Interestingly, no study has investigated the application of PS-CFRP to strengthen two-way slabs instead of using anchors. Additionally, PS-CFRP are manufactured as cured laminates. They can be added to existing structures without the addition of fiber resin required for saturation, which saves labor time and costs (Pandey et al., 2018).

The aforementioned studies serve as a guide to further investigate the effects on the flexural strength of two-way slabs using R-CFRP and PS-CFRP. Knowledge of the flexural strength of two-way slabs using FRPs can assist in finding the most effective strengthening technique. It is of utmost importance to be knowledgeable about the most efficient techniques as they can provide feasible and cost-effective solutions for damage/deterioration in structures. The appropriate techniques found from this current study can be applied worldwide, to assist in strengthening a variety of building structures.

1.2 Problem Statement

Quite often, many structures degrade or deteriorate over time due to various factors, resulting in a negative impact on flexural strength. However, it is impractical to reconstruct each structure that experiences deterioration; therefore, non-destructive methods, such as CFRP wrapping, have been used to significantly assist in increasing the strength of the structures (Fathelbab et al., 2014). Until now, no tests have been conducted to evaluate the practical application of PS-CFRP wrapping on two-way slabs. While studies have shown that the use of R-CFRP used to increase the strength of two-way slabs has been successful, there are some drawbacks. For example, debonding is a major issue when using R-CFRP, and a decrease in ductility was also evident due to brittle nature of FRP materials (Ebead & Marzouk, 2004). To

address these problems, this study aims to evaluate the use of PS-CFRP to strengthen two-way slabs, and the results will be compared to those of R-CFRP.

1.3 Objective

The objective of this study was to compare the effects of using PS-CFRP against R-CFRP laminates, as an external strengthening material for flexure in two-way slabs. The study included experimental and numerical investigations. The experimental segment includes evaluation of strengthening two full-scale, two-way RC slabs using CFRP (regular and pre-saturated, respectively). The numerical investigations were conducted using a finite element software, ABAQUS.

In the experimental phase, a load test was conducted to verify the strength gained by two, two-way slabs, and the results were compared. Load-deflection relationships, load-strain relationships, and ultimate load capacity were additionally obtained from the experiment. The numerical model which was developed using the software also included a variation of strength and performance with respect to a change in aspect ratio for the slabs using finite element analysis (FEA). The objectives of the experimental investigation are summarized below:

1. To investigate the effectiveness and performance of using PS-CFRP and R-CFRP for flexural strengthening of two-way slabs.
2. To optimize the strengthening technique by conducting experimental investigation and numerical modelling.
3. To study the behavior of strengthening material so that the technique can assist in reasonable improvement in the load-carrying capacity of two-way slabs.

4. To conduct parametric studies by changing the properties of the specimen using finite element software.

1.4 Organization of the Thesis

The thesis is divided into seven chapters, and each chapter is further subdivided into various topics to give an in-depth explanation. The outline and organization of the chapters include the following:

Chapter 2 – Literature Review

A background literature review is included in this chapter based upon previous experimental studies on the strengthening of two-way slabs using CFRPs, experimental procedures to test two-way slabs, properties of FRPs, and differences between PS-CFRP and R-CFRP.

Chapter 3 - Sample Preparation

The construction procedure of two full-scale, two-way slabs as well as a detailed description of properties of CFRPs used for strengthening and a process of application of CFRPs are presented in this chapter.

Chapter 4 - Test-Setup and Instrumentation

The instruments used for testing, construction of test set-up, and load-test are described in this chapter.

Chapter 5 - Experimental Results

The results of observation from experimental tests are presented in this chapter. Ultimate load capacity, crack patterns, load-deflection curves, and load-strain curves of PS-CFRP and R-CFRP are presented and compared.

Chapter 6 – Numerical Modelling

This chapter represents the numerical modelling of slab strengthening with CFRP based on a previously conducted study. Material behavior and modelling methodology is also discussed in detail. A numerical model is then calibrated with test results to validate the model.

Chapter 7 – Parametric Study

This chapter presents the results and discussions of each parameter variation that influences the response of slab strengthen with CFRPs.

Chapter 8 – Conclusion and Recommendations

The summary of findings and conclusions from the numerical and experimental study are presented. Lastly, recommendations for further research are discussed.

Chapter 2
Literature Review

2.1 Introduction

The slab is a basic component of a building and is used to construct floors. It is generally constructed using reinforced concrete. The ratio of width and length of the slab to the height is relatively large compared to other parts of a structure, and the thickness is small. Slabs are divided into various categories based upon their shape and support conditions. In addition, slabs can be solid, ribbed, or waffled. Lastly, depending on the load transfer mechanism, slabs are classified as one-way or two-way.

2.1.1 Types of Slabs

A one-way slab is supported on two sides by parallel walls or beams, and/or has a length to breadth ratio greater than or equal to two. Moreover, a one-way slab bends only in one direction (spanning direction) and transfers loads to the walls or beams. Conversely, two-way slabs are generally supported on all four sides by walls or beams. The length to breadth ratio of two-way slabs is less than two, and they bend in both directions while transferring the loads to the walls or beams (Fig. 2.1). Additionally, slabs can be either simply supported or continuously supported (Gharpedia, 2018).

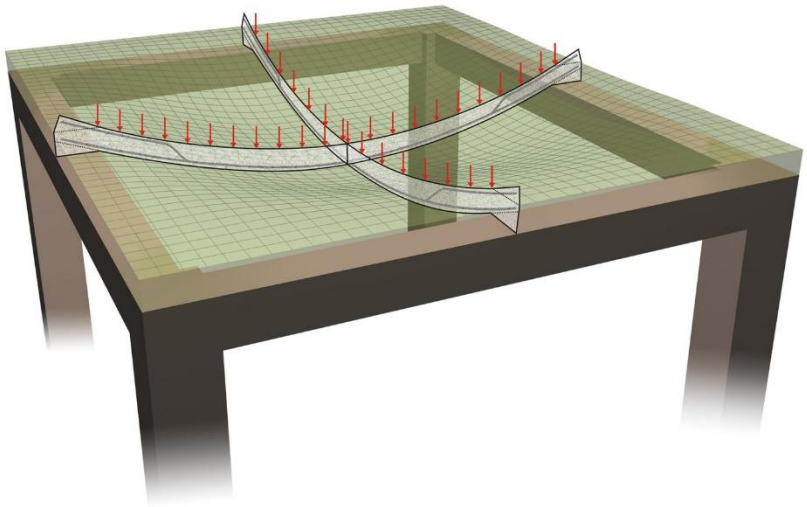

Fig 2.1: Deflection of two-way slabs

2.1.2 Two-way Slabs

The RC two-way slab system is a popular structural system. This system has contributed to the development of RC as a construction material since the construction of the first two-way slab in 1906 in U.S. by Turner (Sozen & Seiss, 1963). In the same year, Maillart of Europe built a two-way slab system in Switzerland. Since these structures were built in 1906, a considerable amount of research has been conducted to investigate the behavior of RC two-way slabs (Ebead, 2002).

The flexural behavior of a two-way slab is comparatively less investigated than punching shear behavior, possibly because of the overly ductile behavior until failure occurs. However, deflection in slabs can cause damage to nonstructural components, such as partitions, ceiling decorations, and doors, although the slab itself may still be able to sufficiently carry more loads.

Therefore, further research is necessary to understand the effects of flexural failure in two-way slabs (Kim et al., 2008).

2.2 Flexural Failure

Structural elements, such as beams and slabs, are susceptible to flexural failure. In general, concrete is strong in compression but weak in tension. Therefore, concrete cracks under tensile forces can cause several issues within the structural system. Cracks indicate concrete's response to applied load in both compression and tension. Furthermore, temperature and shrinkage effects may cause more cracks to develop in the concrete member. Highly apparent cracks can also destroy the aesthetics of the structure and will cause a significant reduction in flexure stiffness of the structural member (Mohamed, 2007).

Flexural tension failure initiates the yielding of steel reinforcement, followed by crushing of concrete on the compression side. The signs of this type of failure include the development of cracks at the tension side of the slabs, which further extend to the compression side. Furthermore, excessive deflection is another sign of flexural tension failure. Fig 2.2 depicts the failure pattern of two-way slabs. Failure of two-way slabs may occur in the form of flexural failure, punching-shear failure, or a combination of both failure modes (Ebead, 2006). When the flexural reinforcement ratio is relatively low, the modes of failure of the slab become unclear as the slabs may first fail in flexure before punching failure can occur (Chanthabouala et al., 2015).

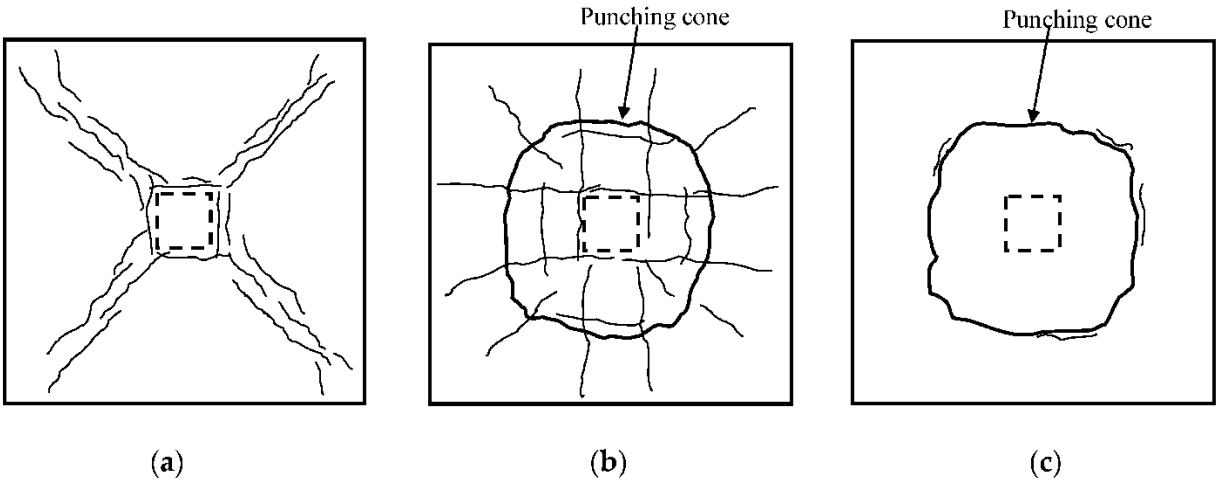

Fig 2.2: Typical cracking patterns on the tension surface of the slab: (a) Flexural failure; (b) Punching shear failure of slabs (c) Punching shear failure of retrofitted slabs (Chen et al., 2020)

The long-term effects of deterioration and other forms of damage on two-way slabs can lead to flexural cracking and reduction in the strength. Cracks may additionally expose rebars to the environment, causing corrosion of steel. Additionally, to protect the structural members from these effects, cracks should be minimized to acceptable limits under normal service loads. The random spread of cracks, moreover, significantly influences the flexural stiffness of the slab, and investigation of the crack propagation is challenging due to the transmission of loads in both directions. As a result, various retrofitting techniques have been introduced after extensive research (Sudha et al., 2017). However, each technique has potential disadvantages. As a result, additional research needs to be conducted to give insight into new techniques for strengthening two-way slabs.

2.3 Need for Retrofitting

The two options available when a RC structure is unable to meet the coding standards are replacement of the entire system or external retrofitting. Replacing the entire system is usually very costly; hence, retrofitting methods are used in structures to accommodate increased loads or

changes in the structural usage. Therefore, the need for localized reinforcement in areas of weakness has increased. Furthermore, structural strengthening may become necessary due to wear and deterioration arising from normal usage or environmental factors (ECT Team, Purdue, 2007).

To maintain structural well-being, concrete structures need to be strengthened for several reasons. Some of these include the following (ECT team, Purdue, 2007):

- Overtime, due to factors such as higher live loads, increased vehicular loads, and installations of heavy machinery, the load bearing capacity of structures may become insufficient to carry the required loads.
- To account for damage to structural parts due to aging construction materials, fire damage, corrosion of the steel reinforcement, or vehicular impact.
- To modify a building's structural system due to the elimination of structural framing elements, inclusive of walls/columns or openings need to be cut through slabs for additional mechanical, electrical and plumbing requirements.
- To accommodate any errors in the design or construction phases.

2.4 Retrofitting Options

In order to regain the strength of deteriorated structural concrete elements and prevent further distress in concrete, RC structural members are often retrofitted (TheConstructor, n.d.). There are several techniques for retrofitting structural members, such as section enlargement, external plate bonding, external post-tensioning, and FRP strengthening. There are also various retrofitting options available for structural-related problems, but the selected solution depends on an economic evaluation (Sudha et al., 2017). In this current study, the various types of retrofitting options are discussed in detail. For example, Sudha et al. (2017) studied retrofitting of RC

structural elements and collected information about the following techniques: concrete replacement, concrete jacketing, steel retrofitting, and FRP.

To begin with, concrete replacement can be used to restore the strength and ductility of reinforced concrete and is one of the most feasible and economical techniques available (Fiorato et al., 1983). In this technique, the damaged concrete is removed and then replaced with fresh concrete. Repair practices using this technique requires attaching external formwork and scaffolding to the structures. However, when using this technique, if a building is functional, concrete replacement can create a disturbance and make the building inaccessible (Sudha et al., 2017).

Concrete jacketing is another technique used where the structure is externally retrofitted by adding reinforcement and concrete to the existing structure. Therefore, the dimension of the structure is increased along with strength (Fiorato et al., 1983). Fiorato et al. tested two RC structures using this technique and concluded that initial stiffness of the structure was not restored. Additionally, when using concrete jacketing techniques, the foundations of some structures are not designed to carry the additional load, which can lead to damage within the structure.

Steel retrofitting is also a frequently used technique. In fact, teel is the most common material used by the construction industry. Steel plates can be directly installed externally on the structure. Adding steel material to concrete mixes increases the ductility and strength of the structure (Ghobarah & Elfath, 2001). As compared to concrete jacketing, the light weight of steel elements serves as an advantage. The major disadvantages of using this technique included corrosion of steel, handling of excessively large steel material, and of the need for scaffolding (Sudha et al., 2017).

To improve steel retrofitting, another method was introduced in which the steel sections were installed only at the required structural area. The plates were only added at the plastic hinge height without affecting the original properties of the structure. U-shaped external confining steel plates has been widely used with epoxy or prestressing to increase the ductility and strength. This method has also been used to enhance the seismic behavior of the structures (Elnashai & Pinho, 1997).

Another method of steel retrofitting is steel bracing. This technique is used to retrofit frame structures. It helps in improving the strength and ductility provided that the steel connections are appropriately designed. Steel bracing also enhances the seismic behavior. Also, vertical steel strips should be added to cross-bracings to counteract the additional vertical compression-tension forces in the diagonal parts (Taghdi et al., 2000). Even with all these techniques available, steel is susceptible to corrosion with time (Sudha et al., 2017). Therefore, FRP strengthening techniques have been explored, and has the potential of being a sustainable technique to strengthen structures.

The use of FRP strengthening is growing rapidly among the construction industry, especially in structural engineering fields. FRP materials are high strength, non-corrosive, and light weight. These factors give this material an upper hand compared to other materials used for retrofitting of structures (Sudha et al., 2017). Because of FRP's advantages, there is a potential increase in the application for recent and older concrete structures. Moreover, FRP has become the most commonly used retrofitting option used worldwide. It provides high strength, high modulus of elasticity, and outstanding fatigue resistance. It is also the most lightweight external strengthening and non-corrosive material that requires minimal preparation of laminates, and it is additionally alkali resistant. To utilize FRP retrofitting practices adequately, several guidelines and journals have been published, such as the American Concrete Institute (ACI) 440.2R.17 guidelines

(Pandey et al., 2018). However, one of the major drawbacks of FRPs is their susceptibility to delamination, which can reduce their strength.

2.5 FRP Composite Materials

FRP composites consist of high-strength fiber embedded in a matrix of polymer resins as shown in Fig: 2.3.

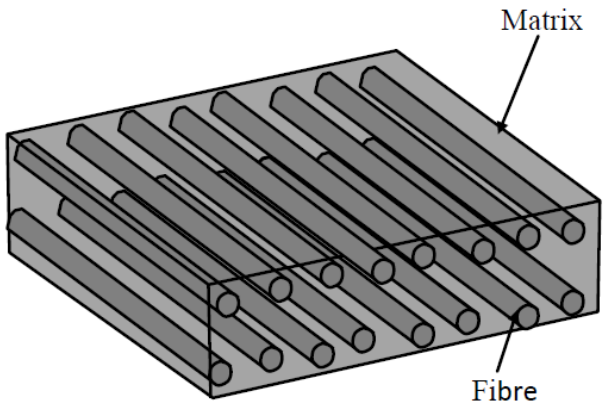

Fig 2.3: A schematic diagram showing a unidirectional FRP plate (Obaidat, 2011)

FRP composite is a system where fibers carry the load and give stiffness to the composite while the resin acts as a protective element to distribute the load evenly among the composite. In addition, FRP materials have high strength and stiffness, but when the load is applied on the composite, the strain in the fiber is much lower than that of composite.

Typically, fiber is made up of three materials: carbon, glass, and aramid. Carbon fiber is the most extensively used due to its mechanical properties. It is the most durable and inexpensive fiber. In contrast, glass fiber has a lower strength, but it is more economical than carbon. Lastly, aramid fiber contains intermediate strength properties (between glass and carbon).

The elastic behavior of fiber is linear, unlike steel which shows an elastoplastic behavior after yielding. Fig 2.4 shows the stress and strain curve for the composite, fiber, and matrix. Before yielding, the composite shows the same behavior, but after yielding (knee point) the matrix does not contribute to stiffness (Obaidat, 2011; Piggot, 2002).

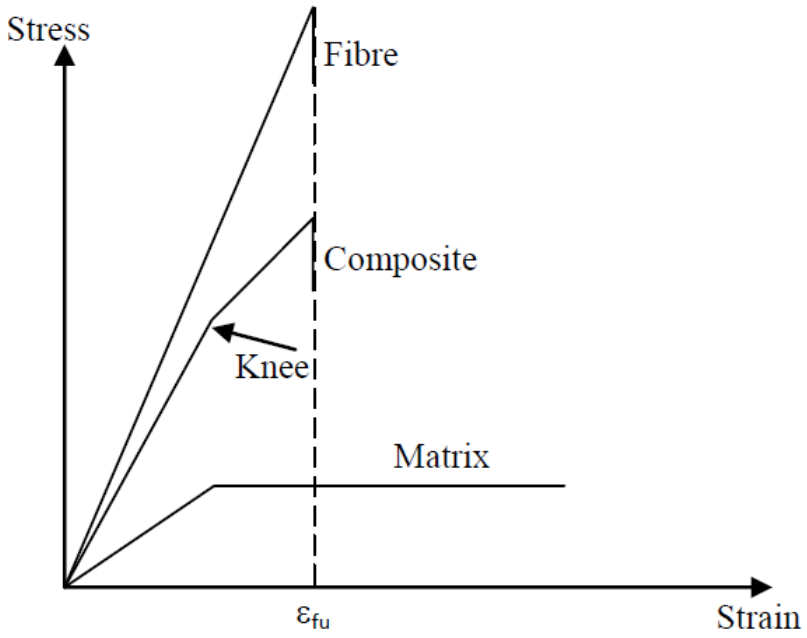

Fig 2.4: Stress vs Strain curve for fiber, resin and FRP composite (Obaidat, 2011; Piggot, 2002).

The mechanical properties of the composite depend upon the fiber properties, matrix properties, orientation of the fiber, and the amount of fiber. The direction of the fiber also plays an important role in the strengthening of the structure. The fiber provides the strength and stiffness to the composite; hence, the composite is an isotropic in the direction of the fiber. Furthermore, a composite with all fibers in one direction is known as unidirectional fiber, but if the fibers are divided into two or more directions, they are known as bi-directional and multi-directional, respectively. Fig 2.3 depicts the layout of a unidirectional fiber. To strengthen the RC structures,

unidirectional fibers are the most widely used (Obaidat, 2011). Table 2.1 shows the typical mechanical properties of the materials used for retrofitting of structures.

Table 2.1: Properties of material used for retrofitting (Obaidat, 2011; Piggot, 2002).

Material	Tensile strength, psi (MPa)	Modulus of elasticity, ksi (GPa)	Density lb/ft^3 (kg/m^3)
Carbon	319083- 812211 (2200-5600)	34809- 120381 (240-830)	112-137 (1800-2200)
Aramid	348090- 522135 (2400-3600)	18854- 23206 (130-160)	87-93 (1400-1500)
Glass	493128- 696181 (3400-4800)	10152- 130679 (70-901)	137-156 (2200-2500)
Epoxy	8702 (60)	362.594 (2.5)	68-87 (1100-1400)
CFRP	217556- 536639 (1500-3700)	23206- 78320 (160-540)	87-106 (1400-1700)
Steel	40610- 275571 (280-1900)	27557- 30457 (190-210)	493 (7900)

2.5.1 Types of Carbon Fiber Reinforced Polymer (CFRP)

Carbon fiber fabrics are high-strength materials that are bonded to structures for strengthening purposes. Manufacturers produce CFRP sheets for concrete application in two forms: regular and pre-saturated. Additionally, the process of application of these fabrics is in four forms: wet layup systems, prepreg systems (pre-saturated), precured systems, and near-surface-mounted systems (ACI Committee 440R, 2017). R-CFRP fabrics are mounted as wet lay-up laminates in which an adequate layer of saturant is spread uniformly on all areas where the CFRP laminate sheet is to be placed. The layer of CFRP laminate sheet is cut to designed lengths and pressed down with a “bubble roller” to eliminate the trapped air and impregnate the laminate sheet with saturant. A second layer of saturant is reapplied to make sure that the CFRP laminate sheet is fully impregnated prior to cure (Tan et al., 2003).

PS-CFRP is a recent invention whereby the CFRP fabric is pre-impregnated with epoxy resin and is sealed in a plastic bag by the manufacturer. It is moistened and cured using polyurethane resin saturant (White, 2018). Once the bag is opened, and the material is exposed to the atmosphere, the moisture activates the epoxy, and the FRP can be conveniently applied to the epoxied concrete surface in a specified timeframe (Yazdani et al., 2020). This saves time and costs over the field application of epoxy resin. Moreover, PS-CFRP has been used successfully in several other industries, such as aerospace and wind energy since the 1970's. Furthermore, it is also important to note that installation of PS-CFRP is possible in wet or submerged conditions (White, 2018).

Fig 2.5: Application of pre-saturated CFRP on RFK bridge (Triborough bridge), NYC (White, 2018)

2.5.2 Bond between FRP and Concrete

Adhesives are used for the bond between concrete and FRP. The most common types of adhesives available in the market are epoxy, acrylics, and urethanes. Epoxies provide high bond strength and temperature resistance; hence, they are widely used in the construction industry as a bonding agent for FRP to concrete. However, acrylics provide moderate temperature resistance but rapid curing. Therefore, bonding of R-CFRP with concrete is conducted using epoxies. Moisture-cured polyurethane resin saturant is used in PS-CFRP (White, 2018) while moisture-cured urethane is used in high humidity and submerged conditions. Damp or wet concrete repairs are possible using this adhesive (Obaidat, 2011). Although the aforementioned adhesives aid in providing a bond between the FRP laminate and concrete, bond failure may still occur.

Bond failure implies loss of composite action between concrete and FRP laminate. This type of failure is often referred to as debonding or delamination of CFRP. The FRP-concrete interface is usually considered to be a more superior bond (Lundqvist et al., 2005; Supaviriyakit et al., 2004). However, it is important to consider the compliance of the bond between FRP and concrete. Consequently, most research indicate that debonding of FRP is the dominating type of failure (Neale et al., 2005).

2.5.3 Failure Modes

A significant amount of previous research and experimentation have reported the common modes of failure of RC members externally strengthened with FRP (Esfahani et al., 2007; Mofidi et al., 2013; Toutanji et al., 2006,). From this observation, the failure modes can be classified into three main categories (Esfahani et al., 2007, Obaidat, 2011). In the first failure mode, the bond between concrete and FRP is not affected. The steel yields are first followed by FRP rupture as shown in Fig 2.6 (a). The second type of failure is caused due to failure in concrete. The concrete

crushes before or after yielding of steel, and the CFRP is unaffected as shown in Fig 2.6 (b) or due to shear crack at the end of the plate, as shown in Fig 2.6 (c). The third type of failure is the most recognized failure and is caused by debonding. In this type of failure, there is complete loss of composite action. The FRP laminates do not contribute to stresses in the steel, thereby leading to brittle failure. Fig 2.6 (d) shows the debonding of FRP. The failure starts at the end due to stress concentration, and then it move inwards. Usually, the cause of this failure is due to shear stresses, but sometimes failure is also caused by normal stresses due to non-zero bending stiffness of the laminate. Fig 2.6 (e) depicts a type of failure where the entire FRP along with the concrete cover is separated from the concrete surface. This failure is caused by the concentration of interfacial shear and normal stresses at or near the end of beam. Due to an increase in loading on the beam, one crack propagates from one end towards the other end of tensile reinforcement. The crack then moves horizontally along the bottom tensile reinforcement. Conversely, the failure depicted in Fig 2.6 (f) and Fig 2.6 (g) is caused by a high concentration of interfacial shear and normal stresses along the beam. As a result, cracks propagate in the concrete parallel to the bonded plate and adjacent to the adhesive to the concrete interface (Obaidat, 2011). In summary, there are various modes of failure which can be exhibited by FRP laminates, however, debonding failure has shown to be the most prevalent.

Studying the various types of failure modes assists in developing various techniques to mitigate the problem. Techniques such as prestressing of CFRP laminates, near surface mounting, and usage of anchors to secure the FRP have emerged in the construction industry (Tan et al., 2003).

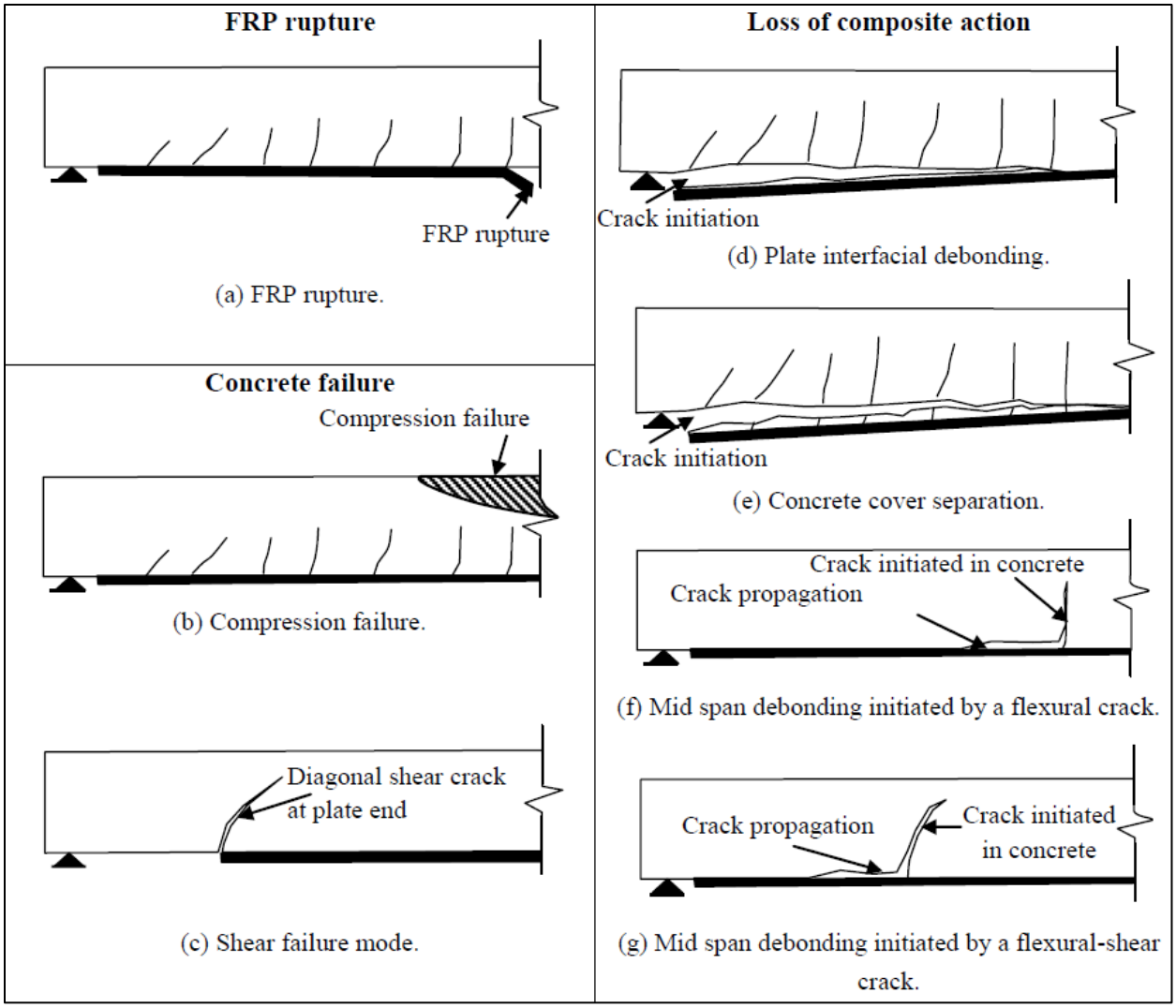

Fig 2.6: Failure modes of beam retrofitted using FRP laminates (Obaidat, 2011)

2.6 Flexure Strengthening of RC Slabs Using FRP

CFRP strengthening has been widely used in the application for retrofitting old structures for many structural engineering projects. Previous research has shown the increase in strength for columns, beams, and one-way slabs (Fathelbab et al., 2014). The flexural capacity of the concrete beam and one-way slabs increases after bonding of the CFRP laminates on the tension side of the beams and slabs. However, CFRP laminates often undergo debonding.

Debonding of CFRP materials was the major drawback observed by past research. However, PS-CFRP application has shown advantages over R-CFRP for strengthening in terms of debonding for beams and columns (Yazdani et al., 2020). Continuous research has assisted in the evolution of CFRP, and its ease of handling has led to extensive application in the structural engineering field. Some of the most important contributions are highlighted in this section (Ebead, 2002; Tan et al., 2003).

Mosallam and Mosalam (2003) conducted an experimental and numerical investigation to evaluate the ultimate response of unreinforced and reinforced two-way slab strengthening using FRPs. The researchers strengthened the specimen using CFRP and GFRP strips. They found that the FRP system increased the ultimate load-carrying capacity by 500% for unreinforced slabs and 200% for reinforced slabs. They observed that the main failure mode was due to the crushing of concrete with some localized debonding of FRP composites. Mosallam and Mosalam used finite element method for comparison between experimental and numerical results, and they found a positive correlation between the two. The results from the research conducted by Mosallam and Mosalam showed that CFRP was effective for flexural strengthening of reinforced and unreinforced two-way concrete slabs. To further evaluate the flexural strength of two-way slabs using CFRP, an experiment conducted by Limam et al. (2003) was reviewed.

Limam et al. conducted load tests on flexural strengthening two-way slabs using CFRP strips. They externally bonded the CFRP strips on the tension side of the slab. The researchers concluded that CFRP plates can be efficiently used for strengthening of two-way slabs. During the test, Limam et al. concluded that the failure of slabs occurred due to early debonding of CFRP strips, as shown in Fig 2.9. Furthermore, the non-strengthened slab showed more ductility than the strengthened one. In summary, the study portrayed the behavior of RC slabs strengthened with

CFRP versus non-strengthened slabs when subject to applied loads. Limam et al.'s study also gave further insight on the prominence on failure modes of CFRPs, such as debonding. Since early debonding of CFRP and reduction in ductility were prominent issues from Limam et al.'s study, these topics were investigated through further research (Ebead and Marzouk, 2004).

Fig 2.7: Debonding failure of CFRP strengthened slab (Limam et al., 2003)

Ebead and Marzouk (2004) used CFRP and GFRP for flexural strengthening of two-way slabs and found a decrease in ductility for the FRP strengthened slab, and debonding failure of FRPs. To evaluate the flexural strength of two-way slabs, they tested slabs with a low reinforcement ratio of 0.35% and 0.5%. The specimens were tested as simply supported slab with monotonous concentrated loading at the center, and FRPs were bonded to the tension side, as shown in Fig 2.7. Ebead and Marzouk observed a 35.5% increase in the flexural strength of the FRP bonded specimen, as compared to the non-strengthened specimen. In addition, there was an increase in the initial stiffness for the strengthened specimen. However, the researchers also observed a 30% decrease in the values of energy absorption and a decrease in ductility due to

brittle nature of FRP materials. The failure of the slabs was caused by debonding of FRPs. To mitigate debonding issues, Vasquez and Kabrbhari (2003) suggested that FRP strips could be made more efficient by ensuring a slightly lower fiber content and better overall resin impregnation.

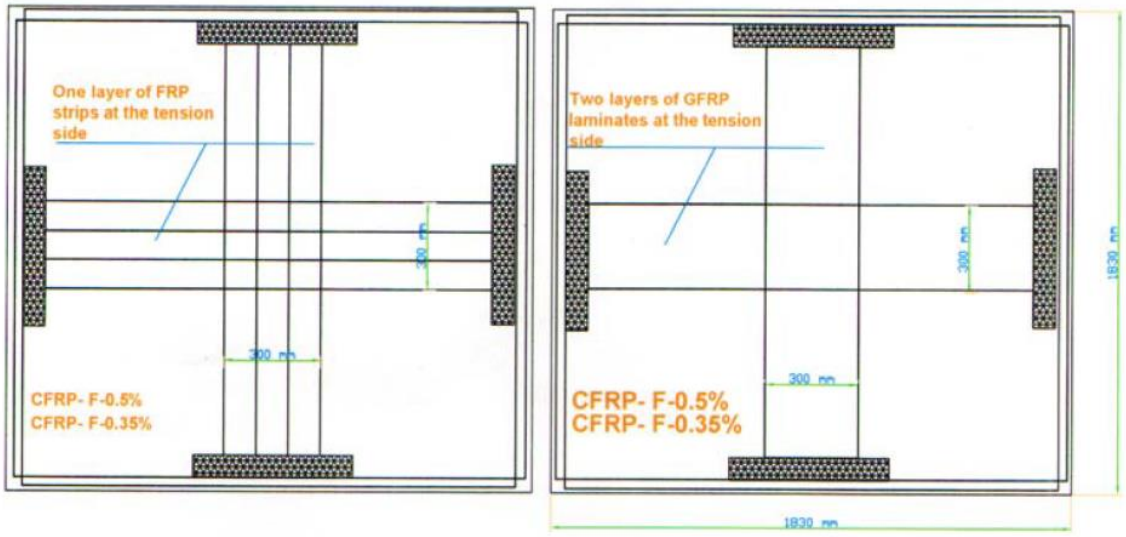

Fig 2.8: Layout of FRPs for flexural strengthening of slabs used by Ebead and Marzouk (2004)

So far, the effects of various types of FRPs were studied for flexural strengthening of two-way slabs. Furthermore, Chen et al. (2008) conducted one collective study on the CFRPs, GFRPs, and basalt fiber reinforced plastics and concluded that CFRP showed the best results as compared to other FRP materials for strengthening of two-way slabs. However, from previous research mentioned above, early debonding of CFRP was the prominent failure mode. Therefore, various methods/techniques of CFRP application were studied (Tan et al., 2003).

Tan et al. (2003) used various methods of CFRP application to strengthen RC slabs. The methods that the researchers used included: cold-cured adhesive bonding, prestressing, manual wet lay-up, and near surface mounting (NSM). All the specimens were tested up to failure. They

found that the flexural strength of the slabs was increased from 44% to 230% using various methods of CFRP application. Different modes of failure were observed after the test. CFRP delamination was observed in cold-cured adhesive bonding and manual wet lay-up, and CFRP rupture was observed in the prestressed CFRP and NSM system. Tan et al. also observed a substantial decrease in the deflection and crack-width using the CFRP. In summary, Tan et al.'s research showed that prestressing and NSM improves the effect of CFRP bonded to concrete.

Furthermore, Kim et al. (2008) tested four large-scale slabs to study the behavior of prestressed and non-prestressed CFRP sheets used for flexural strengthening. They found that there was an increase in the flexural strength of up to 25 % and 72% for non-prestressed and prestressed CFRP sheets, respectively. Kim et al. found that failure of the control slab was very ductile; conversely, a stepwise failure was observed in the strengthened slabs because of the delamination or partial rupture of the CFRP sheets. In comparison to the non-strengthened slab, the slab reinforced with prestressed CFRP sheets had almost the same ductility index. The slab with non-prestressed CFRP sheets, on the other hand, showed no significant improvement. Due to its premature failure, the ductility index of was very low, i.e., 44 percent. Kim et al.'s study was effective in showing that prestressing of CFRP is more effective than non-prestressed CFRP. Moreover, further experiments were studied to investigate the effects of various FRP strengthening techniques (Sorin et al, 2009).

Sorin et al. (2009) used NSM and externally bonded (EB) FRP to determine the effectiveness of strengthening RC two-way slabs (with and without cut-out) using FRP strips. They constructed four large full-scale slabs of dimensions 104 x 155 x 4.72 in. (2650 x 3950 x 120 mm) in which one was without cut-out, and three had different cut-out shapes. The slabs were simply supported along the perimeter and loaded at the center, as shown in Fig 2.8. The specimens were

first tested up to a certain load and then retrofitted using FRP strips. Thereafter, Sorin et al. used a combined strengthening mechanism of near-surface mounted FRP (NSM) and externally bonded FRP. Afterwards, the slabs were re-tested up to failure. The results obtained from the test revealed that the load-carrying capacity was significantly increased by 59.9%. The modes of failure for the FRP mechanism were due to rupture. The researchers also observed a high number of cracks for the retrofitted specimen as the structure gave enough warning signs before failure.

Fig 2.9: Test set-up (Sorin et al., 2009)

Furthermore, Yiyan et al. (2018) investigated two-way slab strengthening with a composite technique of orthogonally bonded CFRP strips and steel strips. They tested seven flat-slabs with a reinforcement ratio of 0.22% and concluded that experimental results indicate that strengthening RC two-way slabs with a CFRP-steel grid were effective in delaying concrete cracking and enhancing the load-carrying capacity when compared to only the CFRP grid. The researchers used the yield line method to analyze the strengthened slabs and found that the analytical model accurately predicts the load-carrying capacity of the strengthened slabs.

In summary, the various methods of slab flexural strengthening included prestressing of CFRPs, NSM, combined use of steel strips and CFRPs, and a combination of NSM and externally bonded CFRPs. These methods were effective in enhancing the load carrying capacity of CFRP strengthened slabs, however, there were some drawbacks. For example, NSM and prestressing techniques require a large labor force which can be costly (Ghaffary & Moustafa, 2020). Therefore, PS-CFRP was used for the current study. PS-CFRP requires reduced labor and has a fast installation time (White, 2018).

2.7 Flexure Strengthening using Pre-saturated CFRP (PSCFRP)

Currently, substantial research has not be conducted on using PS-CFRP for flexural strengthening of RC slabs. However, recently Yazdani et al. (2020) conducted a three-point bending test to determine the flexural strength of beam strengthening using PS-CFRP and R-CFRP. Additionally, they added different anchorage systems to strengthen the CFRPs and then compared the results. The researchers found that PS-CFRP without any anchors was more effective than R-CFRP in increasing the beam flexural capacity. Yazdani et al. also concluded that CFRP laminate application without any anchoring significantly increased the flexural capacity of concrete beam samples in the range of 62–78%. Additionally, PS-CFRP was found to be more effective than R-CFRP for flexural strengthening.

2.8 Cost-Benefit Analysis

After choosing the right material for retrofitting, the next step is to choose the proper application technique. Various factors can be considered when choosing the right material for retrofitting, but one of the crucial factors is the cost of application. Several methods are available

for the application of CFRP as discussed in the previous sections, which are summarized as follows.

EB techniques are the most popular for strengthening of RC slabs. In this technique, the CFRP is directly bonded to the surface of the slab using adhesives. The EB technique is commonly implemented using the wet-layup method in which the fiber is saturated on site. The major advantage of this method is there is no requirement of drilling the concrete surface or removing the concrete before application (Ghaffary & Moustafa, 2020). Therefore, this technique does not require significant labor or cost. However, early debonding of CFRP does not allow the full use of composite, therefore, to overcome this, research scientists are using various techniques.

NSM techniques are conducted by embedding the CFRP bars or strips in the concrete surface to improve the performance of RC structures (Ghaffary & Moustafa, 2020). The two major advantages of this technique are higher bond strength between concrete and CFRP and less material is used compared to EB. The higher bond strength is due to the CFRP being completely enclosed to the concrete surface. However, though less material helps with decreasing the cost, the increased cost for labor affects the material savings (Ghaffary & Moustafa, 2020). Additionally, extra time and efforts are required by the labor force for making the groves (Sobieck & Atadero, 2015).

Prestressing of the FRP is another technique that is used to increase the efficiency of CFRP. The materials used in both EB and NSM can be prestressed. The major advantages of prestressing are full use of composite, delaying crack formation and propagation, enhancing stiffness, and restoration of service level displacements (Ghaffary & Moustafa, 2020). However, despite all the advantages the design of the end anchorage system requires accurate and expensive analysis

(Ghaffary & Moustafa, 2020). Another disadvantage of this technique is added cost and installation.

Another technique to mitigate debonding of CFRP is the use of an anchorage system. A proper anchorage system will allow the use of CFRP composites even after debonding (Ghaffary & Moustafa, 2020). However, a major drawback for many anchorage systems is the cost and complexity of installation (Ghaffary & Moustafa, 2020).

Finally, several techniques have been suggested to reduce early debonding in CFRP, however, those techniques required large amounts of labor and cost. Therefore, PS-CFRP can be used to mitigate early debonding of CFRPs. PS-CFRP is installed as EB-CFRP in which the reinforced fabrics have already been pre-impregnated with the resin (White, 2018). Since the fibers are already saturated, this makes application of the PS-CFRP laminates faster, which allots to time savings. Hence, the major advantages of PS-CFRP are reduced labor and faster installation as compared to EB R-CFRP and other techniques previously mentioned.

2.9 Key-points from Literature Review

EB CFRP successfully increases the flexural capacity of two-way slabs. However, the major cause of failure observed was early debonding of CFRP which also led to reduction in ductility of RC slabs. To overcome this problem, different techniques were used, such as prestressing, CFRP-steel grid, and NSM. These techniques helped in utilizing the full capacity of CFRP, however, the techniques were costly, and required significant amounts of time and labor. Additionally, none of the above-mentioned research studies investigated flexural strengthening of two-way slabs using PS-CFRP. In fact, PS-CFRP has shown effective results for flexural strengthening of beams. Therefore, the primary objective of this study is to investigate the effects

of flexural strengthening of two-way slabs using PS-CFRP and R-CFRP experimentally and analytically.

Chapter 3
Sample Preparation

This chapter gives a detailed description of sample preparation for the experiment. It includes the properties of materials used, preparation of formwork, and CFRP application. The materials used include concrete, steel, R-CFRP and PS-CFRP.

The experiment was conducted on two-way slabs. Two identical RC slabs were cast on-site. Furthermore, to strengthen the flexural capacity of the slabs, they were externally retrofitted using CFRPs.

3.1 Materials

3.1.1 Concrete and Steel Reinforcement Properties

The concrete mix used to cast the slabs was designed to obtain compressive strength of 3000 psi (20.7 MPa) after 28 days. The concrete mix proportions used in the experimental program are listed in Table 3.1. Concrete cylinders were poured to evaluate the compressive strength of concrete after seven days and 28 days. The average compressive strength of concrete obtained after the cylinder tests are illustrated in Table 3.2.

Table 3.1: Mix proportions for concrete

Material	lb/ft^3 (kg/m^3)
Cement	12.5 (201)
Fly Ash	3.2 (51)
Water	8.8 (141)
Coarse aggregate	68.5 (1098)
Fine aggregate (Bristol sand)	13.3 (214)
Fine aggregate (Bridgeport sand)	40.0 (640)

Table 3.2: Average compressive strength of concrete cylinders

Days tested	Average compressive strength, psi (MPa)
7	1769 (12.19)
28	3254 (22.43)

ASTM A615 Grade 60 steel rebars with a yield strength of 60 ksi (414 MPa) were used as the flexural reinforcement. The properties of the rebar used for the reinforcement of the slabs are mentioned in Table 3.3.

Table 3.3: Properties of steel reinforcement rebars

Bar no.	Size, in	Diameter, in (mm)	Cross-sectional area, in^2 (mm^2)	Elongation %	Yield strength, psi (MPa)	Tensile strength, psi (MPa)
#4	1/2	0.5(12.7)	0.2(129)	9	60,000(420)	90,000(620)

3.1.2 Strengthening Material Properties

For strengthening the specimen, unidirectional CFRP laminates were used. PS-CFRP and R-CFRP were used to strengthen structural concrete slabs. The two CFRPs possess unique physical properties which are discussed in detail below.

3.1.2.1 Regular CFRP (R-CFRP)

R-CFRP is a high strength, unidirectional carbon fiber fabric. The material is field-laminated using Sikadur-330/Sikadur Hex-300 epoxy to form a CFRP (Sika, 2019). The dry fiber comes in a roll of 25 in. x 50 ft. (63.5 cm x 15.2 m); 25 in. x 300 ft. (63.5 cm x 91.4 m). The thickness of cured CFRP laminate is 0.04 in. (1.0 mm). The properties of R-CFRP material are listed in Table 3.4. In addition, the properties of the epoxy used to strengthen the slab are mentioned in Table 3.5.

Table 3.4: Properties of R-CFRP*

Nominal Ply Thickness	Tensile Strength (*fu*)	Tensile Modulus (*Ef*)	Tensile % Elongation (*εfu*)	Tensile Stiffness (*AfEf*)
0.04 in. (1.0 mm)	160.9 ksi (1,110 MPa)	10.39 msi (71.7 GPa)	1.45%	416 kips/in. width (74,289 kg/cm width)

*(Regular CFRP)

Table 3.5: Properties of epoxy adhesive used to strengthen CFRP laminates.

Flexural Strength	Modulus of Elasticity in Flexure	Tensile Strength	Elongation at Break
8,800 psi (60.6 MPa) (7 days)	5.06 x 105 psi (3,489 MPa) (7 days)	4,900 psi (33.8 MPa) (7 days)	1.2 % (7 days)

*(Sikadur-330)

3.1.2.2 Pre-saturated CFRP (PS-CFRP)

Pre-saturated dry fibers are unidirectional carbon fiber fabric pre-saturated used to form a CFRP (Sika, 2016). The fiber comes in a roll of 24 in. x 30 ft. (61 cm x 9.1 m). The laminates must be applied within two hours. after the foil is opened. The thickness of the laminates was 0.019 in. (0.48 mm). Properties of PS-CFRP are mentioned in table 3.6.

Table 3.6: Properties of PS-CFRP*

Nominal Ply Thickness	Tensile Strength (*fu*)	Tensile Modulus (*Ef*)	Tensile % Elongation (*εfu*)	Tensile Stiffness (*AfEf*)
0.019 in. (0.48 mm)	93,662 psi (645 MPa)	8,973,997 psi (61,873 MPa)	1.04	170.5 kips/in. width

*(Pre-saturated CFRP)

3.2 Preparation of the Specimen

To prepare the specimens used for this study, activities, such as formwork preparation and laying of reinforcing bars were conducted. To construct the specimens, plywood formwork was prepared to cast them as shown in Fig 3.1. The specimens had the same geometrical configurations. The dimension of the slabs was 48 in. x 28in. x 6in. Firstly, two formworks were prepared, and

the plywood formwork was prepared to obtain the following geometry as shown in Table 3.6. After, reinforcement was added to the formwork. A cover of 1.5 in. (38.1 mm) was added on all sides of the formwork.

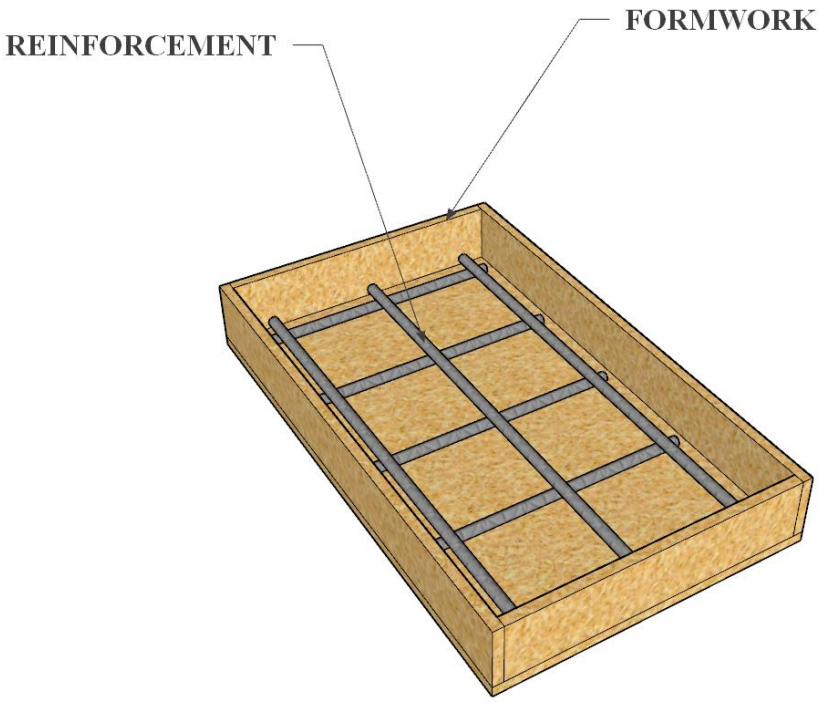

Fig 3.1: Plywood formwork with reinforcement

Table 3.6: Slab Geometry

Slab Dimensions	
	in(m)
Length	48(1.22)
Width	28(0.71)
Depth	6(0.15)

For flexular strenghtening of the slab, No. #4 rebar was used as the main tension reinforcement based on the minimum steel required for the specimen. Both of the slabs were lightly reinforced to have a low flexular capacity, simulating flexular deficient slabs similar to that of corroded steel or an increase in slab loading. Additionally, rebars were distributed at 10.875 in.,

center to center. The short-side rebars were placed below the long-side rebars. Steel wires were also used to tie the reinforcement to maintain the spacing between and the orientation of the rebars. The tension rebars had different lengths: the length along the long direction of the rebar was 45 inches (1.14 m), and the length of the short direction was 28 inches (0.72 m). The reinforcement rods were straight and not bent in any directions.

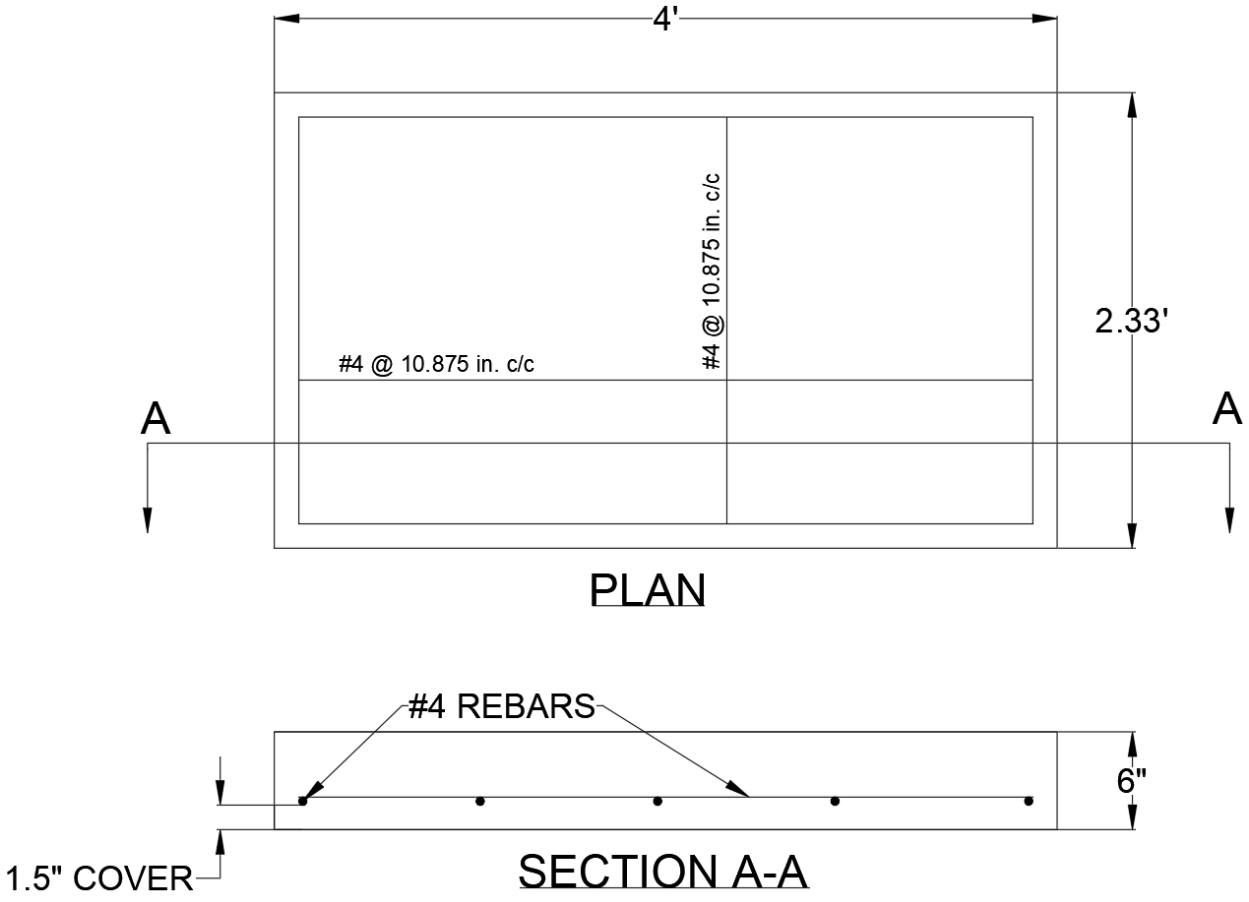

Fig 3.2: Detail drawing of slab reinforcement and dimension

3.3 Pouring of Concrete

The RC slab specimens were cast after the preparation of the formwork. The specimens were cast using a single batch of ready-mix concrete in the Civil Engineering laboratory (CELB) at the University of Texas Arlington (UTA). A slump test was conducted to calculate the workability of the concrete, and the slump of the concrete mix was 8 inches (200 mm). During the pour, the concrete was spread using shovels and consolidated using a vibrator as shown in Fig 3.3(c). After the completion of the casting, the slabs were sprayed with the curing compound to attain the targeted compressive strength of 3000 psi (20.7 MPa). The slabs were cured daily for 28 days, and a plastic sheet was laid over the slabs for curing. The process of casting of slabs is shown in Fig 3.3. Afterwards, the slabs were removed from the sheet and kept in ambient temperature for testing.

(a) (b)

(c) (d)

Fig 3.3: Casting of slabs: (a) Batch of ready-mix concrete (b) Specimen ready to cast (c) Casting of specimen (d) Application of curing compound on the specimen

Cylinders were cast along with the specimen per the ASTM standards (ASTM C39/39M (2017)) to calculate the compressive strength of the concrete ($f'c$) as shown in Fig 3.4. The standard size specimen used for compressive strength testing was a 4 x 12-inch (10.2 x 30.5 cm) cylinder.

Fig 3.4: Pouring of concrete cylinders

3.5 Application of CFRP on Concrete Surface

3.5.1 Sandblasting

To install the CFRPs, the concrete surface must be prepared. The surface must be clean and sound. According to the International Concrete Repair Institute (ICRI) as required by ACI 440.2R-17 code and manufacture specifications, the surface should be roughened to profile 3(CSP 3) to ensure bond-critical applications between CFRP and the concrete surface. The range of roughness is shown in Fig 3.5 (a). For this study, sandblasting was conducted on the slab to obtain the desired surface as shown in Fig 3.5 (b). The sand particles were blown using a blower.

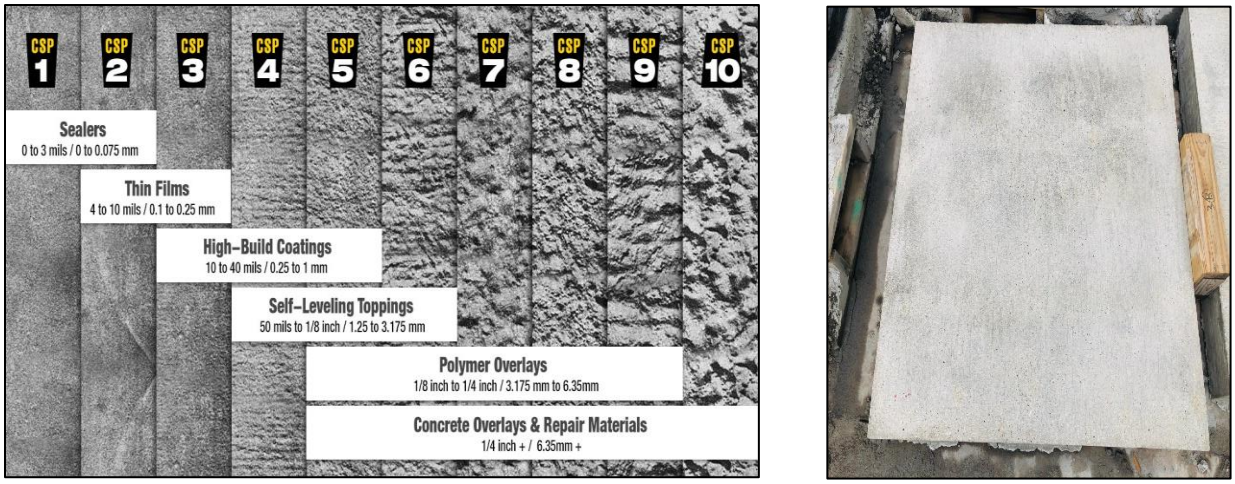

(a) (b)

Fig 3.5: (a) ICRI concrete surface profile levels (CSP) (b) Sand blasted concrete slab surface

3.5.2 Application of CFRP

Since the slabs were two-way, the CFRPs were applied in both directions (short span and long span) on the tension side. For application of CFRPs, the specimen was first marked with the location at which the CFRPs must be applied as shown in Fig 3.6 (a). The location to apply the CFRPs was selected based upon the previous research conducted by Ebead (2002) for flexural strengthening of slabs.

For the application of R-CFRP, Sikadur-31 was applied on the concrete surface to fill in the voids and was left to be cured. The R-CFRP was then cut according to the application area. Next, the epoxy adhesives were applied on both the concrete surface and the CFRP as shown in Fig 3.6 (b). After the application of CFRP, a steel roller was used to clear the air pockets between the CFRP and the concrete. The concrete slab, after application of CFRP is shown in Fig 3.6 (c)

For application of PS-CFRP, the package was open only at the time of application since the laminates must be applied within two hours of opening. Sikadur-31 was applied to the

specimen. PS-CFRP does not require application of epoxy, therefore, the PS-CFRP was directly applied on the surface of the slab.

(a) (b) (c)

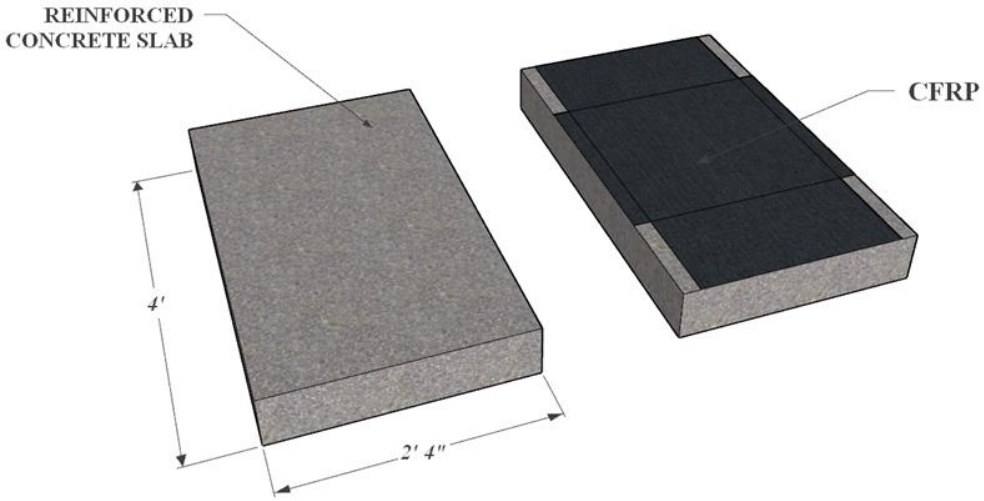

(d)

Fig 3.6: Application of CFRPs : (a) Marked locations for CFRP (b) Applying CFRP on the surface of the slab (c) Concrete slab strengthen with CFRP (d) 3-D representation of slab before and after CFRP application

Chapter 4
Test-Setup and Instrumentation

This chapter discusses the experimental test-setup and the instrumentation, including compression testing machine, supports, linear variable differential transformers (LVDTs), and strain gauge installation. The specimens were simply supported at the perimeter to obtain a two-way action and then subjected with monotonic loading until failure. The experiment explored the specimen subjected to a concentrated load applied at the center by using a compression testing machine. The results obtained from the test are analyzed in the next chapter. A 3-D representation of the test set-up constructed for conducting the experiment is shown in Fig 4.1.

According to ACI 318 (2019), to obtain the two-way action of the slabs, the long to short span ratio should be less than two. For this experiment, the test-setup was designed to ensure that this condition was satisfied. The support conditions for the slabs are shown in Fig 4.2. The rigid steel supports in the figure show that the slab is simply supported. The effective flexural span in the shorter direction was 20 inches (50.8 cm), and along the longer direction, it was 36 inches (91.44 cm.). The long span to short span ratio was $1.8 < 2$.

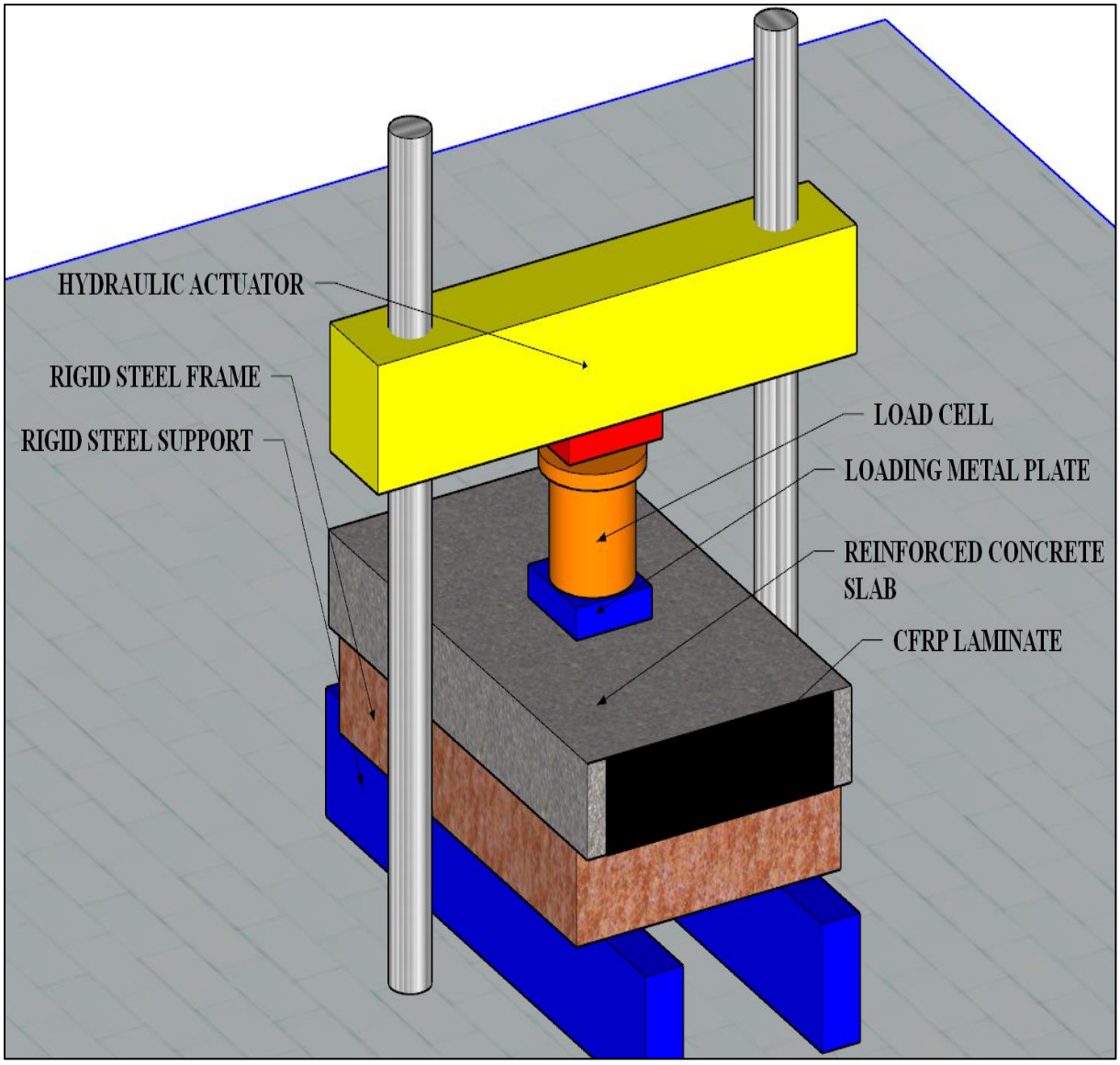

Fig 4.1: 3-D representation of the test set-up

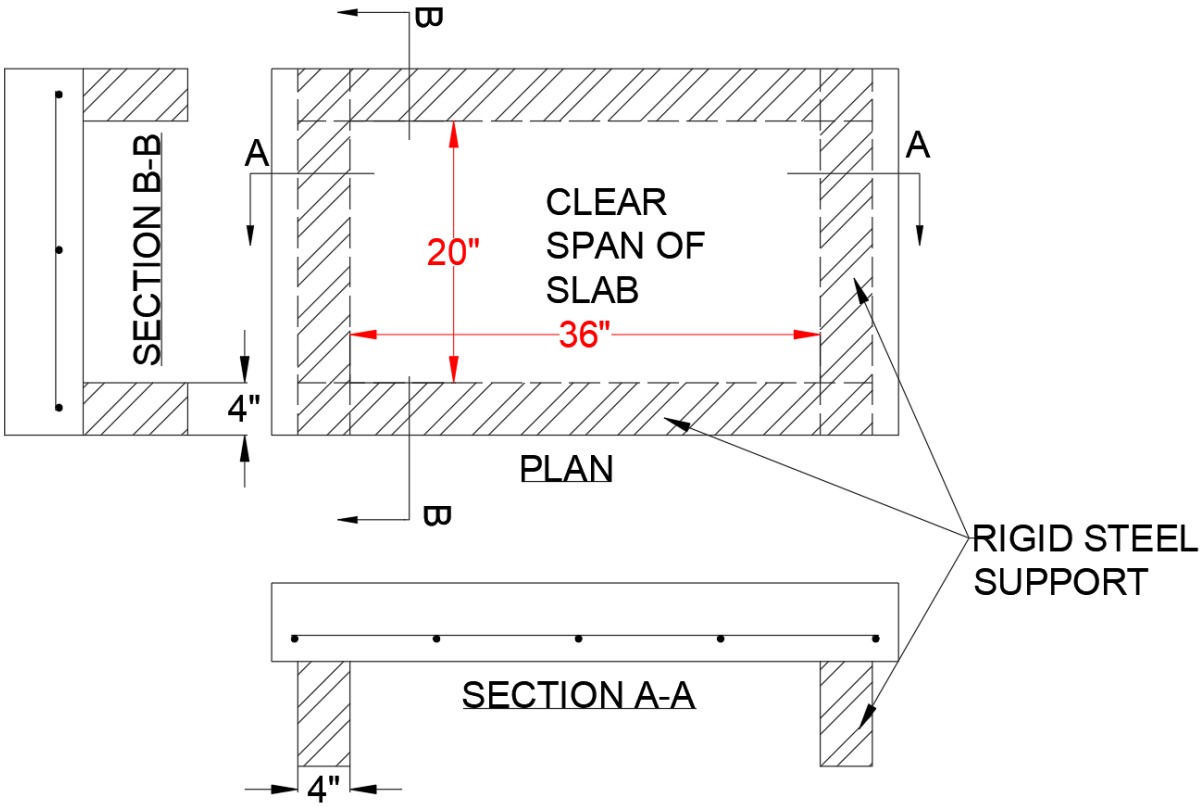

Fig 4.2: Support condition for the slab

4.1 Compression Testing Machine

A 400-kip (1779.29 kN) compression testing machine was used for testing the slabs. A central actuator is fixed in the machine and was used to directly apply the load onto the slabs. The machine was alsoconnected to the computer set-up to allow adjustments of the loading rate applied to the specimen. The computer was used to apply a concentrated load of 150 psi. The machine is shown in Fig 4.3. The machine is not equipped with a loading frame to test the slabs. Therefore, to test the specimen, a loading frame composed of four steel beams was constructed.

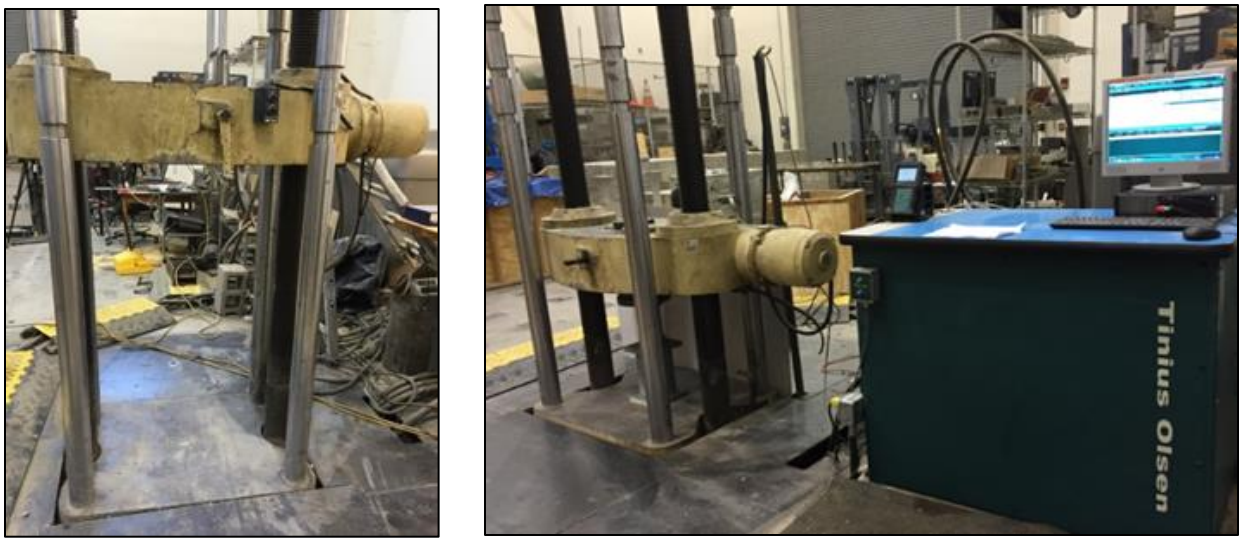

Fig 4.3: 400-kip compression testing machine

4.2 Loading Frame

To obtain a two-way simply supported action, a loading frame was developed comprised of rigid steel sections. The frame was constructed using four HSS sections which were first cut to the appropriate size and then welded together to obtain a box frame. Four HSS 8 x 4 x 5/16 were cut. There were two with a length of 36 inches along the long direction and two with a length of 28 inches along the short direction. Additionally, the dimensions of the frame were fixed according to the support conditions shown in Fig 4.1. High-strength steel sections were selected for the support, to ensure that there was no bending of the steel sections during the application of the load. To avoid movement of the frame during the application of load, these sections were welded using an electric welding machine.To increase the strength of the frame, external steel plates were welded at each corner as shown in Fig4.4 (c). The process of constructing the steel frames is shown in Fig 4.4.

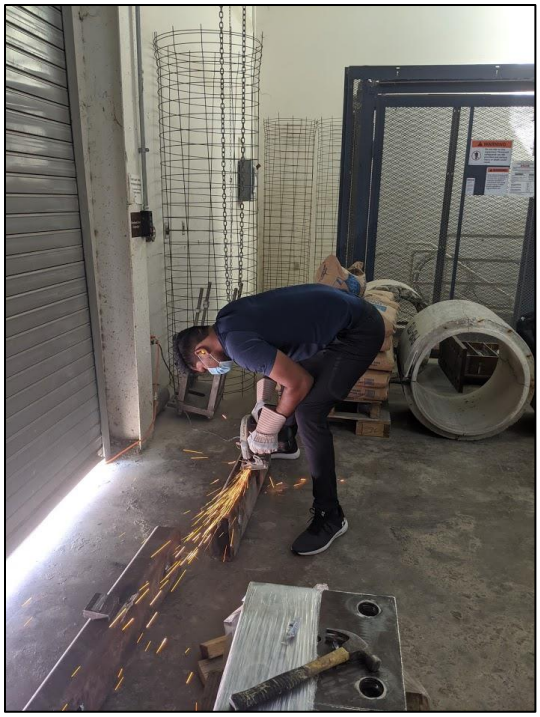

(a)

(b)

(c)

(d)

Fig 4.4: Loading frame (a) Cutting of HSS sections (b) Welding of steel sections together (c) Plate welding for increasing the strength (c) Completed box frame

4.3 Instrumentation

The strain and deflection of the specimens corresponding to the applied load were measured using strain gauges, LVDT, and a load cell. These instruments were then connected to a data acquisition box (DAQ). The data acquisition system was pre-installed with the software to obtain the results from LVDT, strain gauges and load cell. Afterwards, the results were transferred to the computer. The location of the strain gauges and LVDT is shown in Fig 4.5. The location of the instrumentation was determined to obtain accurate data.

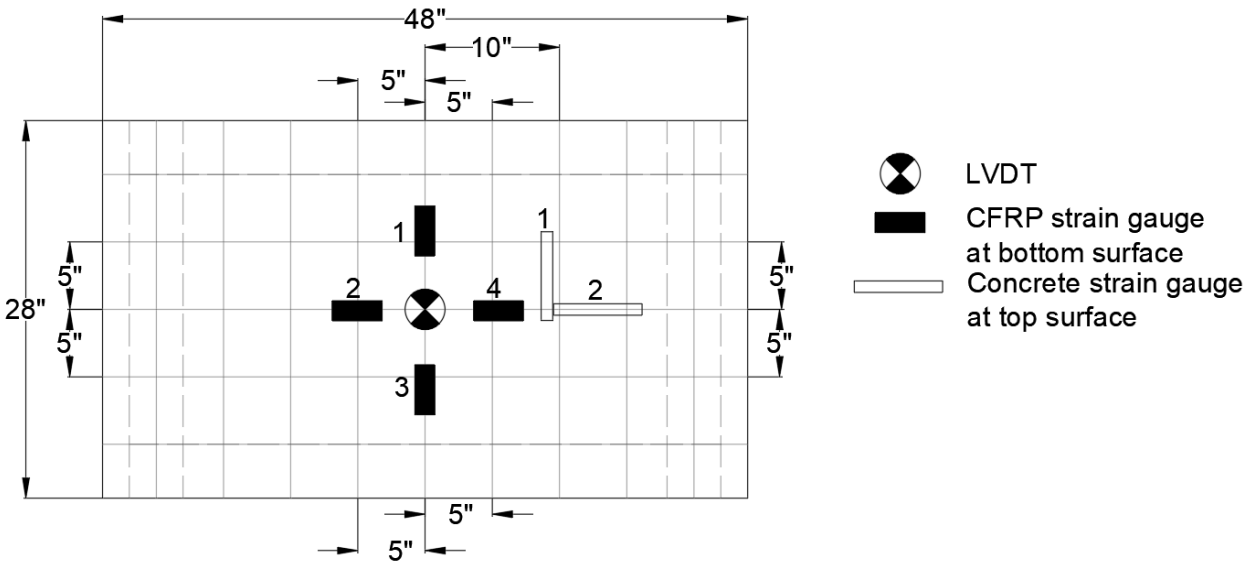

Fig 4.5: Instrumentation of the specimen

A total of twelve strain gauges were installed on the two slabs (six on each slab). Four strain gauges were installed on the CFRP surface on the tension side, and two were installed on the concrete surface on the compression side. The process of installation and the type of strain gauges were different for the concrete and CFRP surface.

For installation of strain gauges on CFRP, the CFRP surface was first cleaned using a blower to remove the dust particles. The location of installation of the strain gauges was marked on the slabs. Furthermore, the surface was abraded using an 80-grit sandpaper, and to further smoothen the surface, it was re-abraded using a 320-grit sandpaper as shown in Fig 4.6 (b). The surface was then visually inspected and was finally cleaned using acetone. The strain gauge with a gauge length of 5 mm (0.19 in.) was used to attach to CFRP since the strain in CFRP is small. These strain gauges were attached using CN adhesives and then covered using tape to protect them from damage.

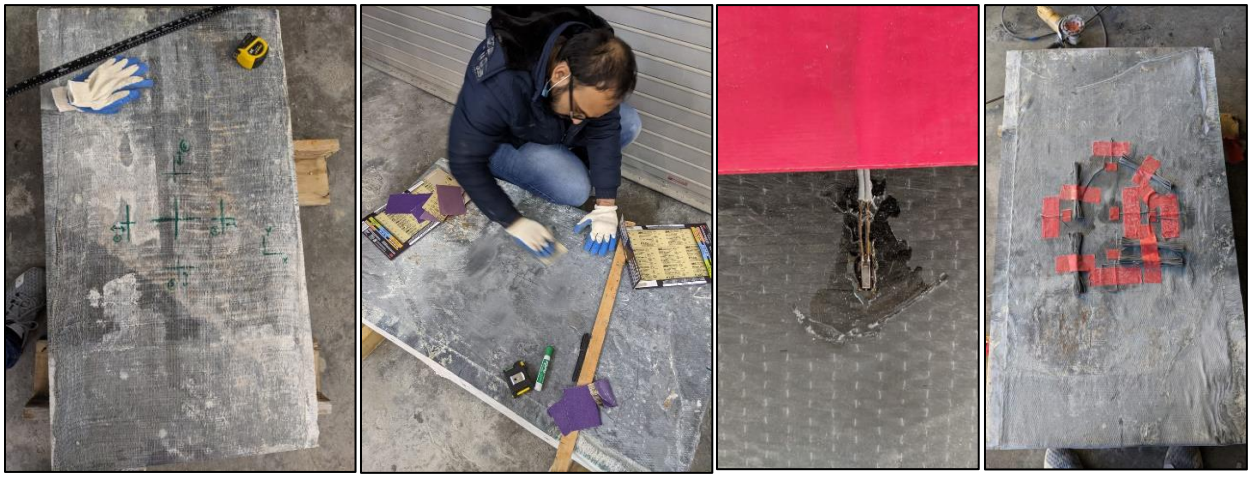

(a) (b) (c) (d)

Fig 4.6: Installation of CFRP strain gauges (a) Marking the location of strain gauge (b) abrasion of CFRP surface using sandpaper (c) CFRP strain gauge installed (d) Tape covering for protection purpose

For installation of the strain gauges on the concrete surface, a similar process to the installation of strain guages on the CFRP surface was undertaken. The concrete surface was grinded using a concrete grinder as shown in Fig 4.7 (a). The strain gauge with a gauge length of 60 mm (2.36 in.) was installed on the concrete surface as shown in Fig 4.7 (b). The concrete strain gauges were installed on the top surface to measure the compression strain.

(a) (b)

Fig 4.7: Installation of concrete strain gauges: (a) Grinding of concrete surface (b) concrete strain gauge installed

To measure the vertical deflection along with the application of the loads, LVDT and a load cell were used as shown in Fig 4.8 (a) and Fig 4.8 (b), respectively. The load cell was also used to measure the strain for the applied load.

All the instruments were then connected to the DAQ as shown in Fig 4.8 (c). The values of load, deflection, and strains in the form of analog electrical signals were converted through the DAQ to digital signals and were additionally saved in digital computer files.

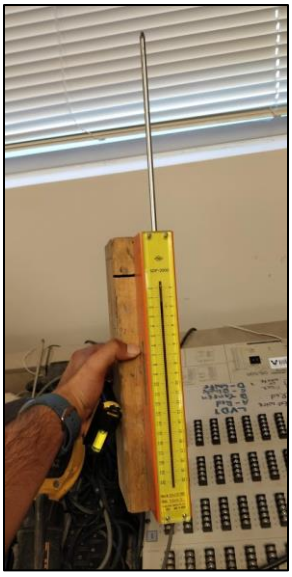

(a)

(b)

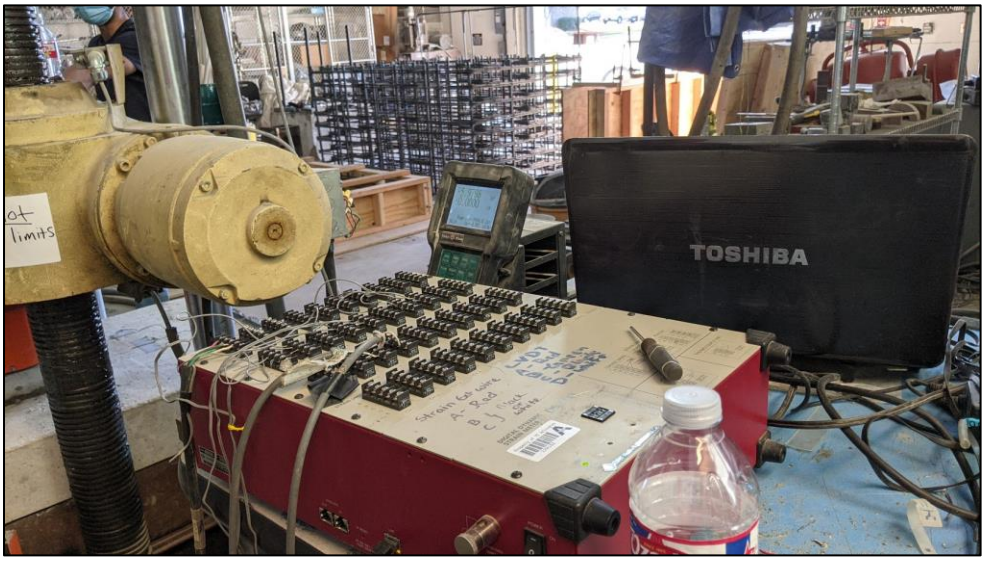

(c)

Fig 4.8: Instruments used during the test (a) linear variable differential transformer (LVDT) (b) load cell (c) Data acquisition box (DAQ)

4.4 Test Set-up

A crane was used to lift and install the specimen horizontally inside the loading frame during and after the test as shown in Fig 4.9 (a). The specimen was laid on the loading frame, which in turn was supported at the bottom using C-sections as shown in Fig 4.10. Geometrical

imperfections on the slab surface led to small gaps between the loading frame and the slab. These gaps were then filled using a grout made from Quick-Crete and water to ensure full compaction during the test. The top surface was levelled using the same process as shown in Fig 4.9 (c). Both the specimens were subjected to a monotonous central load of 150 psi which was applied through a metal plate that was 8 x 9 inches. (203.2 mm x 228.6 mm). The load was applied as an ultimate central failure load. Crack initiation, crack propagation, and CFRP debonding was continuously monitored during the test.

(a)

(b)

(c)

Fig 4.9: Specimen placement (a) A specimen carried using a crane (b) Filling the voids between specimen and support using a grout (c) Checking the level of metal plate for loading

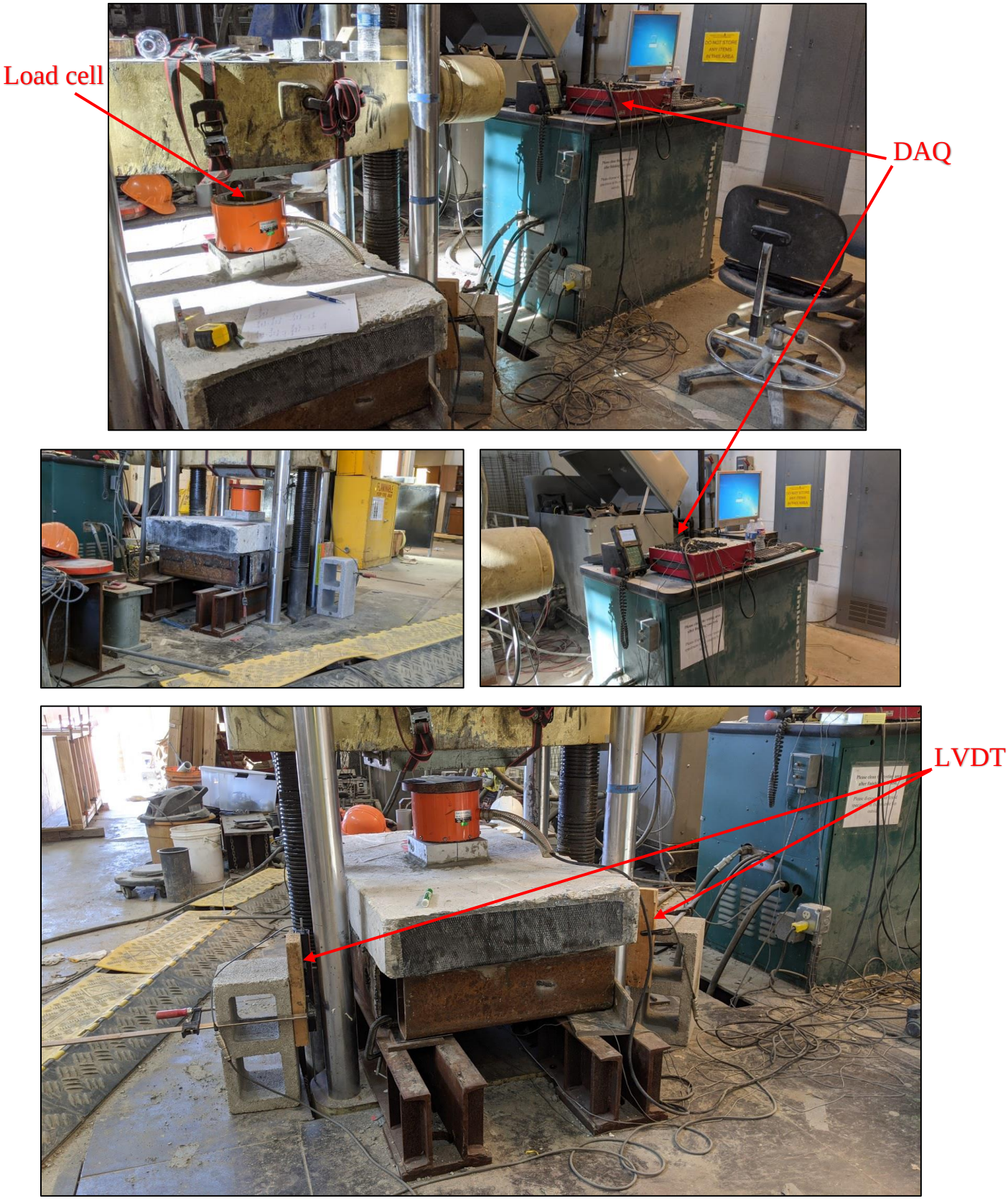

Fig 4.10: Final test set-up

Chapter 5
Experimental Results

This chapter discusses the results obtained from testing two slabs with PS-CFRP and R-CFRP. The performance behavior of these materials for flexural strengthening of two-way slabs is discussed in detail.

5.1 Compressive Strength Test

To determine the average compressive strength of the slabs, three cylinders were tested in accordance with ASTM C39/39M (2017). The cylinders were tested after the slab testing to obtain the exact compressive strength of the slabs during the time of testing. Three cylinders that were 4 inches (101.6 mm) in diameter and 8 inches (203.2 mm) in height were tested. To obtain optimum results, the cylinders were capped to avoid irregularities on the surface. A compressometer was attached to the cylinders to determine the strain for finite element modelling. The results obtained from the test are summarized in Table 5.1. A stress versus strain graph using the experimental results was also plotted as shown in Fig 5.2.

Fig 5.1: Concrete compressive testing of the cylinders

Table 5.1: Cylinder compression test results

Specimen No	Dimensions	Average stress, psi (MPa)
1.	4 in. (101.6 mm) x 8 in. (203.2 mm)	3254 (22.43)

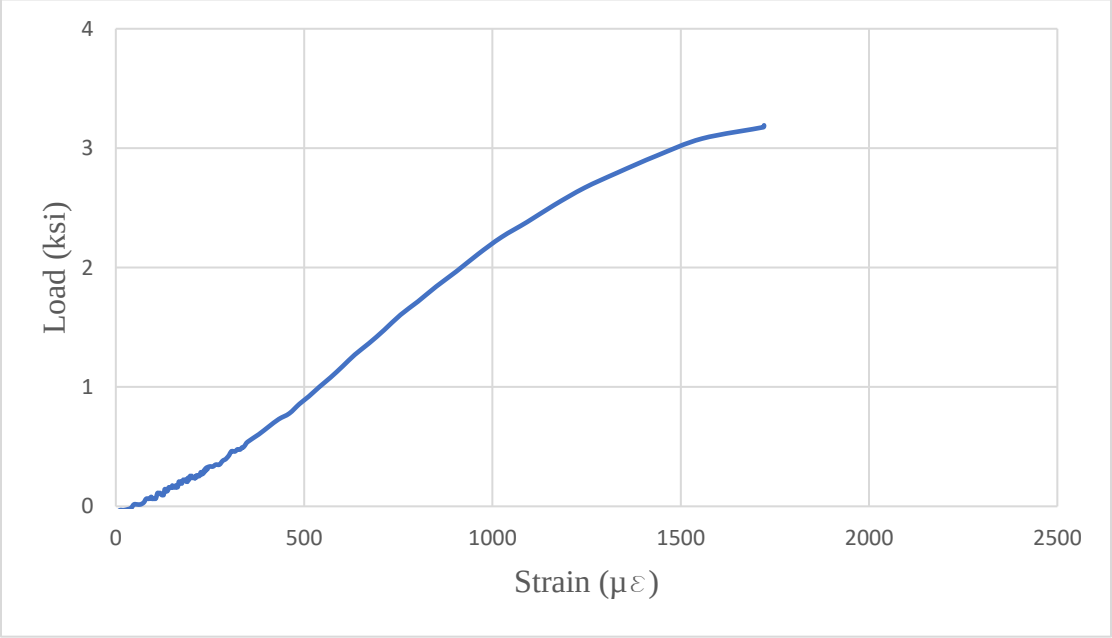

Fig 5.2: Stress versus strain graph for compressive cylinders

5.2 Test Results of the Specimens

The results are divided into two parts: R-CFRP and PS-CFRP. A complete description of crack, load-deflection, load-strain, ultimate loads, and failure characteristics are shown below.

5.2.1 Crack and Ultimate Loads

Cracks for each specimen were visually inspected and the load corresponding to it were recorded.

5.2.1.1 Pre-saturated CFRP Slab

Each slab was loaded until failure. The failure mode of the specimen was observed to be flexure. The first visible crack for this specimen appeared at 50 kip (222.41 kN) on the edge of the slab. The crack propagated from the bottom of the slab towards the top. This crack was observed to be close to the center of the long span as shown in Fig 5.3. Another crack appeared around the similar load (56 kip) on the other edge towards the end of the slab. This crack also followed the same pattern and propagated towards the top of the slab. Crack propagation and crack size were continuously increasing as the load on the specimen continued to increase. Since the bottom of the slab was bonded with CFRP, it was not possible to visually inspect the crack on the tension side. Lastly, the initial flexural cracks appeared under the loading area and propagated towards the edges of the slab as the slab was further loaded.

Before the ultimate failure of the specimen, multiple cracks were observed. These cracks propagated from the previous cracks and were seen moving upwards. Delamination of CFRP was observed before the ultimate failure as shown in Fig 5.4. The ultimate failure of the specimen was observed to be 81.56 kip (362.8 kN). Following delamination of CFRP, the failure was brittle, and sudden failure of the concrete was observed. Multiple diagonal cracks were observed on the top of

the slab moving from the center towards the end of the slabs and joining with the previous occurred cracks as depicted in Fig 5.5. The experiment concluded that the load-carrying capacity of the PS-CFRP specimen was increased by 1.14 times from the R-CFRP strengthen specimen.

To observe the mode of failure of the slab, the slab was lifted using a forklift. The data suggests that the cause of failure was delamination of CFRP followed by crushing of concrete. The CFRP was delaminated at various locations and stretched in the opposite directions of the fiber as shown in Fig 5.6. It can be concluded that excessive cracking in concrete caused delamination of CFRP.

(a)

(b)

Fig 5.3: First visible crack on the slab (a) Crack on the edge of slab (b) Zoomed view of the crack

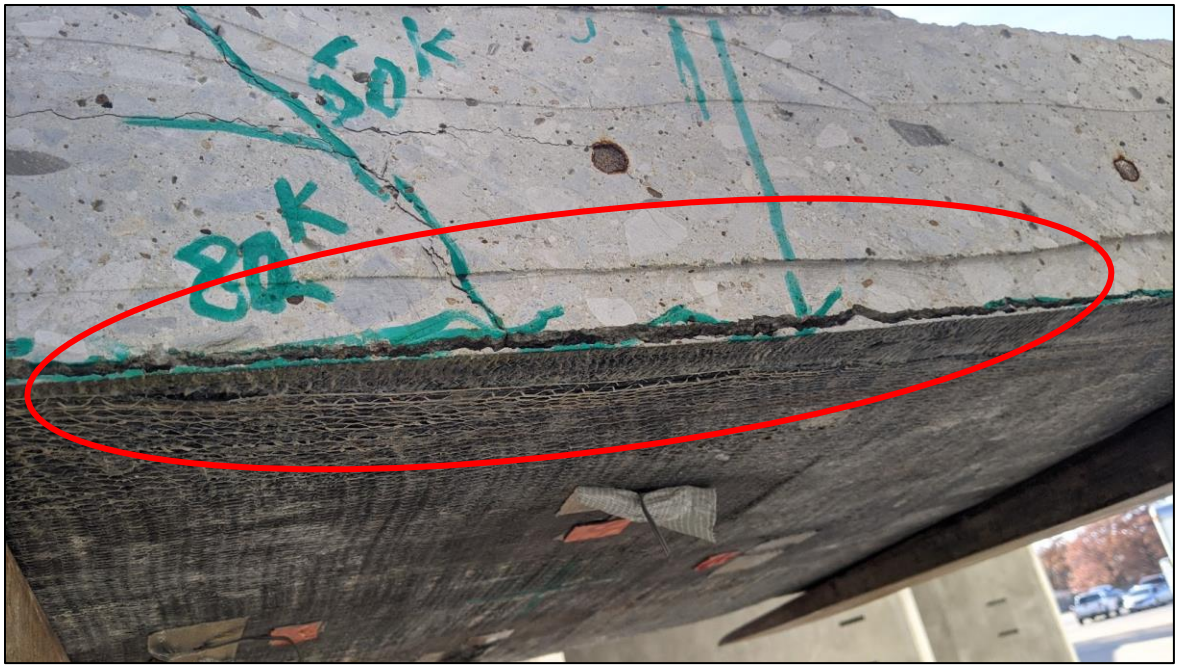

(a)

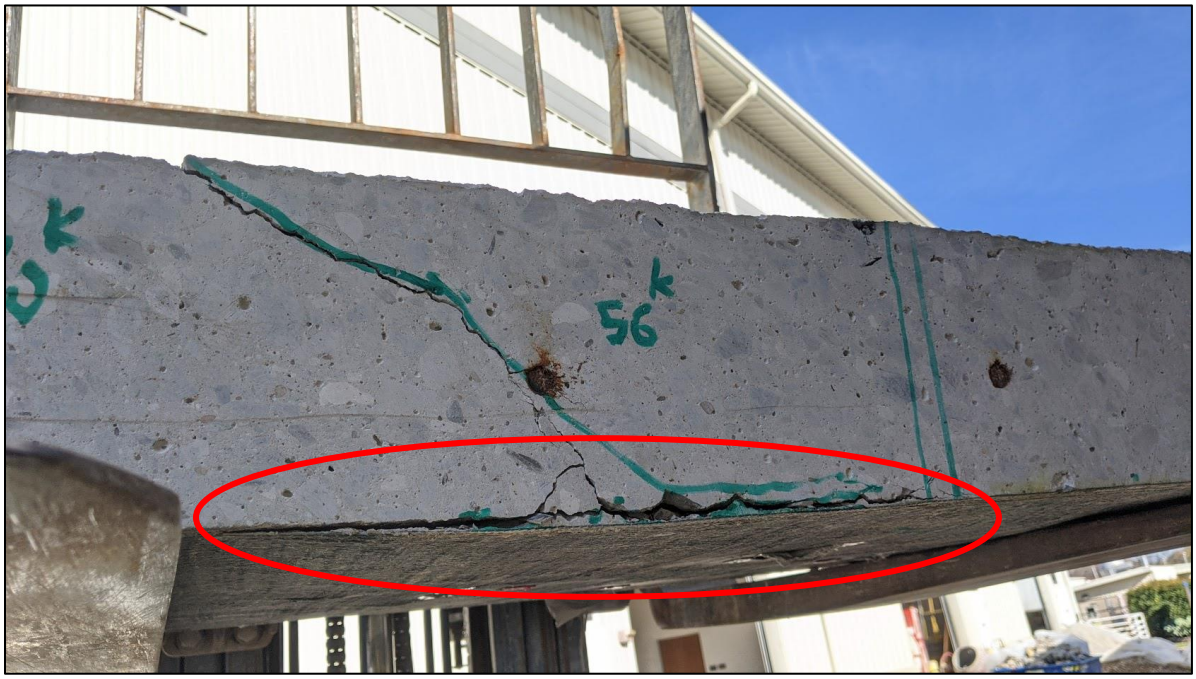

(b)

Fig 5.4: Observed delamination of PS-CFRP (a) along long span (b) along long span

(a)

(b)

Fig 5.5: Multiple diagonal cracks visible on top of the slab (a) side view (b) top view

Fig 5.6: Stretching of unidirectional fiber in transverse direction

5.2.1.2 Regular CFRP

The failure mode of this specimen was also observed to be flexure. The R-CFRP showed a lower load capacity compared to PS-CFRP. There was no visible crack on the sides of slab until 69 kip (306.93 kN). This crack propagated from bottom reinforcement of the slab towards the top. The crack was close to the center of the long side as shown in Fig 5.7. The second crack was visible near the same location, but this crack propagated from the bottom of the slab near the CFRP and moved towards the reinforcement, joining the first crack. Ultimately, the slab reached a maximum load of 71.36 kip (317.43 kN). At this point, the slab formed a circular-shaped crack, which appeared at the top of slab as shown in Fig 5.8. This circular crack was in the same location as other local cracks at the top of slab.

To observe the reason of failure of the slab, the slab was carried away from the testing site and lifted using a forklift. At the bottom of the slab, delamination of CFRP was observed at various

locations. The CFRP used to strengthen the short span was delaminated as shown in Fig 5.9. Furthermore, there was rupture of CFRP, but the rupture was not along the direction of the fiber as shown in Fig 5.10. The delamination was most likely induced by excessive shear stress concentrations at the cut-off points of the CFRP sheets and a lack of adequate anchorage.

(a)

(b)

Fig 5.7: First visible crack on edge of slab (a) right edge (b) left edge

(a)

(b)

Fig 5.8: Circular-shaped crack on top of the slab (a) side view (b) top view

Fig 5.9: Delamination of R-CFRP

Fig 5.10: Rupture of transverse CFRP fabric

5.2.2 Load-Deflection Relationship

The variation of load-deflection was dependent on the type of CFRP. For the R-CFRP strengthened specimen at the same load level, the tangents to the load-deflection curve were higher than that of PS-CFRP strengthened specimen as shown in Fig 5.11. Accordingly, the R-CFRP specimen showed higher stiffness over that of PS-CFRP strengthened specimen. Due to the brittle

nature of CFRP materials, the overall load-deflection relationship of both specimens showed a stiffer behavior. The ultimate failure for R-CFRP was more brittle as compared to PS-CFRP.

The deflection value at the ultimate load of R-CFRP was 0.76 times higher than the deflection value associated with the PS-CFRP strengthened specimen. It was found from the previous research conducted on two-way slab strengthened with CFRP that the deformations of the strengthened specimens were reduced (Kim et al., 2008). The results obtained from this study showed that the R-CFRP reduces the deformation of the specimen as compared to PS-CFRP, due to its stiff behavior. The results of the study also suggest that PS-CFRP showed more ductile behavior.

The LVDT was used to measure the displacement of the specimen. However, the LVDT was longer than the space available beneath the slab; hence, to compute the displacement of the specimen, the LVDT was attached directly to the testing machine. Therefore, the results obtained from LVDT measured the overall displacement of the loading plate rather than the displacement of a point on the slab. Consequently, conducting the numerical analysis based on the data was difficult. For this reason, a numerical model based on previous research by (Hawileh et al., 2016) was conducted and is discussed in the next chapter.

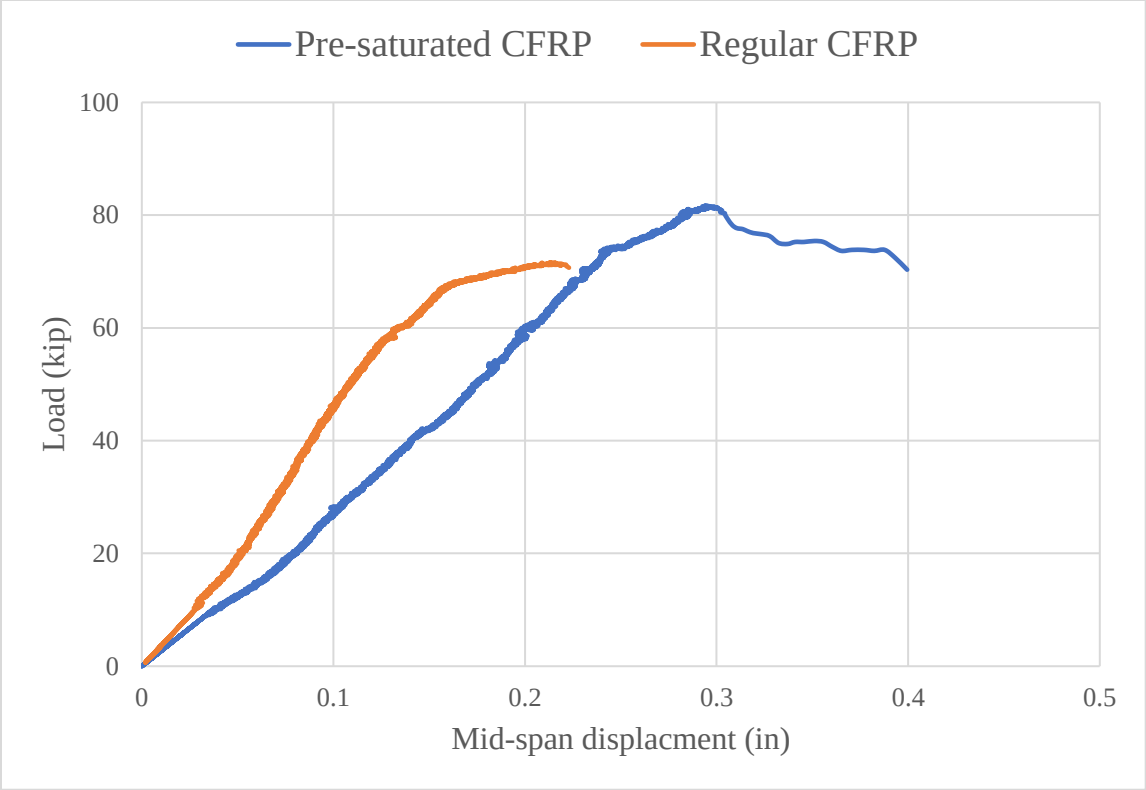

Fig 5.11: Load versus deflection relationship

5.2.3 CFRPs Strain

Measurements were made to determine the strain in the R-CFRP and PS-CFRP at selected locations from the center of the slab. Strain in CFRP was investigated at four locations as discussed in Chapter 4. The strain was measured along the short span and long span. After the cracks were fully developed, the CFRP strain increased linearly as shown in Fig 5.12.

Along the short and long span of the PS-CFRP, the strain slightly increased until 40 kip (177.93 kN). After this point, the strain increased almost linearly. In the case of R-CFRP, the concrete cracking was observed to be 30 kip (133.45 kN) at that point. After cracking of the concrete on tension side, the load was carried by the CFRPs. The ultimate strain for PS-CFRP and R-CFRP along the short span was observed to be 5144 and 3841 ($\mu\varepsilon$), respectively. Along the

long span, the ultimate strain was observed to be 2413 and 2247 ($\mu\varepsilon$), respectively, as shown in Fig 5.12.

Results from the present study also suggest that the strain in PS-CFRP was greater than R-CFRP at ultimate load. Before ultimate failure, the strain at all four points in PS-CFRP was greater than R-CFRP as shown in Appendix B. This indicates that the bond between PS-CFRP and concrete was intact for greater loads as compared to R-CFRP. More composite action can be achieved in PS-CFRP as the matrix and fiber carried more strain for higher loads. Conversely, the R-CFRP portrayed early delamination.

The load versus strain curve in Fig 5.10 (a) for PS-CFRP in the short span exhibited the illustrated pattern is possibly due to the placement of the CFRPs. The CFRPs overlapped each other in the short and long direction (Fig 3.6). For the short span, the strain gauge was placed over the CFRP spanning in the long direction. However, the set up was designed to measure the strain in the short direction. As a result, there was a possible discrepancy as shown in Fig 5.10.

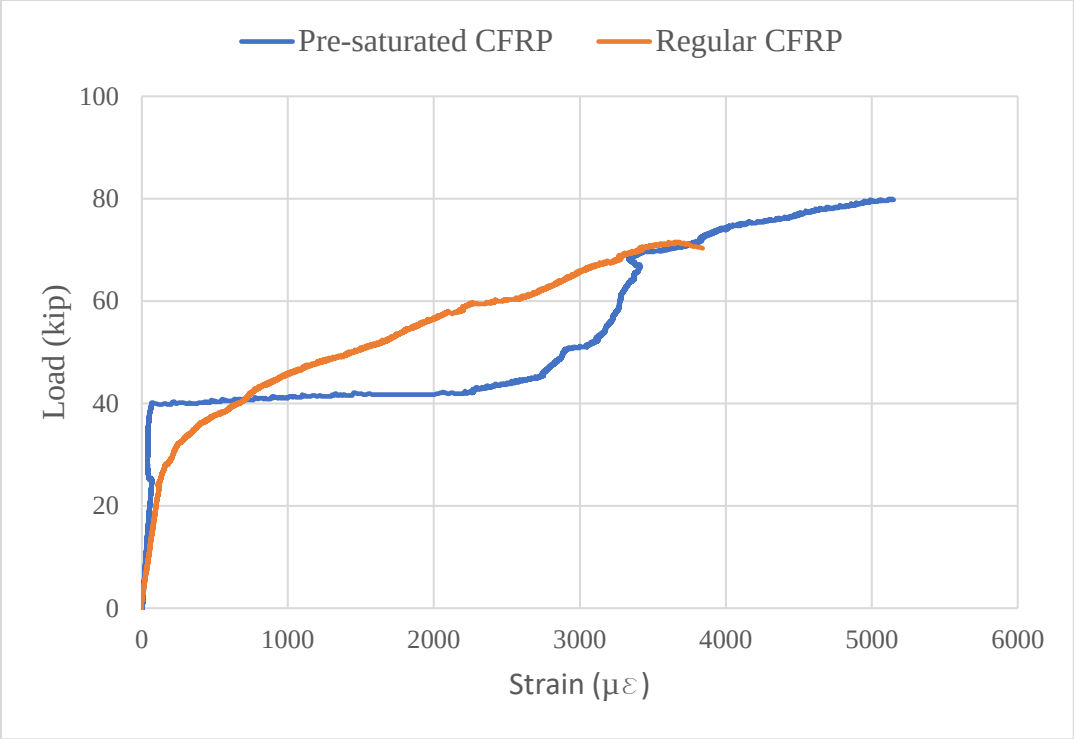

(a)

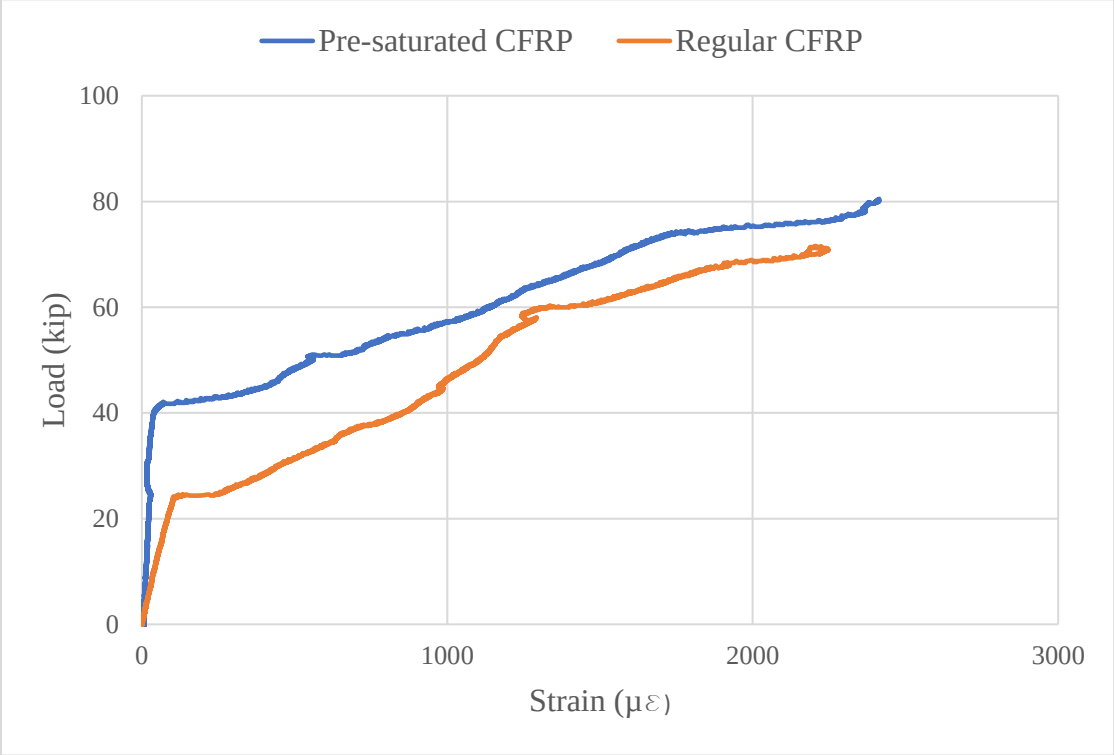

(b)

Fig 5.12: Load versus strain: (a) Short-span (b) Long- span

Table 5.2: Test results summary of the specimen

Title	First visible crack load, P_{cr}	Ultimate load, P_u	Deflection at ultimate load, δ_v	CFRP strains at ultimate load, ε_c (10^{-6})		Mode of Failure
	kip (kN)	kip (kN)	in (mm)	Short span	Long span	
R-CFRP	69 (306.93)	71.36 (317.43)	0.215 (5.46)	3841.484	2175.457	Flexure-Brittle
PS-CFRP	50 (222.41)	81.56 (362.8)	0.295 (7.51)	5149.966	2414.135	Flexure-Ductile

Chapter 6
Numerical Modelling

Hawileh et al. (2016) studied the flexural performance of thin RC slabs cast with concrete compressive strength of 50 MPa and 100 MPa, which were externally strengthened with CFRP laminates on the tension side.

The experimental program consisted of six specimens: three specimens for compressive strength 50 MPa (7.54 ksi) and three specimens that were 100 MPa (14.5 ksi). The three 50 Mpa (7.54 ksi) specimens consisted of a control slab and two strengthened slabs. The two strengthened slabs contained one and two layers of CFRP laminates, respectively. The length, span length, width, and height of the cast specimens were 2000 (78.7), 1700 (66.9), 300 (11.81), and 75 (3) mm (in.), respectively. The slabs were reinforced with two 12 mm diameter steel bars located at a depth of 50 mm from the top compression fiber. Fig 6.1 shows the details of the specimen. The slabs were externally retrofitted using 100 mm (3.93 in.) wide unidirectional MapeWrap CFRP laminates (Mape, 2013) and were bonded using adhesives on the tension side.

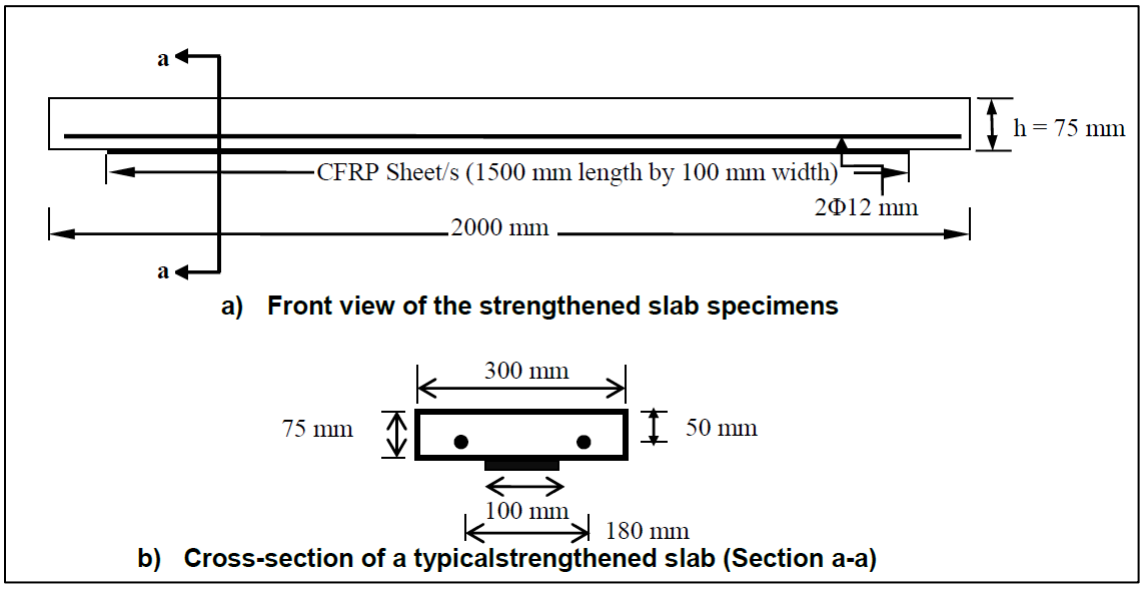

Fig 6.1: Details of the slab specimens (Hawileh et al., 2016)

Hawileh et al. conducted a four-point bending test on all of the specimens as shown in Fig 6.2. The results obtained from the test were summarized, and load versus displacement curves were plotted to display the results.

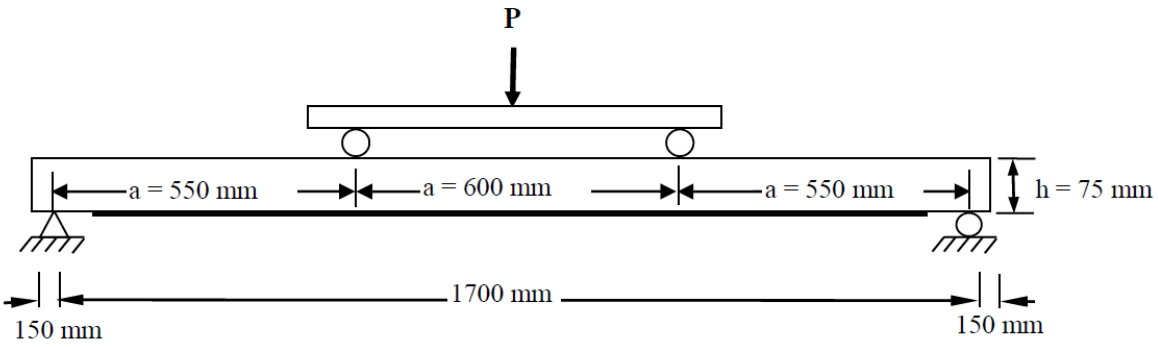

Fig 6.2: Test set-up by (Hawileh et al., 2016)

Based on the results obtained from his study, a numerical model has been developed in my study to validate the experimental results. For my study, a single layer of CFRP slab specimen with a compressive strength of 50 MPa (7.54 ksi) was utilized. To validate the results, a numerical method was used. The numerical method employs the discretization technique to subdivide the mathematical model into small components with simple geometry known as elements or finite elements. This type of study is known as finite element analysis (FEA), which provides accurate results in the analysis of complex structures. The FEA was performed using ABAQUS computer software, and the theories, methodologies, and results obtained are summarized in this chapter.

6.1 Concrete Damage Model (CDP)

Reinforced concrete is a complicated material. Hence, it is important to develop a finite element model which can calculate the elastic and plastic behavior of concrete under tension and compression. Wahalathantri et al. (2011) proposed a concrete material model that is capable of representing the formation of cracks and post-cracking behavior of reinforced concrete

elements. Three numerical material models were used by ABAQUS to simulate complete stress-strain behavior of concrete under compression and tension, including damage properties. Wahalathantri et al. proposed a concrete damage plasticity model for the inelastic behavior of concrete. The CDP behavior assumes two main factors, such as tensile cracking and compression crushing.

6.1.1 Concrete Compression Behavior

Wahalathantri et al. (2011) modified the model proposed by Hsu and Hsu (1994). The model can be used to develop a stress versus strain relationship of concrete in compression using maximum compressive stress (σ_{cu}). This model can only be developed for uniaxial compression up to $0.3\sigma_{cu}$ of stress in the descending part of σ_{cu}. The model also obeys Hooke's law up to 50% of σ_{cu} in the ascending portion of the stress-strain curve. Fig 6.3 shows the ultimate compressive stress σ_{cu} and strain at $\sigma_{cu}(\varepsilon_0)$ as well as the strain corresponding to $0.3\sigma_{cu}$ in the descending portion ε_c. This model can only be used for a high compressive strength of 62 MPa. The equation provided by Hsu and Hsu (1994) to calculate the compressive stress σ_c from $0.3\sigma_{cu}$ to $0.5\sigma_{cu}$ is:

$$\sigma_c = \left(\frac{\beta\left({}^{\varepsilon_c}/_{\varepsilon_0}\right)}{\beta - 1 + \left({}^{\varepsilon_c}/_{\varepsilon_0}\right)^{\beta}} \right) \sigma_{cu} \qquad [1]$$

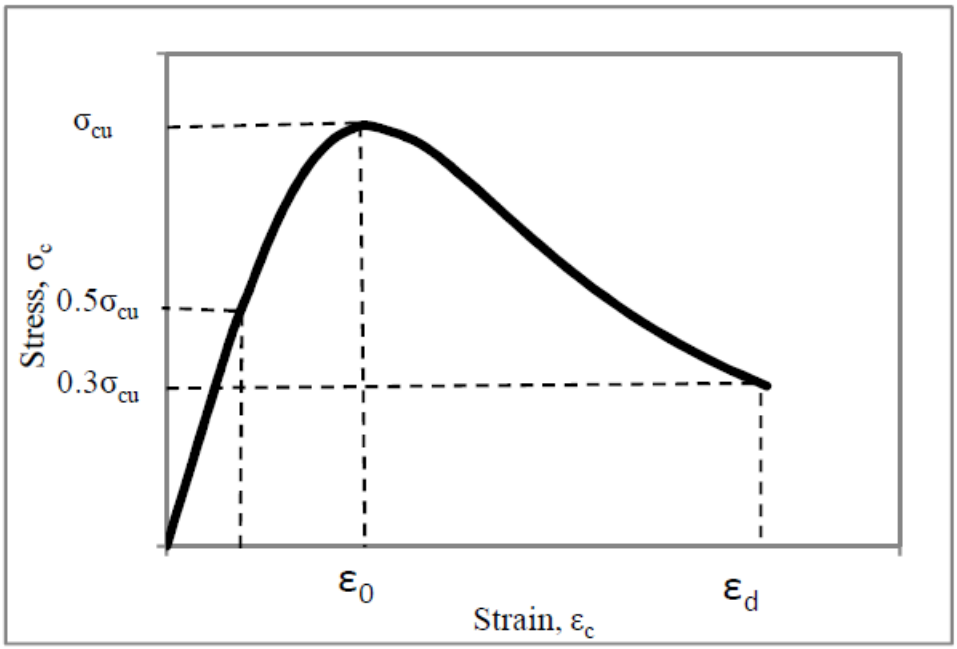

Fig 6.3: Compressive stress-strain relationship for ABAQUS (Wahalathantri et al., 2011)

where β is the parameter that relies on the shape of the stress-strain curve and can be calculated based on the following equation (Wahalathantri et al., 2011):

$$\beta = \frac{1}{1 - \left[\sigma_{cu}/(\varepsilon_0 E_0)\right]} \quad [2]$$

E_0 is defined as the initial tangential modulus, and ε_0 is the corresponding strain of the ultimate compressive strength. E_0 and ε_0 are calculated using the following equations, respectively (Wahalathantri et al. 2011):

$$E_0 = 1.2431 * 10^2 \sigma_{cu} + 3.28312 * 10^3 \quad [3]$$

$$\varepsilon_0 = 8.9 * 10^{-5} \sigma_{cu} + 2.114 * 10^{-3} \quad [4]$$

To define the stress-strain relationship of concrete in ABAQUS, the user needs to enter inelastic strain ($\tilde{\varepsilon_c^{in}}$) corresponding to the stress value (σ_c) and damage parameter (d_c). The total

strain value is converted into inelastic strain using the following equation (Wahalathantri et al., 2011):

$$\varepsilon_c^{\sim in} = \varepsilon_c - \varepsilon_{oc}^{el} \quad [5]$$

where, $\varepsilon_{oc}^{el} = {}^{\sigma_c}/_{E_0}$, ε_{oc}^{el} = Elastic strain corresponding to the undamaged material and ε_c= Total compressive strain.

Damage parameter is a scalar variable in the range between 0 and 1 where 0 represents no damage, and 1 represents full damage. Damage parameter is used to characterize the degradation of the elastic stiffness on the strain softening range of the stress-strain curve (Tao & Chen, 2014). The damage parameter of the concrete in the compression damage in ABAQUS can be calculated using the following equation (Lubliner et al., 1989):

$$d_c = 1 - \frac{\sigma_c}{f_c'} \quad [6]$$

where, σ_c = corresponding compressive strength and f_c' = ultimate compressive strength.

The concrete compressive stress-strain values and damage parameters are summarized in Table 6.1, and these values are used in the concrete compression section in ABAQUS. The values for the stress versus strain graph are also calculated using the aforementioned formulae, and the graph was plotted as shown in Fig 6.4. The f_c' is 52 MPa and the ultimate strain (ε_0) corresponding to this value is 0.00278 and was calculated using equation [4]. Finally, the initial tangential modulus was calculated using equation [3] and the value was 29098.75 MPa.

Table 6.1: Concrete compressive behavior

Concrete Compressive Behavior				Concrete Compressive Damage	
Yield Stress (Mpa)	**Total Strain (m/m)**	**Elastic Strain (m/m)**	**Inelastic Strain (m/m)**	**Damage Parameter (dc)**	**Inelastic Strain (m/m)**
0.00	0.0000	0.0000	0.0000	0.0000	0.0000
26.15	0.0009	0.0009	0.0000	0.0000	0.0000
28.24	0.0010	0.0010	0.0000	0.0000	0.0000
33.21	0.0012	0.0011	0.0001	0.0000	0.0001
39.76	0.0015	0.0014	0.0001	0.0000	0.0001
43.41	0.0017	0.0015	0.0002	0.0000	0.0002
46.42	0.0019	0.0016	0.0003	0.0000	0.0003
47.68	0.0020	0.0016	0.0004	0.0000	0.0004
48.77	0.0021	0.0017	0.0004	0.0000	0.0004
49.69	0.0022	0.0017	0.0005	0.0000	0.0005
51.49	0.0025	0.0018	0.0007	0.0000	0.0007
51.80	0.0026	0.0018	0.0008	0.0000	0.0008
52.00	0.0028	0.0018	0.0010	0.0000	0.0010
51.92	0.0029	0.0018	0.0011	0.0016	0.0011
51.73	0.0030	0.0018	0.0012	0.0053	0.0012
51.06	0.0032	0.0018	0.0014	0.0181	0.0014
49.48	0.0035	0.0017	0.0018	0.0484	0.0018
46.66	0.0039	0.0016	0.0023	0.1026	0.0023
45.88	0.0040	0.0016	0.0024	0.1177	0.0024
30.27	0.0060	0.0010	0.0050	0.4179	0.0050
27.17	0.0065	0.0009	0.0056	0.4775	0.0056
24.45	0.0070	0.0008	0.0062	0.5298	0.0062
22.07	0.0075	0.0008	0.0067	0.5755	0.0067
20.00	0.0080	0.0007	0.0073	0.6154	0.0073
19.50	0.0081	0.0007	0.0075	0.6249	0.0075

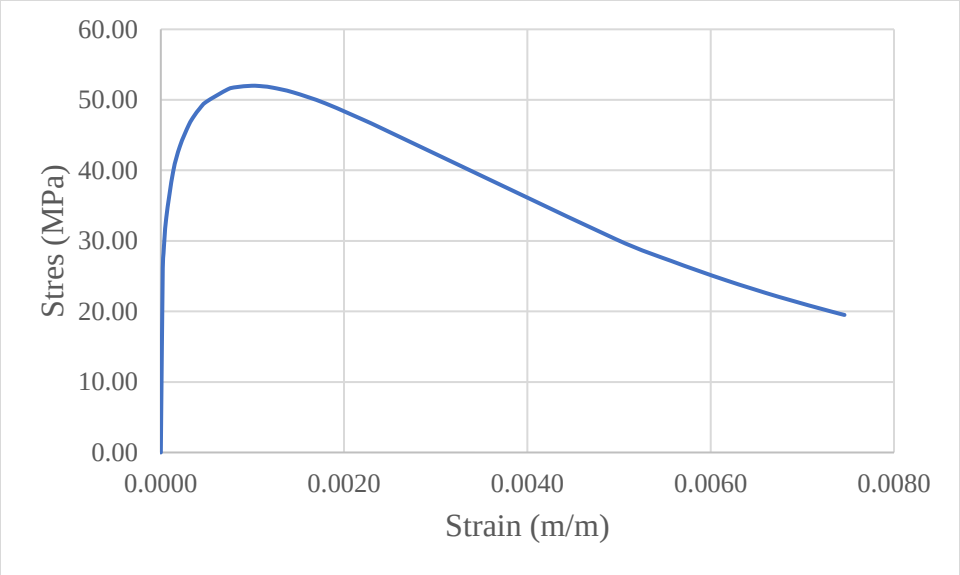

Fig 6.4: Stress versus strain relationship of concrete in compression

6.1.2 Concrete Tensile Behavior

To simulate the tensile behavior of concrete in ABAQUS, a post failure stress-strain relationship for concrete subjected to tension is displayed in Fig 6.5 (Wahalathantri et al., 2011). To develop the model, the following parameters need to be entered: Young's Modulus (E_0), stress (σ_t), cracking strain ($\varepsilon_t^{\sim in}$), and the damage parameter (d_t). The cracking strain $\varepsilon_t^{\sim in}$ is calculated using the following equation (Wahalathantri et al., 2011).

$$\varepsilon_t^{\sim in} = \varepsilon_t - \varepsilon_{ot}^{el} \quad [7]$$

where, $\varepsilon_{ot}^{el} = {}^{\sigma_t}/_{E_0}$, ε_{ot}^{el} = Elastic strain corresponding to the undamaged material and ε_t= Total tensile strain.

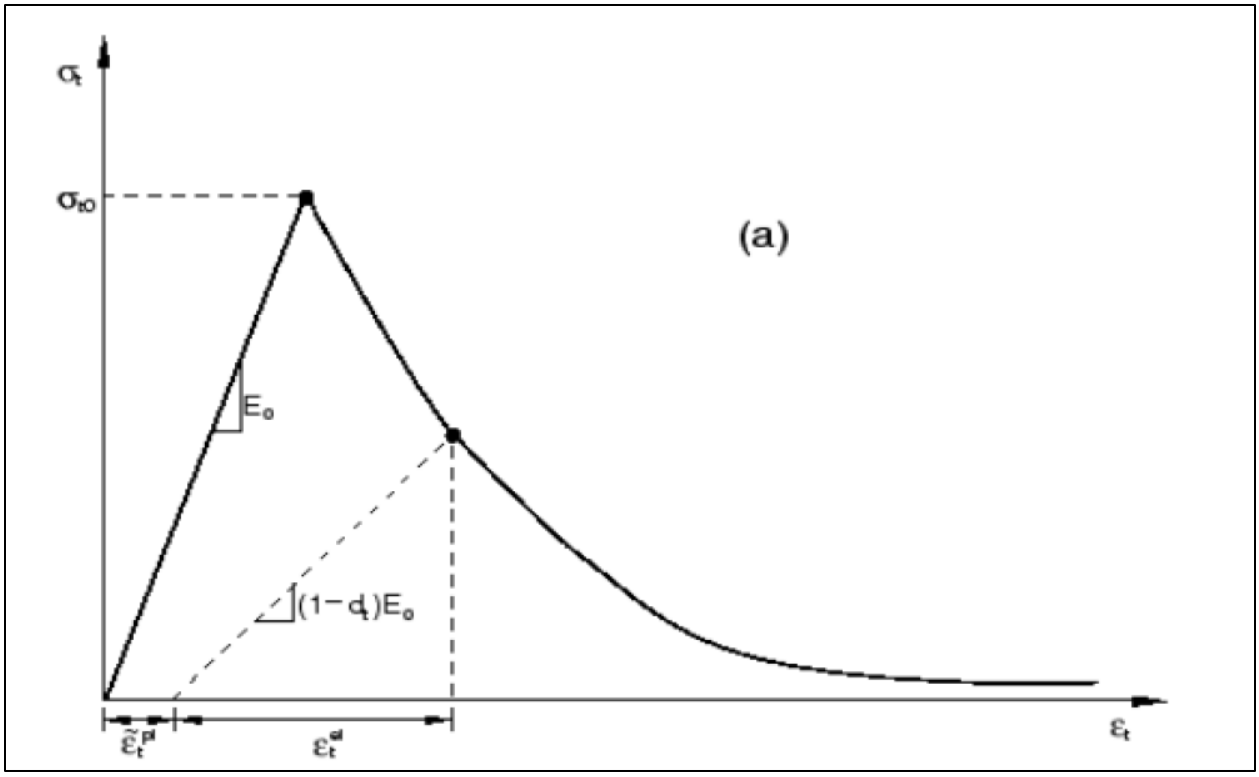

Fig 6.5: Response of Concrete to Uniaxial Loading in Tension (Dassault Systèmes Simulia et al. 2013)

Wahalathantri et al. (2011) modified the model proposed by Nayal and Rasheed (2006) in which they changed a sudden drop at critical strain (ε_{cr}) from maximum tensile stress σ_{to} to $0.8\sigma_{to}$ and made the resulting graph slanted as shown in Fig 6.6. This change was made to avoid run-time error in ABAQUS material models. Nayal and Rasheed (2006) developed the model based on the tension stiffening model presented by Gilbert and Warner (1978) to capture the stress-strain behavior of concrete under uniaxial tension. The primary and secondary cracking stages were represented by two descending parts after the sudden drop at the tensile strain (ε_{cr}) corresponding to the maximum tensile stress (f_t) as shown in Fig 6.5.

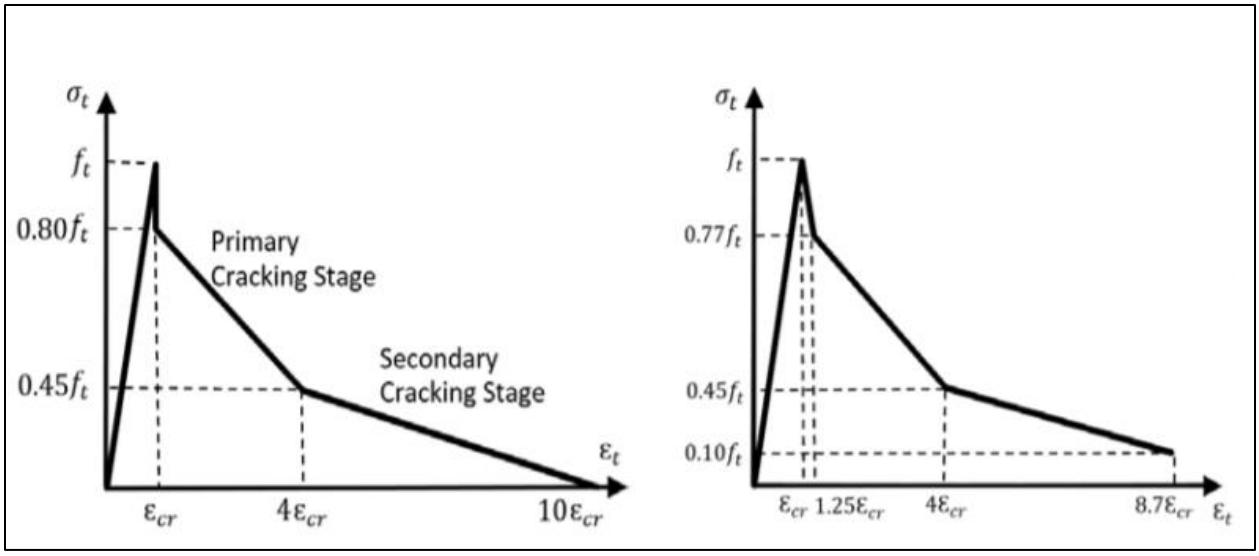

Fig 6.6: Tension stiffening model (a) (Nayal and Rasheed 2006) (b) (Wahalathantri et al. 2011)

The ultimate splitting tensile stress (f_t) of the concrete can be calculated according to ACI Committee 318 2019, which is given in the following equation:

$$f_t = 6.7\sqrt{f_{cm}} \quad [8]$$

where, f_{cm} is the measured average compressive strength.

The damage parameter is calculated using the following equation (Lubliner et al. 1989):

$$d_t = 1 - \frac{\sigma_t}{f_t'} \quad [9]$$

where, σ_{tc} = corresponding tensile strength and f_t' = ultimate tensile strength.

The ultimate tensile strength (f_t) calculated using equation [8] was 4.01 MPa, and the corresponding tensile strain was 1.38 x 10^{-4}. The value of the critical tensile strain was calculated based on dividing the ultimate tensile stress over the initial tangential modulus (E_0). Table 6.2

summarizes the concrete tension behavior, and Fig 6.7 depicts the stress versus strain curve of concrete in tension.

Table 6.2: Concrete Tensile Behavior

Yield Stress (MPa)	Tension Damage (d_t)	Cracking Strain (m/m)
0	0	0.000000
4.01	0.23	0.000138
3.0877	0.45	0.000172
1.7644	0.77	0.000551

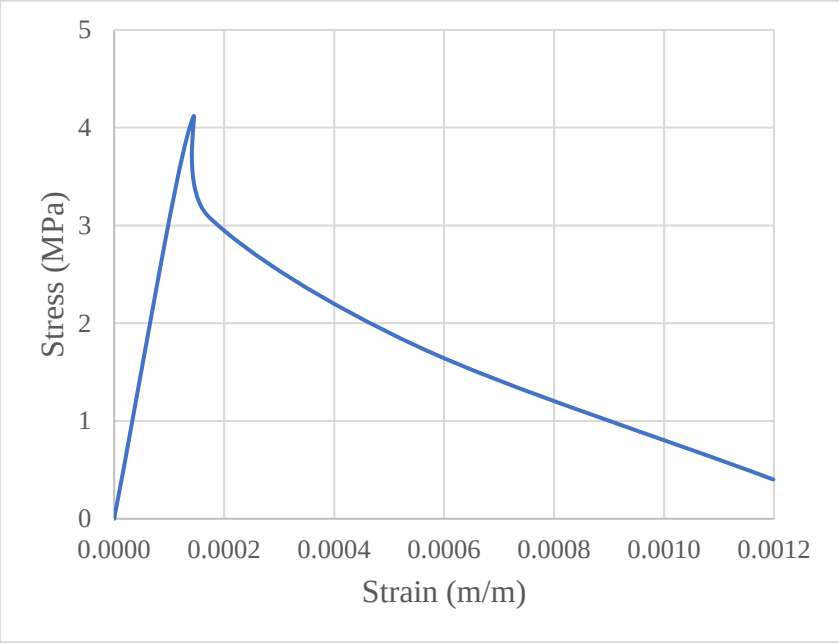

Fig 6.7: Stress versus strain relationship of concrete in tension

6.2 Steel Constitutive Behavior

A bilinear elastic-plastic model was used to describe the stress-strain behavior of the steel. The tangent modulus of the strain hardening branch was estimated to be one-hundredth of the elastic modulus. E_s is defined as the modulus of steel, which has a magnitude of 205 GPa. Perfect bond was assigned to the interface between the concrete and internal reinforcement. To assign this

bond, an embedded constraint was used in ABAQUS. The values of stress and plastic strain were calculated using the data provided by Retno et al. (2019), assuming yield strength and tensile strength to be 506 MPa and 580 MPa, respectively.

Table 6.3: Tensile Data of the Steel Material.

Yield Stress (MPa)	Total Strain (m/m)	Plastic Strain (m/m)
506.21	0.002564	0.000095
542.85	0.008320	0.005672
556.11	0.016005	0.013292
562.99	0.023116	0.020370
569.87	0.028793	0.026013
576.50	0.034470	0.031658
582.64	0.040147	0.037304
588.41	0.045823	0.042953

6.3 CFRP Constitutive Behavior

The FRP laminate was modeled as a linear elastic isotropic material, and its stress-strain response was determined to be a linear elastic relationship. The elastic modulus of FRP composites in the direction to the fibers, E_{11} = 95 GPa were taken from the properties table provided by MapeWrap CFRP laminates (Mape, 2013), and Poisson's ratio ν_{12} was assumed to be 0.3 for the analysis. There is no significant difference in the results for cases when the fiber was modeled as an orthotropic material. Thus, it is preferable to use the simpler assumption of isotropy (Obaidat, 2011).

6.4 Interaction Between CFRP and Concrete

The interaction between CFRP and concrete can be evaluated using two different methods. The methods include a perfect bond between CFRP and concrete i.e., using tie-constraint in ABAQUS and a cohesive bond which describes the surface separations. The perfect bond

overestimates the ultimate load and stiffness of the specimen (Obaidat, 2011). Hence, a cohesive model is a more appropriate choice for representing the interface behavior (Obaidat, 2011). Lu et al. (2005) proposed a bilinear bond-slip model which was utilized to represent the behavior of the FRP-concrete interface in terms of the local shear stress, τ and effective displacement/slip, δ between the FRP and the concrete as shown in Fig 6.8.

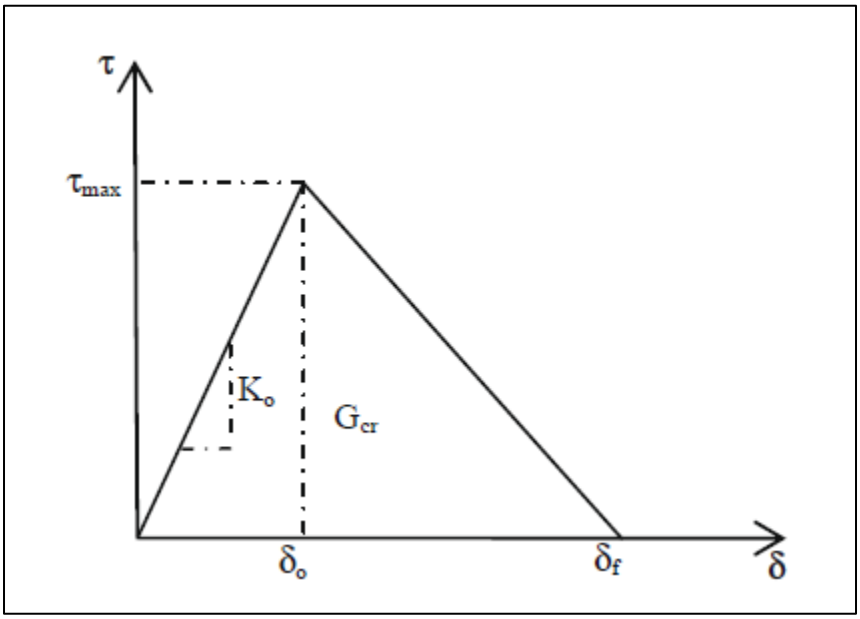

Fig 6.8: Bilinear traction–separation constitutive law (Obaidat, 2011)

The initial stiffness K_o is defined as,

$$K_o = \frac{1}{\frac{t_i}{G_i} + \frac{t_c}{G_c}} \quad [10]$$

where, t_i = resin thickness, t_i = 1 mm (0.04 in) (assumed)

t_c = concrete thickness, t_c = 5 mm (0.19 in) (assumed)

G_i = shear modulus of resin, G_i = 665 MPa ()

G_c = shear modulus of concrete, G_c = 10309.35 MPa

From Fig 6.8, it can be concluded that the relationship between traction stress and opening displacement depends on initial stiffness K_o, local shear stress τ, characteristics of opening displacement at fracture δ_f, and the energy needed to open the crack G_{cr} which is equal to the area under the traction – displacement curve (Guo et al., 2005; Obaidat, 2011).

Maximum shear stress τ_{max} is given by (Lu et al., 2005),

$$\tau_{max} = 1.5\beta_w f_t \quad [11]$$

Where:

$$\beta_w = \sqrt{\left(2.25 - \frac{b_f}{b_c}\right) \Big/ \left(1.25 + \frac{b_f}{b_c}\right)} \quad [12]$$

and b_f = CFRP plate width

b_c = Concrete width

f_t = Concrete tensile strength

The initiation of damage depends on factors such as cohesive tensile strength (σ_n^0) which is equal to the tensile strength of concrete (f_t) and shear stresses of the interface (τ_s^0 and τ_t^0). Where n, s, and t refer to the direction of the stress component (Obaidat, 2011). The values input in ABAQUS are provided in Table 6.4.

Table 6.4: CFRP-concrete interfacial properties for surface-based cohesive behavior material model and damage model.

K_{nn}, N/mm^3(lb/in^3)	K_{ss}, N/mm^3(lb/in^3)	K_{tt}, N/mm^3(lb/in^3)	Normal, MPa(ksi)	Shear-1, MPa(ksi)	Shear-2, MPa(ksi)
1834(6756379.86)	503(1853031.11)	503(1853031.11)	4.01(0.581)	8.582(1.23)	8.582(1.23)

Obaidat (2011) defines the interface damage evolution in terms of energy release. He defined the dependence of the fracture energy on the mode mix based on the Benzaggah–Kenane fracture criterion. Obaidat further claimed that the Benzaggah–Kenane fracture criterion is particularly useful when the critical fracture energies during deformation which are purely along the first and the second shear directions are the same i.e., $G_s^c = G_t^c$ and the fracture energies are given by:

$$G_n^c + (G_s^c - G_n^c)\left(\frac{G_\delta}{G_\tau}\right)^\eta = G^c \quad [13]$$

where, $G_\delta = G_s + G_t$, $G_\tau = G_n + G_s$, and η are the material parameter. $G_n, G_s, and\ G_t$ refer to the work done by the traction and its conjugate separation in the normal, the first and the second shear directions, respectively. The values used for this study were $G_n^c = 90\,J/m^2$, $G_t^c = G_s^c = 900\,J/m^2$, and $\eta = 1.45$.

6.5 Modeling Methodology

The slab was modeled as simply supported with proper boundary conditions. Eight-node linear brick elements with reduced integration (C3D8R) were used for the concrete. The W00WF or reinforcement was modeled using two-node truss elements (T2D3E). Four-node doubly-curved thin shell elements with reduced integration (S4R) were used to represent CFRP laminates. The element types are shown in Fig 6.9. The FRP-to-concrete interface was defined as surface-based cohesive behavior, which neglects the small interface thicknesses using the above bond-slip constitutive model. The model geometry and assembly are shown in Fig 6.10 in which the color red depicts the RC slab, and green depicts the CFRP laminate.

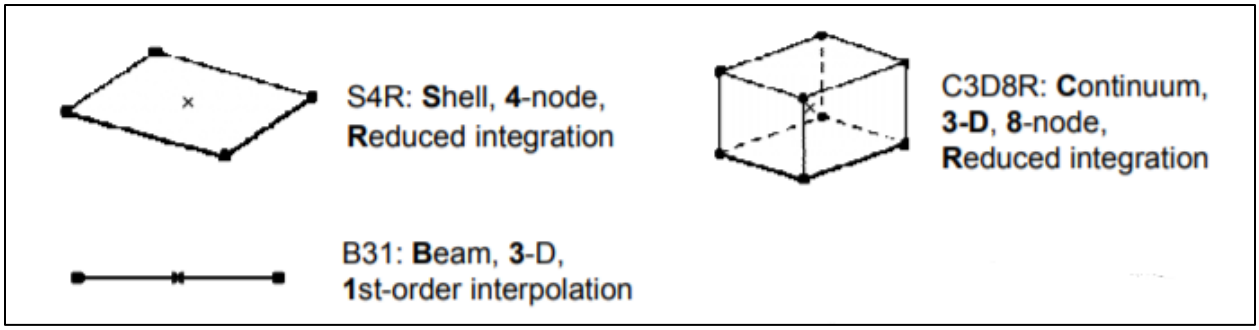

Fig 6.9: Element types in ABAQUS, 2005

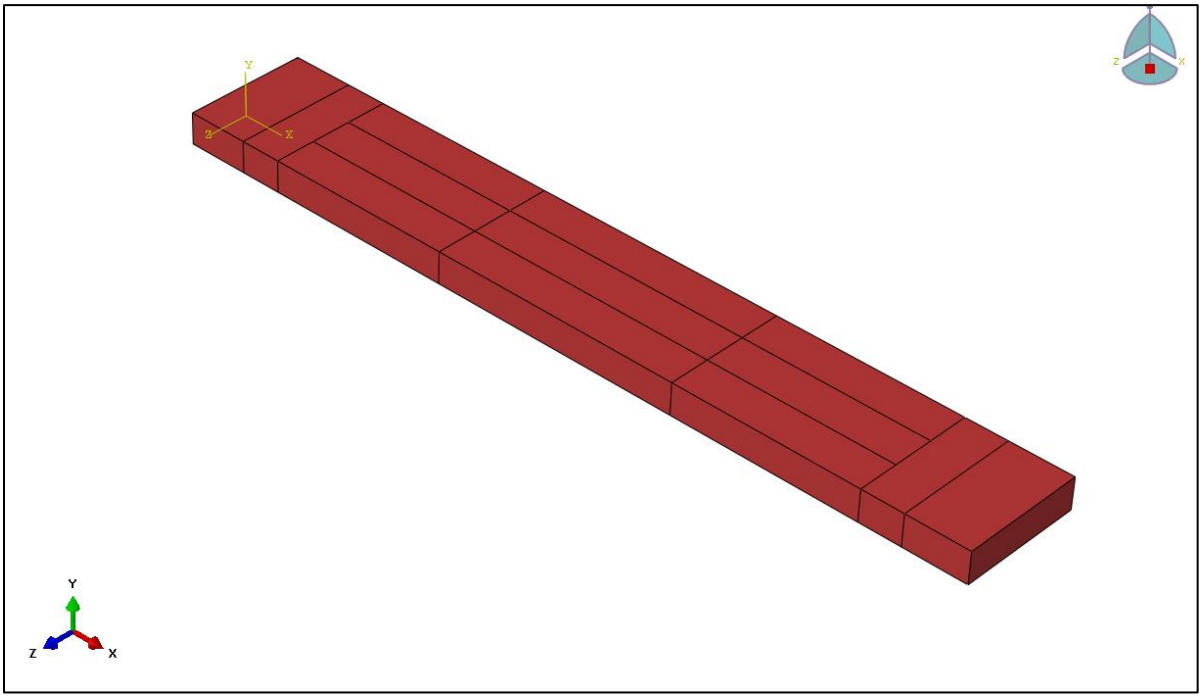

(a)

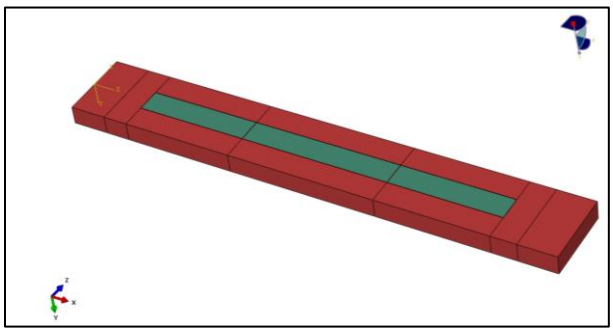

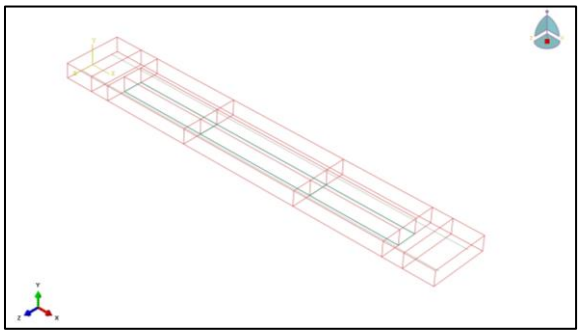

(b) (c)

Fig 6.10: Model Geometry and type (a) Concrete slab modelled as eight-node brick element (b) CFRP at the bottom surface modelled as four-node shell element (c) Reinforcement modelled as two-node truss element

6.5.1 Meshing of Parts

The meshing was applied for part instances with a reasonable part-to-part mesh with an element size of 25 mm for each part as shown in Fig 6.11. The reduced integration property was adopted in the analysis to reduce computer run time.

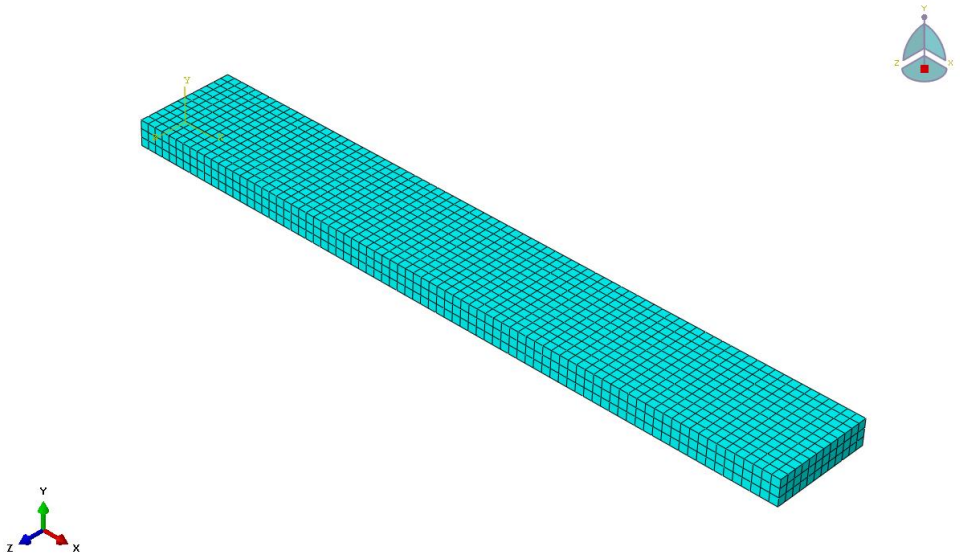

Fig 6.11: Mesh size of 25 mm use for model

6.5.1.1 Mesh Refinement Study

A mesh refinement study was conducted using Richardson's formula to determine an acceptable mesh density. This study utilized an extrapolation formula to determine a quantity of interest calculated with an infinitely fine mesh using the following formula (Cook et. al., 2002; Rajek, 2010).

$$\phi_\infty = \frac{\phi_1 h_2^q - \phi_2 h_1^q}{h_2^q - h_1^q} \quad [14]$$

Where, ϕ_∞ = Quantity from infinite mesh

ϕ_1 = Quantity from 1st mesh

h_2 = Characteristic length (longest line segment that fits within an element) of 2nd mesh

q= Extrapolation exponent

ϕ_2= Quantity from 2nd mesh

h_1= Characteristic length of 1st mesh

The analysis was conducted using three different mesh sizes 15 mm, 30 mm, and 45 mm for the slabs. The sizes are shown in Fig 6.12.

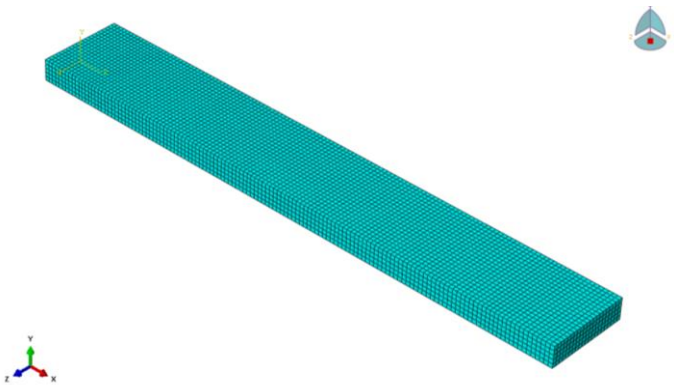

(a)

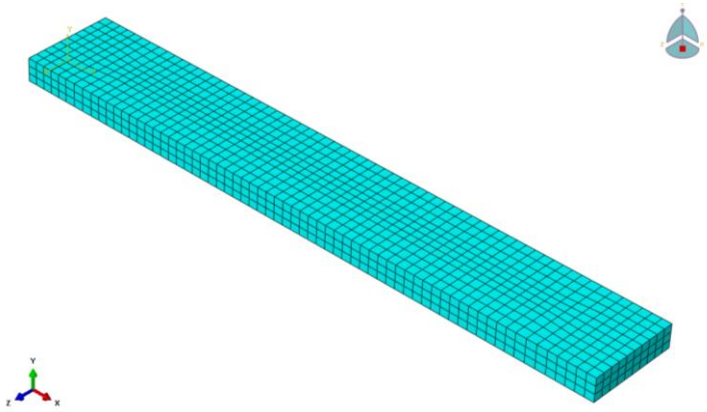

(b)

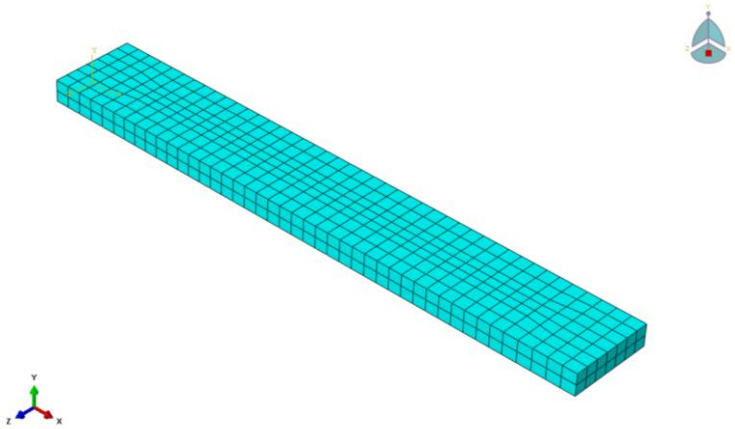

(c)

Fig 6.12: Different mesh sizes (a) 15 mm mesh size (b) 30 mm mesh size (c) 45 mm mesh size

Ultimate load was used as the quantity to compare the mesh densities. The extrapolation exponent (q) was determined using methods outlined by Cook et al. (2002) and Rajek (2010). Cook recommended determining the value of q graphically. Ultimate load (φ) identified in Fig 3.16 was plotted against the characteristic length (h) raised to the q power. The value of q was altered until the plot of φ vs. h_q plotted a straight line. A value of 1.6 for q was used to plot the straight line. The values used to determine q are shown in Table 6.5. Fig 6.13 displays the plot used to determine q.

Table 6.5 Ultimate load and q value with respect to the mesh

Length (Mesh Size) (mm)	**Load (kN)**	**q=1.6**
0	31.49	0
15	30.2	132.6080873
30	27.6	401.9925496
45	24	769.0667202

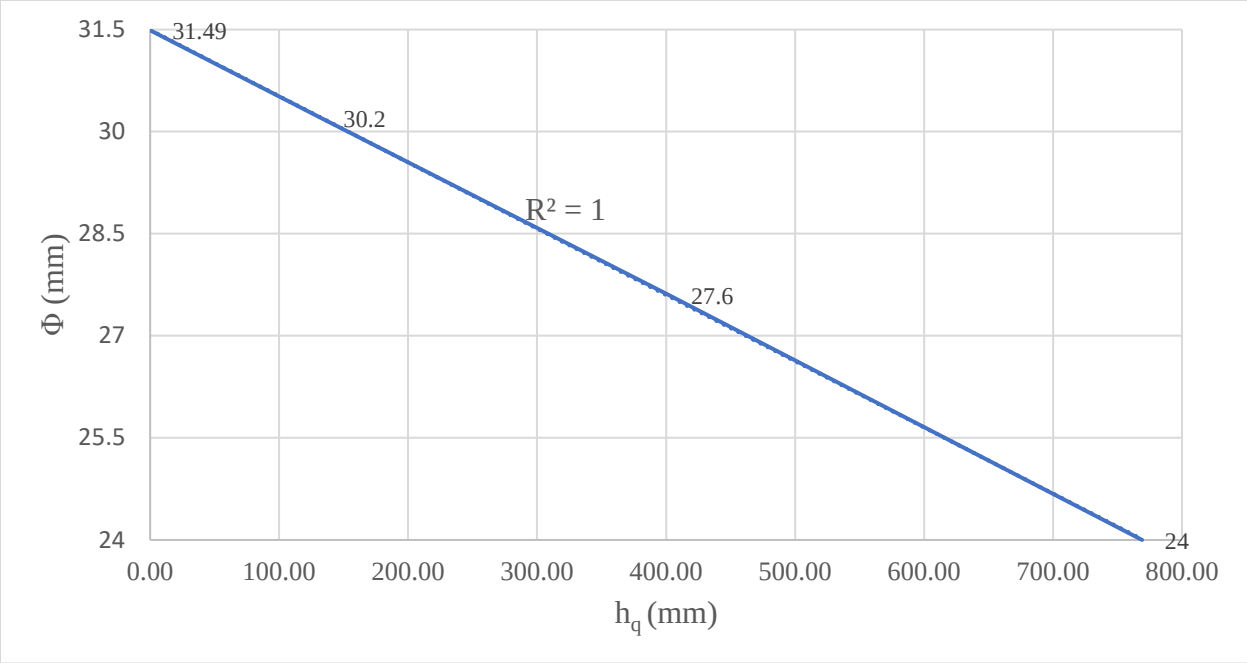

Fig 6.13: h_q verses φ plot used to determine q for Richardson's extrapolation

The ultimate load for infinite mesh was found to be 31.49 kN using equation [14]. The error between the mesh sizes was determined using the percentage formula.

$$e_2 = \frac{\phi_2 - \phi_\infty}{\phi_\infty} * 100 \qquad [15]$$

Where, e_2= Error in 2nd mesh

ϕ_2= Ultimate load from 2nd mesh

ϕ_∞= Ultimate load from infinite mesh

The runtime of the model with 25 mm elements was reduced by approximately seven hours when compared to the model with 15 mm elements. The error with different mesh sizes is presented in Table 6.6.

Table 6.6: Percentage of error using different mesh sizes

Length (Mesh Size) (in.)	Load (kN.)	Difference	Difference (%)
15	30.2	-0.042774464	4.277
30	27.6	-0.141006841	14.101
45	24	-0.312157867	31.216
25	28.5	-0.104975046	10.498

6.5.2 Boundary Conditions and Load

Loads are applied to the specimen using a displacement. In a displacement-controlled analysis, as opposed to a load-controlled analysis, the displacement changes incrementally while the reaction force results depend on the stiffness of the structure. To apply the load, the surface was partitioned as shown in Fig 6.14.

The assembly was also partitioned at the surfaces where the boundary conditions was to be assigned. The left support was assigned as a pin with the restriction of the vertical and horizontal displacement (U1, U2=0), and right support was assigned as a roller with vertical displacement equal to zero (U2=0).

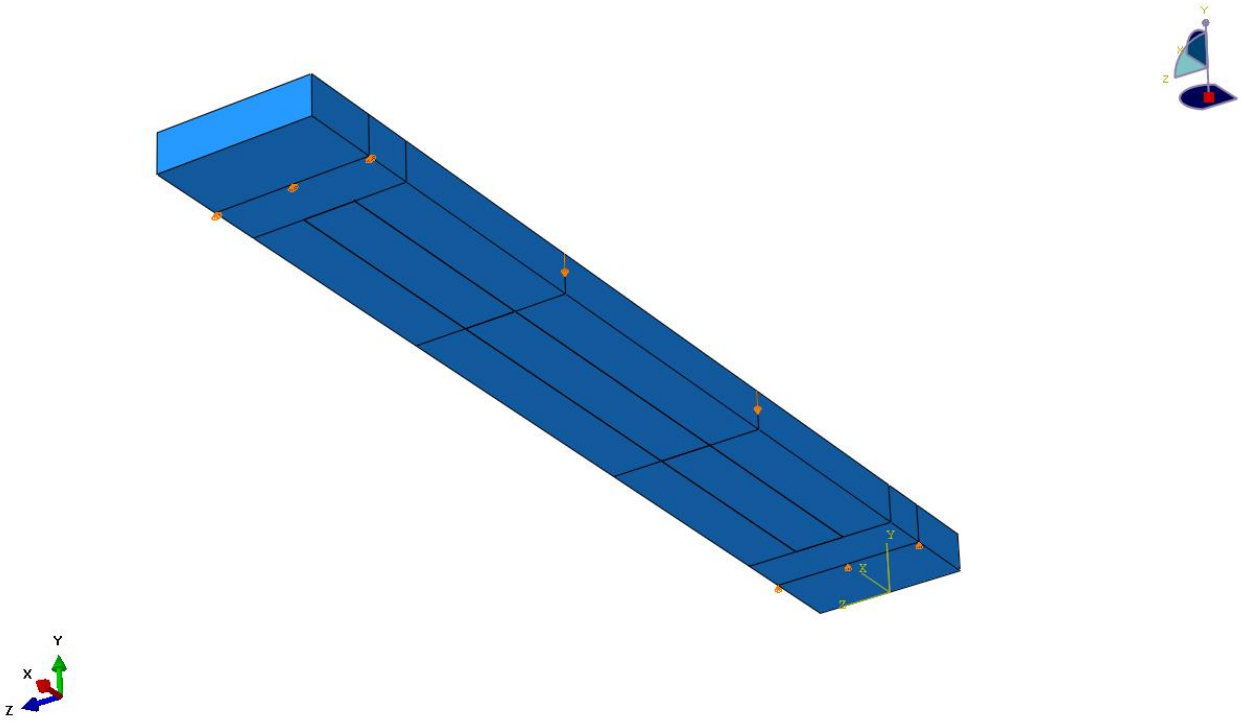

Fig 6.14: Boundary condition and applied load on the specimen

6.6 Result Validation and Discussion

The load-deflection response of the slab from a finite elements model was compared to the experimental program to calibrate the model. The mid-span deflection of the slab was measured during the experiment and plotted in the graph as shown in Fig 6.15. For my model validation, we use the experimental results of concrete with compressive strength of 50 MPa (7.54 ksi) and single layer CFRP laminate.

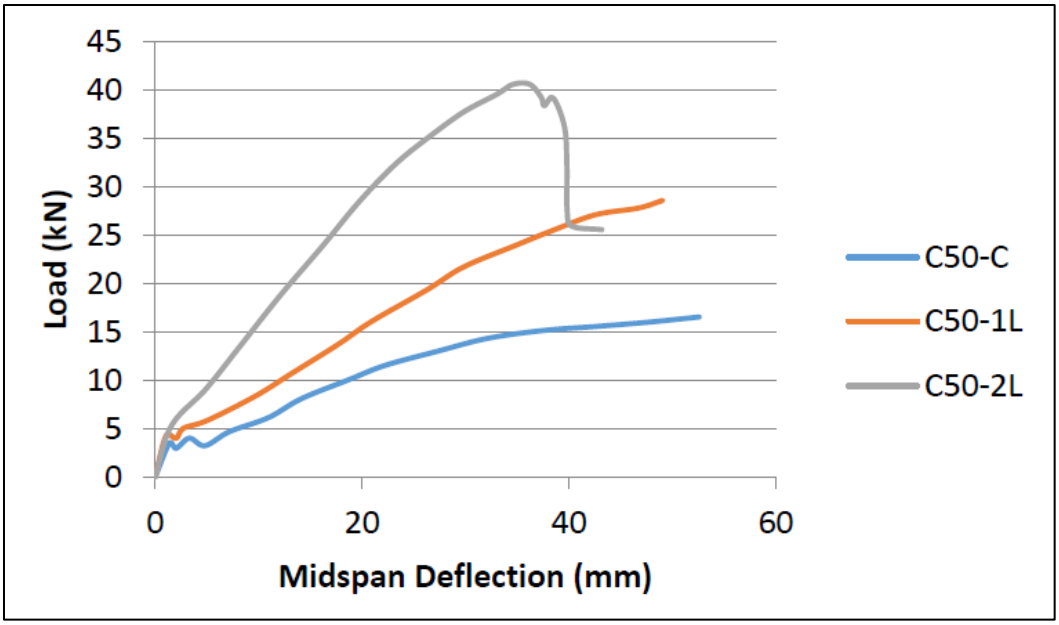

Fig 6.15: Load versus displacement by Hawileh et al. (2016)

The load versus deflection curve of the slab showed a good agreement between experimental and numerical results as shown in Fig 6.16. This indicated that the FEM can precisely depict the fracture results of concrete. There was a slight difference in the curve of test results, possibly because the study by Hawileh et al. did not include the stress versus strain relationship of the concrete in tension and compression. The following data was calculated based on the equations mentioned in section 6.1. The ultimate load from the experiment was measured to be 28 kN, which caused the failure of the slab due to delamination of CFRP. The deflections corresponding to the ultimate load is 48 mm.

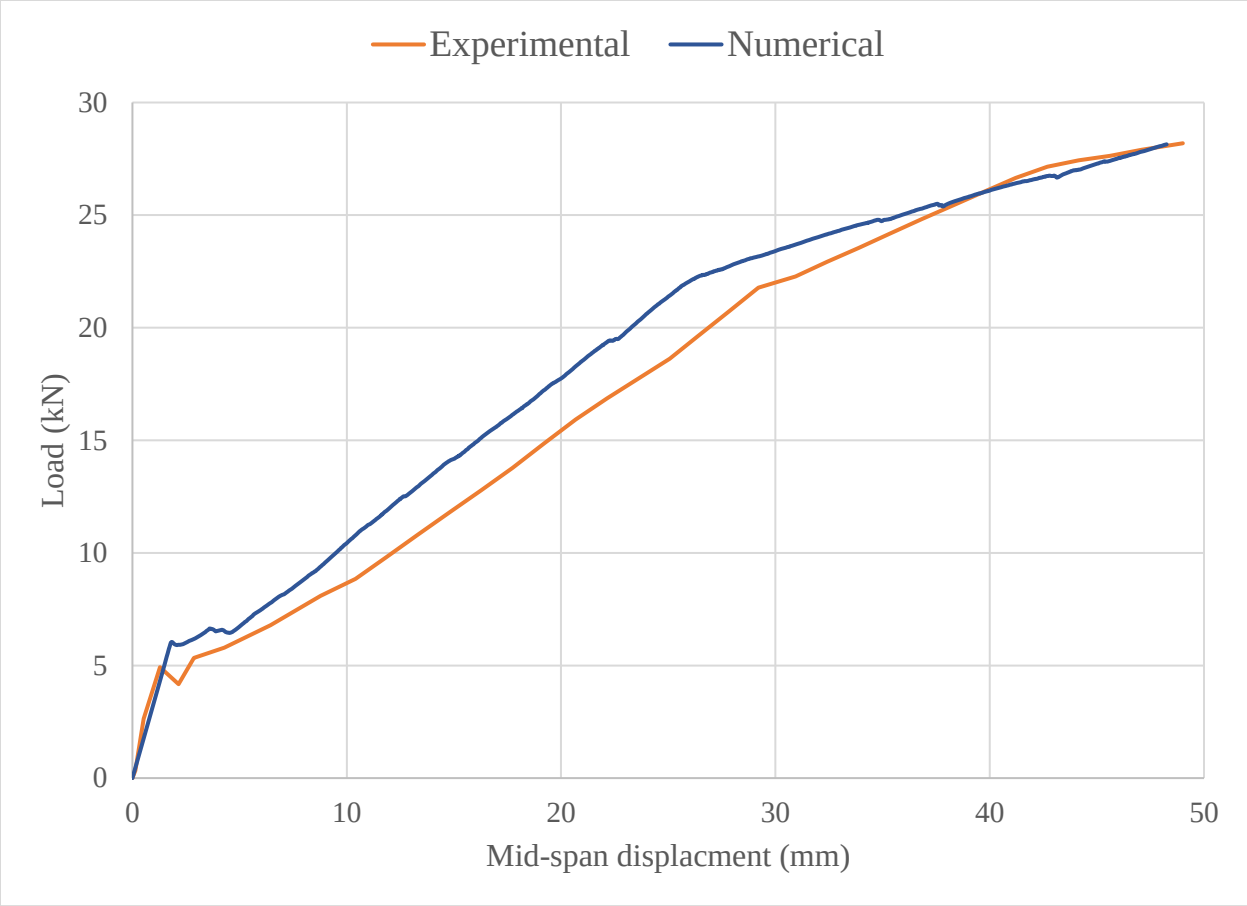

Fig 6.16: Comparisons between experimental and numerical results of the strengthened slab

In addition to load-deflection behaviors of the slabs, the crack patterns from experimental and numerical results were also compared to provide accurate validation of the numerical model. It was apparent that all the crack patterns and failure surface of the slab from the test and the numerical model took place at the same locations as illustrated in Fig 6.17.

The strengthened specimen failed by the debonding of CFRP laminates. The failure was initiated by flexural cracking of concrete in the maximum bending moment zone. This ultimately led to the debonding of CFRP laminates (Hawileh et al., 2016). The damage can be predicted in the specimen when the region at the mid-span of the specimen is the color red as shown in Fig 6.17.

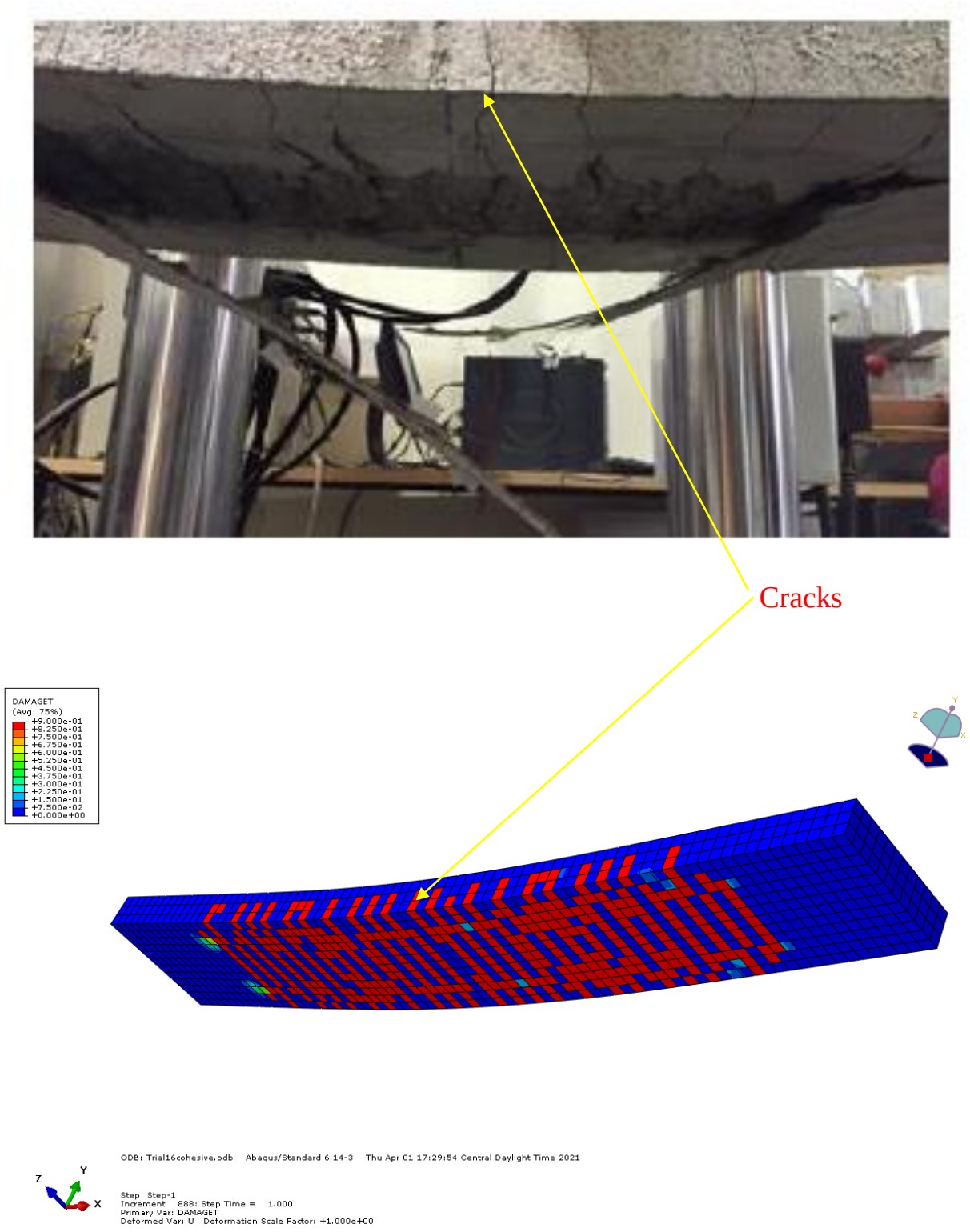

Fig 6.17: Crack pattern comparison between experimental (Hawileh et.al., 2016) and numerical results of the strengthened slab

The maximum stress was observed at the midspan of the specimen as shown in Fig 6.18 (a), which led to debonding of CFRP. The deformed shape of the specimen is also shown in Fig 6.18 (b).

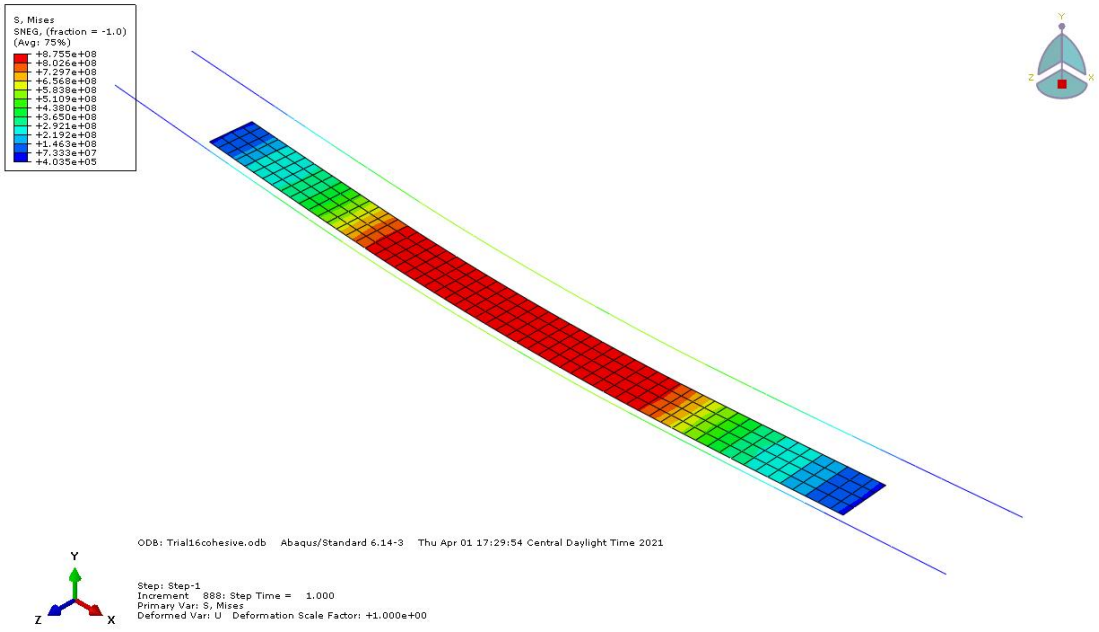

(a)

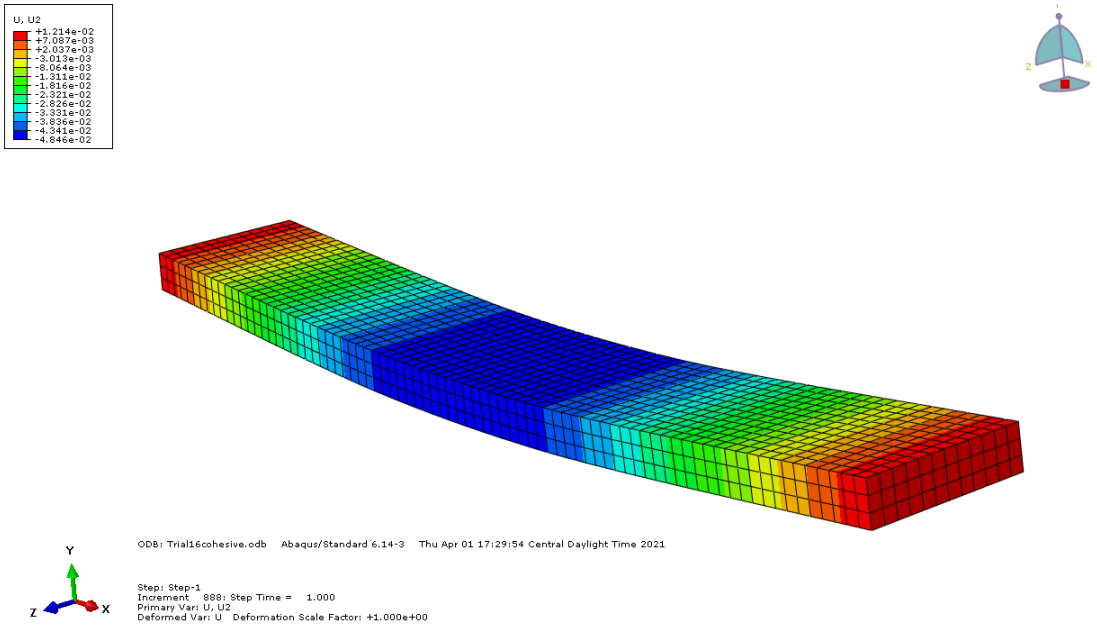

(b)

Fig 6.18: (a) Stresses on CFRP and reinforcement (b) Deformed shape of the slab

Chapter 7
Parametric Study

The numerical analysis was further extended to study the variations in results by changing the parameters. This study aims to understand the various factors affecting the CFRP strengthened slab. The parameters used for the study include compressive strength of concrete, types of CFRPs and number of layers of CFRP. The validated FEA model from the previous chapter was utilized for these purposes.

7.1 Effect of Concrete Strength

In order to understand the behavior of the CFRP strengthened slab, the slab was modelled with two different concrete compressive strengths of 52 MPa (7.54 ksi) and 20.6 MPa (2.98 ksi). A load versus displacement diagram of different concrete strength is plotted and shown in Fig 7.1. There was observed reduction in load-carrying capacity of the slab with lower compressive strength. The initial cracking was also observed at an early stage. The cracks also developed on the top surface of slab, which are not visible in 52 MPa (7.54 ksi) concrete as shown in Fig 7.2.

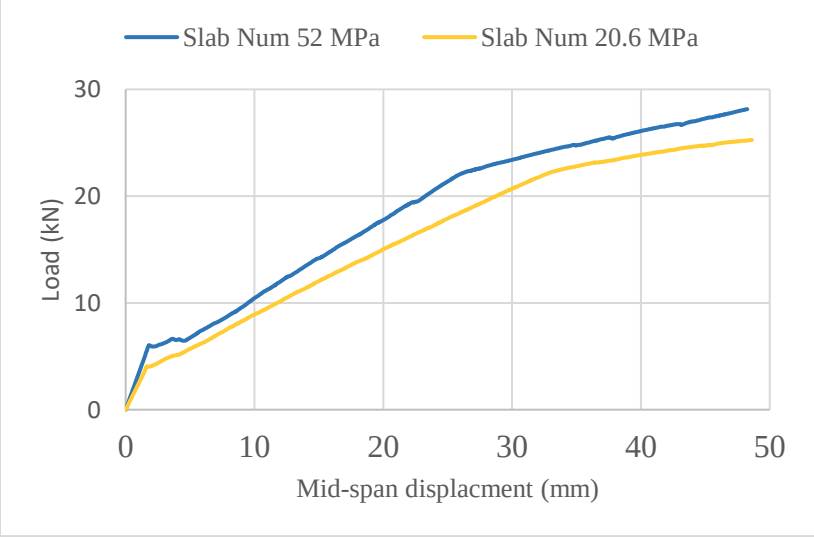

Fig 7.1 Load versus displacement diagram of different compressive strength

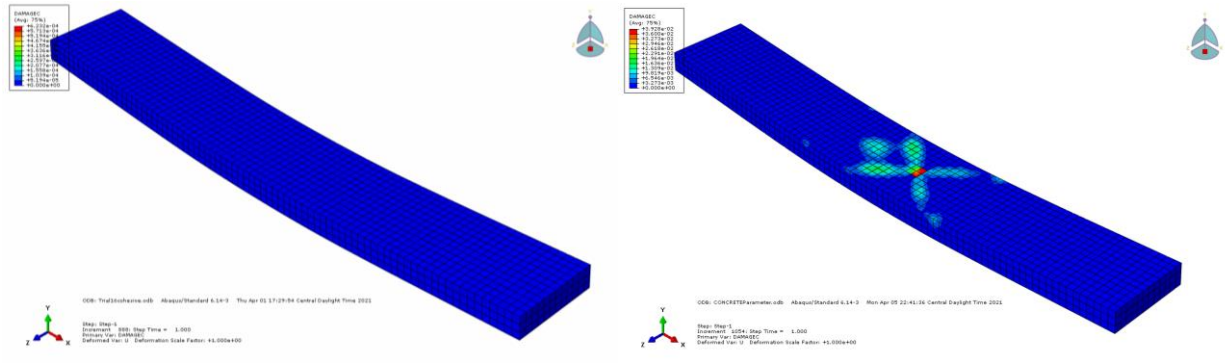

(a) (b)

Fig 7.2 Slab top surface (a) Cracks on 52 MPa (7.54 ksi) compressive strength concrete (b) Cracks on 20.6 MPa (2.98 ksi) compressive strength concrete

7.2 Effect of Types of CFRPs

For the investigation on the effect of CFRP strengthening system, the compressive strength of concrete was determined to be 52 MPa (7.54 ksi). Load capacities of three different type of CFRPs were investigated. The CFRPs used for the purpose of modelling were Sika PS-CFRP, Sika R-CFRP, and MapeWrap CFRP. The material properties of the CFRPs were different and were discussed in detail in previous chapters. The stiffness of the slab is greatly affected by the type of CFRP and is shown in Fig 7.3. For Sika R-CFRP at the same load level, the tangents to the load-deflection curve were higher than that of PS-CFRP and MapeWrap CFRP. This result suggests that slab strengthened with Sika R-CFRP showed stiffer behavior as compared to Sika PS-CFRP and MapeWrap CFRP.

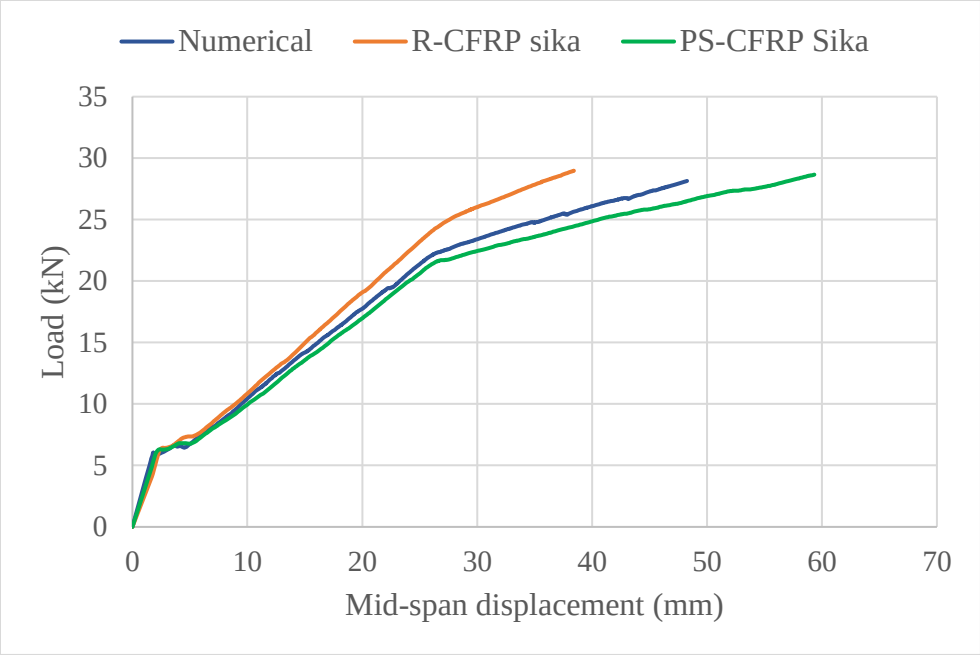

Fig 7.3: Load vs deflection for different types of CFRPs

7.3 Effect of Layer of CFRP

To study the effect of layers of CFRP on the slab, a double layer of CFRP was modeled, and the results were compared with the single layer. The overall stiffness with the double layer was increased as shown in Fig 7.4.

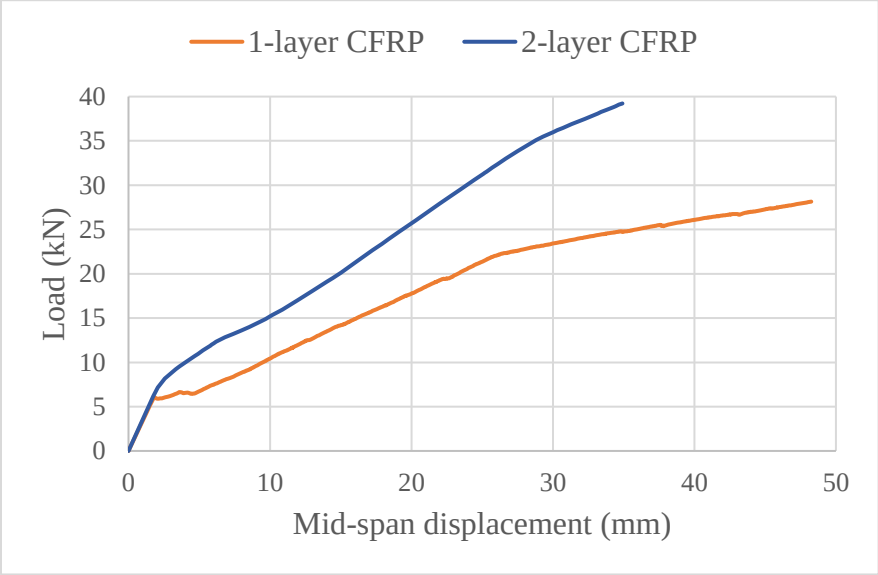

Fig 7.4: Load versus displacement for 1-layer and 2-layers of CFRP

The ultimate load was increased, but there was a significant decrease in the overall deformation. The model also showed good agreement with the experimental results as shown in Fig 7.5.

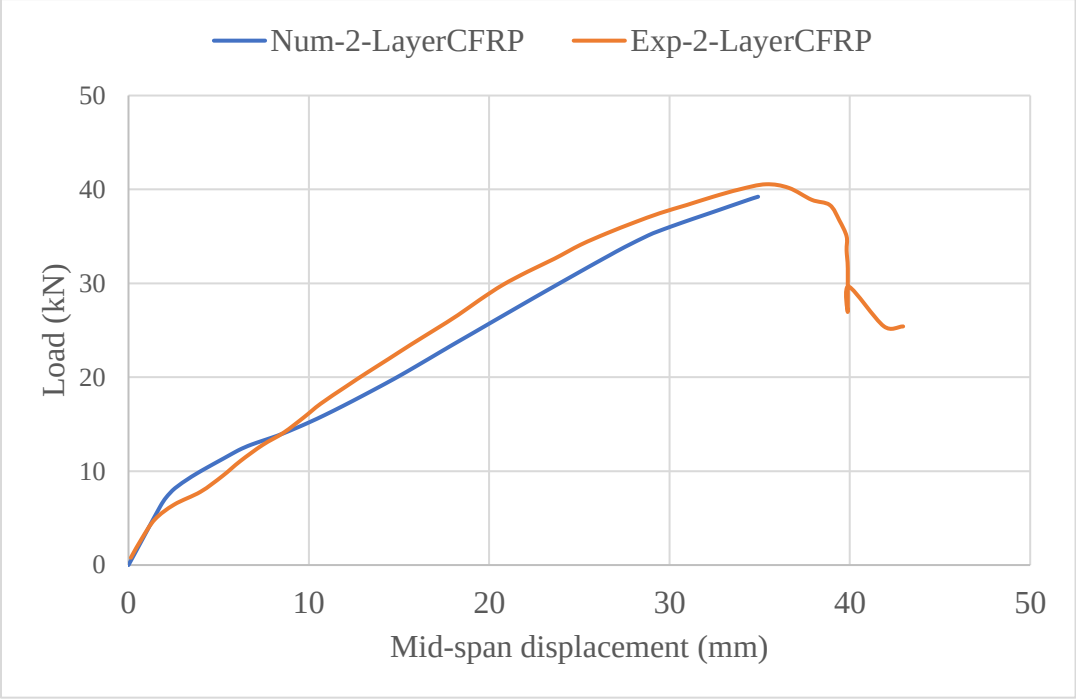

Fig 7.5: Load versus displacement for 2-layers of CFRP

Chapter 8
Conclusions and Recommendations

6.1 Conclusions

The current study aims to evaluate and develop a better understanding of flexural strengthening of two-way slabs using PS-CFRP and R-CFRP. The structural behavior of the two-way slabs was investigated after the experiment, and a numerical model was developed based on previous research. This study was successful in providing appropriate flexural strengthening techniques for two-way slabs. The following conclusions were made from this study:

- The experiment concluded that the load-carrying capacity of the PS-CFRP specimen was increased by 14.29 % as compared to the R-CFRP strengthened specimen.
- PS-CFRP demonstrated ductile behavior as compared to R-CFRP.
- The mode of failure for R-CFRP specimen was brittle flexure failure.
- The mode of failure for PS-CFRP was ductile flexure failure.
- The matrix (resin) of PS-CFRP carried more load than R-CFRP.
- At ultimate load, the strain in PS-CFRP was more than R-CFRP.
- Delamination of CFRP was the prominent failure for both R-CFRP and PS-CFRP.
- Intermediate flexure cracks induced interfacial debonding between the concrete surface and CFRP.
- The FE model was successfully calibrated using the experimental data to investigate the effectiveness of the strengthening of slabs using CFRP.

6.2 Recommendations for Future Studies

- More experimental tests are recommended to be carried out on two-way slabs strengthened with PS-CFRP. This will also help in developing numerical models for two-way slabs strengthened with PS-CFRP.
- Conduct an experiment on a cracked specimen to observe the behavior of R-CFRP and PS-CRFP since CFRP strengthening techniques are practically applied on older and damaged structures.
- Investigate the use of anchorage systems to strengthen PS-CFRP in two-way slabs since the systems have shown successful results using R-CFRP.
- Investigate the use of PS-CFRP for punching shear in slabs.
- Provide a more detailed analysis for various slab sizes, reinforcement ratios, and strengths of concrete.
- Calculate the ductility and energy absorption values for a PS-CFRP strengthened slab.

Appendix A
Installation Procedure of R-CFRP VS PS-CFRP (White, 2018

	Pre-saturated CFRP	**Regular CFRP**
Definition	Reinforced fabrics that have been pre-impregnated with a resin system	Dry carbon fiber fabric
Installation procedure	1. ~~Order & Ship Resin~~ 2. Order & Ship Fabric 3. Prepare concrete 4. ~~Bring Saturator on site~~ 5. Mix Epoxy Primer 6. Prime Concrete 7. Fabric is cut on site (if necessary) 8. ~~Set up saturator~~ 9.~~Fabric is then saturated (saturator or table/rollers)~~ 10. ~~Piece by piece, saturated fabric transported and given to installers~~ 11. Applied to primed surface 12. Left to cure 13. ~~Clean up saturator and site~~ 14. ~~Dispose of Resin pails~~	1. Order & Ship Resin 2. Order & Ship Fabric 3. Prepare concrete 4. Bring Saturator on site 5. Mix Epoxy Primer 6. Prime Concrete 7. Fabric is cut on site (if necessary) 8. Set up saturator 9.Fabric is then saturated (saturator or table/rollers) 10. Piece by piece, saturated fabric transported and given to installers 11. Applied to primed surface 12. Left to cure 13. Clean up saturator and site 14. Dispose of Resin pails

Appendix B
Load Versus Strain

(R-CFRP)

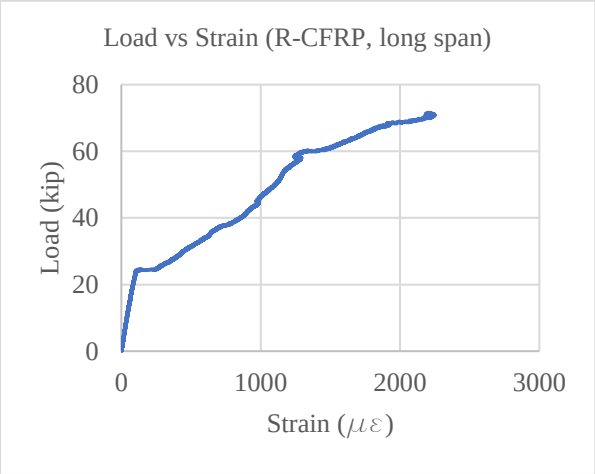

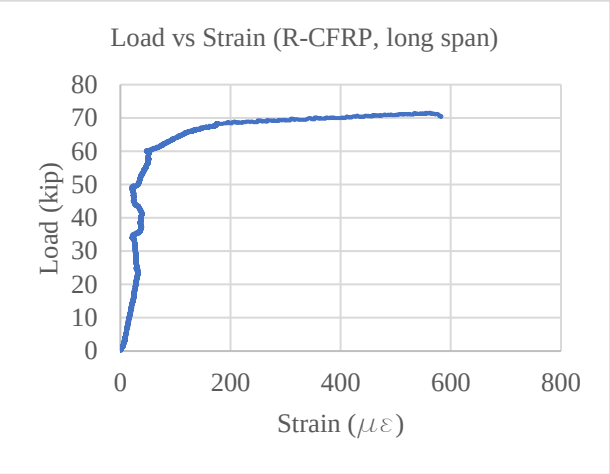

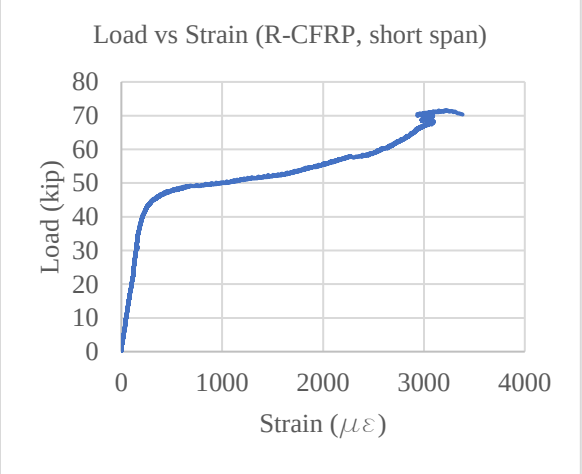

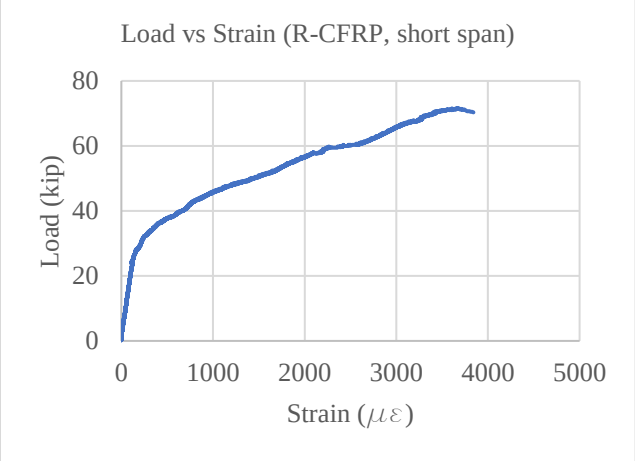

(PS-CFRP)

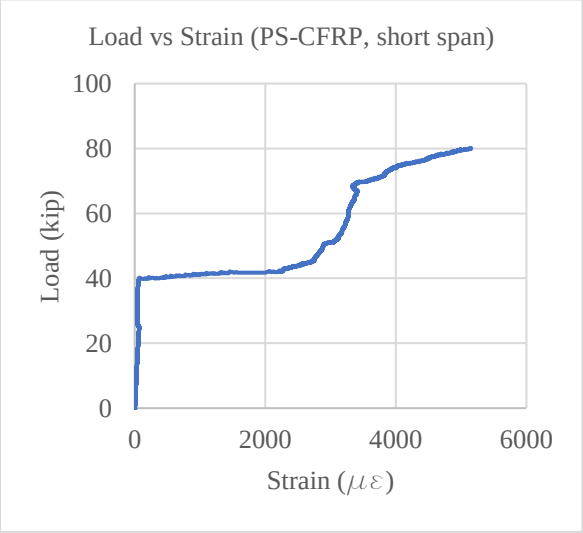

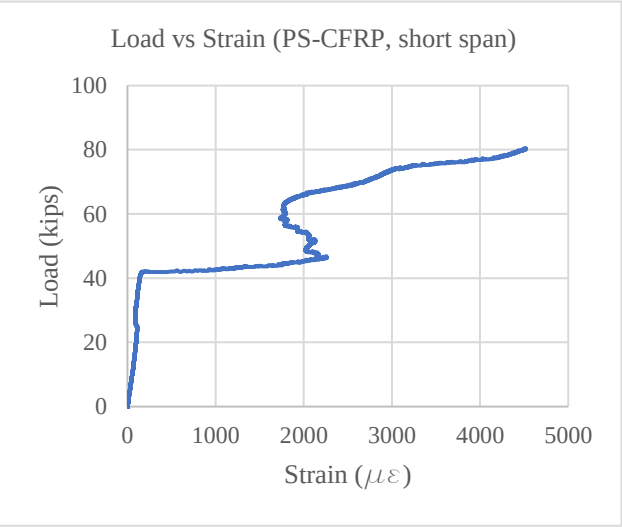

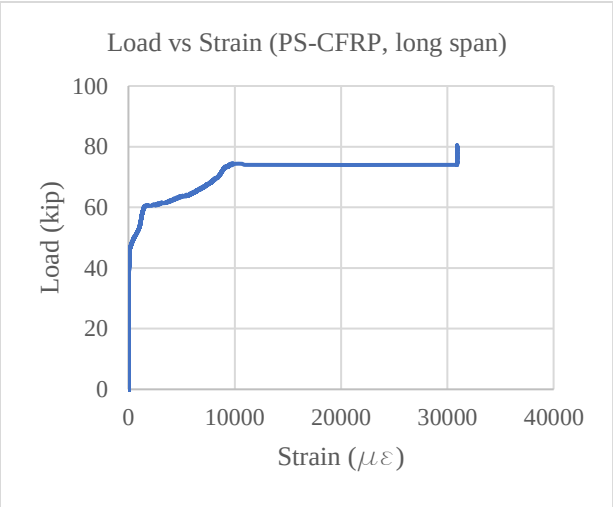
Load vs Strain (PS-CFRP, long span)
Load (kip)
100
80
60
40
20
0
0
10000
20000
30000
40000
Strain (με)

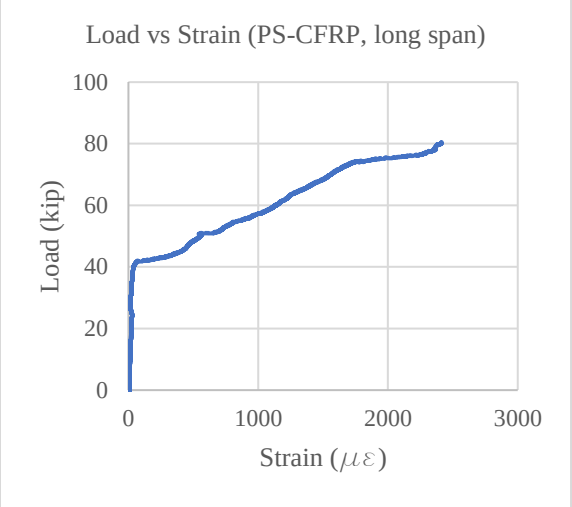
Load vs Strain (PS-CFRP, long span)
Load (kip)
100
80
60
40
20
0
0
1000
2000
3000
Strain (με)

References

1. ABAQUS Inc. (2005). Elements. Retrieved from https://imechanica.org/files/l2-elements.pdf

2. Abbaszadeh, M. A., Sharbatdar, M. K., & Kheyroddin, A. (2017). Performance of Two-way Rc SLABS retrofitted by different configurations of high Performance fibre Reinforced CEMENTITOUS Composite Strips. *The Open Civil Engineering Journal*, *11*(1), 650-663. doi:10.2174/1874149501711010650

3. Abou-Elfath, H., & Ghobarah, A. (2000). Behaviour of reinforced concrete frames rehabilitated with concentric steel bracing. *Canadian Journal of Civil Engineering*, 27(3), 433-444. doi:10.1139/l99-092

4. ACI Committee 421 (2015). Guide to design of reinforced two-way slab systems: (ACI 421.3-15). Farmington Hills, MI*: American Concrete Institute*

5. ACI Committee 440. (2002). Guide for the Design and Construction of Externally Bonded FRP Systems for Strengthening Concrete Structures (ACI 440.2R-02). Farmington Hills, MI: *American Concrete Institute*

6. ACI Committee 318. (1995). Building code requirements for structural concrete : (ACI 318-95) ; and commentary (ACI 318R-95). Farmington Hills, MI: *American Concrete Institute*

7. Anggraini, R., Tavio, Raka, I. G., & Agustiar. (2018). Stress-strain relationship of high-strength steel (HSS) reinforcing bars. *AIP Conference Proceedings*. doi:10.1063/1.5038307

8. Chen, Z. F., Wan, L. L., Lee, S., Ng, M., Tang, J. M., Liu, M., & Lee, L. (2008). Evaluation of CFRP, GFRP and BFRP Material Systems for the Strengthening of RC Slabs. *Journal of Reinforced Plastics and Composites*, *27*(12), 1233–1243. https://doi.org/10.1177/0731684407084122

9. Chen, C. & Chen, S. (2019). Strengthening of Reinforced Concrete Slab-Column Connections with Carbon Fiber Reinforced Polymer Laminates. Applied Sciences. 10. 265. 10.3390/app10010265.

10. Cook, R. D., & Cook, R. D. (2003). *Concepts and applications of finite element analysis*. India: John Wiley & Sons (Asia).

11. Demeter, I., Nagy-György, T., Stoian, V., Dăescu, C., & Dan, D. (2011). Strengthening strategies using FRP composites For PRECAST RC wall panels With cut-out openings. *International Review of Applied Sciences and Engineering, 2*(1), 19-24. doi:10.1556/irase.2.2011.1.3

12. Demeter, I., Nagy-György, T., Stoian, V., Dăescu, C., & Dan, D. (2011). Strengthening strategies using FRP composites For PRECAST RC wall panels With cut-out openings. *International Review of Applied Sciences and Engineering, 2*(1), 19-24. doi:10.1556/irase.2.2011.1.3

13. Ebead, U., & Marzouk, H. (2004). Fiber-reinforced polymer strengthening of two-way slabs. *ACI Structural Journal, 101*(5). doi:10.14359/13387

14. Ebead, U., Hesham, M. & Leonard, L. (2002). Strengthening of Two-Way Slabs Using FRP Materials: A Simplified Analysis Based on Response Surface Methodology.

15. ECT Team, Purdue. Carbon Fiber Reinforced Polymer (CFRP) Laminates for Structural Strengthening. (2007). *Purdue University*. doi:10.5703/1288284315732

16. ElSafty, A., Graeff, M. K., & Fallaha, S. (2014). Behavior of Laterally Damaged Prestressed Concrete Bridge Girders Repaired with CFRP Laminates Under Static and Fatigue Loading. *International Journal of Concrete Structures and Materials, 8*(1), 43-59. doi:10.1007/s40069-013-0053-0

17. Externally Bonded FRP Reinforcement for RC Structures (Rep. No. 14). (2001). Fib Bulletin. ISBN 978-2-88394-054-3

18. Farghaly, A. S., & Ueda, T. (2011). Prediction of punching shear strength of two-way slabs strengthened externally with frp sheets. *Journal of Composites for Construction, 15*(2), 181-193. doi:10.1061/(asce)cc.1943-5614.0000177

19. Fathelbab, F. A., Ramadan, M. S., & Al-Tantawy, A. (2014). Strengthening of RC BRIDGE slabs using CFRP sheets. Alexandria Engineering Journal, 53(4), 843-854. doi: 10.1016/j.aej.2014.09.010 7. Jiho Moon, Mahmoud M. Reda Taha, and Jung J. Kim (2017).

20. Fiorato, A., Oesterle, R. and Corley, W. (1983). Behavior of Earthquake Resistant Structural Walls Before and After Repair. *ACI Journal* 80:5, 403-413

21. Ghaffary, A., & Moustafa, M. A. (2020). Synthesis of Repair Materials and Methods for Reinforced Concrete and Prestressed Bridge Girders. *Materials*, *13*(18), 4079. https://doi.org/10.3390/ma13184079

22. Guo, Z. & Cao, S. & Sun, W. & Lin, X. (2005). Experimental Study on Bond Stress-Slip Behaviour Between FRP Sheets and Concrete.

23. Hawileh, H., Abdalla, J. & Mahmoud, H. (2016). Strengthening of Thin Reinforced Concrete Slabs with CFRP Laminates**.** *7th International Conference on Advanced Composite Materials in Bridges and Structures***.** Vancouver, British Columbia, Canada

24. HM-20 Unidirectional Carbon Fiber Wrap. Retrieved April 10, 2021, from https://www.horseen.com/carbon-fiber-strengthening-system/unidirectional-CFRP-wrap

25. Kim, Y. J., Longworth, J. M., Wight, R. G., & Green, M. F. (2008). Flexure of Two-Way Slabs strengthened with prestressed Or NONPRESTRESSED CFRP Sheets. *Journal of Composites for Construction, 12*(4), 366-374. doi:10.1061/(asce)1090-0268(2008)12:4(366)

26. Limam, O., Foret, G., & Ehrlacher, A. (2003). RC two-way slabs strengthened with CFRP STRIPS: Experimental study and a LIMIT analysis approach. *Composite Structures, 60*(4), 467-471. doi:10.1016/s0263-8223(03)00011-4

27. Lu, X., Teng, J., Ye, L., & Jiang, J. (2005). Bond–slip models for FRP Sheets/plates bonded to concrete. *Engineering Structures, 27*(6), 920-937. doi:10.1016/j.engstruct.2005.01.014

28. Lubliner, J., Oliver, J., Oller, S., & Oñate, E. (1989). A plastic-damage model for concrete. *International Journal of Solids and Structures, 25*(3), 299-326. doi:10.1016/0020-7683(89)90050-4

29. Lundqvist, J., Nordin, H., Täljsten, B., & Olofsson, T. (2005). Numerical analysis of concrete beams strengthened with CFRP: a study of anchorage lengths.

30. Moon, J., Reda Taha, M. M., & Kim, J. J. (2017). Flexural strengthening of Rc Slabs using a hybrid FRP-UHPC system including Shear Connector. *Advances in Materials Science and Engineering*, 1-7. doi:10.1155/2017/4387545

31. Mosallam, A. S., & Mosalam, K. M. (2003). Strengthening of TWO-WAY concrete slabs with FRP composite laminates. *Construction and Building Materials, 17*(1), 43-54. doi:10.1016/s0950-0618(02)00092-2

32. Nayal, R., & Rasheed, H. A. (2006). Tension stiffening model for concrete beams reinforced with steel and Frp bars. *Journal of Materials in Civil Engineering, 18*(6), 831-841. doi:10.1061/(asce)0899-1561(2006)18:6(831)

33. Neale, K., Ebead, U., Abdel Baky, H., Elsayed, W., & Godat, A. (2005). Modelling of debonding phenomena in FRP-strengthened concrete beams and slabs. *Proceedings of the international symposium on bond behaviour of FRP in structures (BBFS).*

34. Obaidat, Y. T. (2011). Structural retrofitting of concrete beams Using FRP: Debonding issues (Doctoral dissertation, Diss. Lund: Lunds universitet, 2011). Lund: Department of Construction Sciences, Structural Mechanics, Lund University.

35. Orton, S. L., Jirsa, J. O., & Bayrak, O. (2008). Design Considerations of Carbon Fiber Anchors. *Journal of Composites for Construction, 12*(6), 608-616. doi:10.1061/(asce)1090-0268(2008)12:6(608)

36. Pandey, P. (2018). *Evaluation of Beams and Columns Strengthening with Pre-Saturated and Regular CFRP* (Unpublished master's thesis). The University of Texas at Arlington.

37. Piggott, M. (2002). *Load Bearing Fibre Composites*. New York, NY: Springer US.

38. Rajek, G. S. (2010). *Numerical Modeling of the Performance of Highway Bridge Approach Slab* (Unpublished master's thesis). University of Wisconsin - Madison.

39. Reinforced concrete slab repair. (2019, February 12). Retrieved April 10, 2021, from https://www.structuraldynamics.com/reinforced-concrete-slab-repair

40. *Retrofitting of RCC Structural Members, Types, Selection, and Procedures*. The Constructor. (2019, February 20). https://theconstructor.org/concrete/retrofitting-rcc-structural-members/7363/.

41. Sika. (2019). SikaWrap® Hex-103 C - CARBON FIBER FABRIC FOR STRUCTURAL STRENGTHENING. Lyndhurst, NJ; Sika Corporation.

42. Sika. (2016). SikaWrap® Pre-saturated 117C - CARBON FIBER FABRIC FOR STRUCTURAL STRENGTHENING. Lyndhurst, NJ; Sika Corporation.

43. Sobieck T., Atadero R., Mahmoud H. *Predicting Fatigue Service Life Extension of RC Bridges with Externally Bonded CFRP Repairs.* Mountain Plains Consortium, Department of Civil and Environmental Engineering, Colorado State University; Fort Collins, CO, USA: 2015.

44. Taghdi, M., Bruneau, M., & Saatcioglu, M. (2000). Seismic retrofitting of low-rise masonry and concrete walls using steel strips. *Journal of Structural Engineering*, 126(9), 1017-1025. doi:10.1061/(asce)0733-9445(2000)126:9(1017)

45. Tan, K.Y., Tumialan, G. & Nanni, A. (2003). Evaluation of externally bonded CFRP systems for the strengthening of RC slabs. 10.1142/9789812704863_0038.

46. Tao, Y., & Chen, J. F. (2015). Concrete damage plasticity model for modeling frp-to-concrete bond behavior. *Journal of Composites for Construction, 19*(1), 04014026. doi:10.1061/(asce)cc.1943-5614.0000482

47. Teeraphot, S., PhuwanatAmorn, P., & Pimanmas, A. (2004). A. Finite Element Analysis of FRP Strengthened RC Beam. *Songklanakarin Journal of Science and Technology*.

48. Vanderbilt, M. D., Sozen, M. A. & Seiss, C. P. (1963). Investigation of Multiple Panel Reinforced Concrete Floor Slabs: Design Methods - Their Evaluation and Comparison. *ACl Journal Proceedings,* 60(8):9W-1027

49. Vasquez, A., & Kharbari, V. M. (2003). Fiber-Reinforced Polymer Composite strengthening of concrete slabs with cutouts. *ACI Structural Journal, 100*(5). doi:10.14359/12808

50. W.E. El Sayed, U.A. Ebead, and K.W. Neale "Modelling of Debonding Failures in FRP-Strengthened Two-Way Slabs" SP-230—27

51. What is Two-way Slab? (2020, June 15). Retrieved April 10, 2021, from https://gharpedia.com/blog/two-way-slab/

52. White, D. (2018). Bridge Preservation with Presaturated FRP Composite Materials. *National Bridge Preservation Partnership*.

53. Yazdani, N., Aljaafreh, T., & Beneberu, E. (2020). Concrete Beam Flexural Strengthening with Anchored Pre-saturated CFRP Laminates. *Composite Structures, 235*, 111733. doi: 10.1016/j.compstruct.2019.111733

54. Yiyan, L., Tao, Z., Shan, L., & Haojun, Z. (2018). Behaviour of RC two-way slabs strengthened with CFRP-steel grid under concentrated loading. *Journal of Southeast University (English Edition), 34*(1003-7985), 331-339.